EUROPEAN ORGANIZATION FOR NUCLEAR RESEARCH (CERN)

CERN-EP-2026-243
2026/11/18

CMS-TAU-25-001

A machine-learning method for the estimation of the background from jets misidentified as hadronic tau lepton decays

The CMS Collaboration*

arXiv:2610.13634v2 [hep-ex] 16 Nov 2026

Abstract

Backgrounds arising from quark- and gluon-initiated jets misidentified as hadronically decaying tau leptons constitute a major experimental challenge for analyses involving tau leptons. The MUltivariate Fake-Factor INference (MUFFIN) approach, a machine-learning-based method for estimating this background directly from observed events, is presented. Boosted decision tree reweighting is used to learn multi-dimensional, per-object correction factors directly from observed data, thereby modelling the jet to hadronic tau lepton misidentification probability across the kinematic and topological phase space without relying on low-dimensional parametrisations. Performance studies are presented using proton-proton collision data collected by the CMS experiment at the CERN LHC at $\sqrt{s} = 13.6\,\text{TeV}$, corresponding to an integrated luminosity of $62.4\,\text{fb}^{-1}$. Compared to low-dimensional parametrisation methods, improved modelling of key kinematic observables is achieved, particularly in regions of high p_{T}. The improved modelling leads to a reduction of up to 70% in the systematic uncertainty associated with jets being misidentified as hadronically decaying tau leptons. The MUFFIN method provides a robust and scalable method for background estimation in precision measurements and searches for beyond-the-standard-model physics involving tau lepton final states.

Published in the Journal of Instrumentation as doi:10.1088/1748-0221/21/11/P11012.

© 2026 CERN for the benefit of the CMS Collaboration. CC-BY-4.0 license

*See Appendix A for the list of collaboration members

1 Introduction

In the standard model (SM) of particle physics, tau (τ) leptons are the heaviest leptons and play a crucial role in measurements involving the Higgs boson (H), as well as in searches for physics beyond the SM (BSM). Measurements involving τ leptons provide a sensitive probe of Higgs boson properties, including its couplings to fermions, its charge-parity (*CP*) properties, and its self-coupling via the Higgs boson pair production mechanism [1–11]. The τ leptons are also key signatures in many BSM scenarios, including models with extended Higgs sectors, supersymmetry, and heavy gauge bosons [12–19]. The τ leptons can decay either leptonically or hadronically, with the latter mode, denoted as τ_{h}, being the most abundant and occurring in approximately 65% of the τ lepton decays. Since τ_{h} decays consist of charged and neutral hadrons and are accompanied by neutrinos, they represent a complex experimental signature that requires dedicated reconstruction and identification techniques. Despite significant advances in τ lepton reconstruction and identification at the CERN LHC, analyses involving τ_{h} candidates remain challenging due to substantial backgrounds from quark- and gluon-initiated jets that can mimic τ_{h} decays (jet $\rightarrow \tau_{\mathrm{h}}$). An accurate estimation of these backgrounds is therefore essential for precision measurements and searches involving τ leptons.

These backgrounds, primarily originating from quantum chromodynamics (QCD) multijet production, W boson production in association with jets ($\mathrm{W}+\mathrm{jets}$), and top quark pair production ($\mathrm{t\bar{t}}$) processes, can mimic the signature of τ_{h} decays and thus complicate the extraction of signal processes. Additional processes such as $\mathrm{Z}/\gamma^{*}+\mathrm{jets}$ or diboson production can also contribute depending on the final state. The dominant background from jet $\rightarrow \tau_{\mathrm{h}}$ misidentification is often estimated using data-driven methods, among which the "Fake Factor" (F_{F}) method is widely used [4, 12, 20–22]. This method relies on the definition of determination regions (DRs), enriched in misidentified τ_{h} candidates, and application regions (ARs), which are kinematically similar to the signal regions (SRs) but differ in the τ_{h} identification requirements. Transfer factors (TFs) are measured in the DRs and applied in the ARs to estimate the misidentified background in the SRs.

While the F_{F} method is robust and effective, it relies on a number of limiting assumptions. In particular, F_{F}s are typically parametrised using fixed binning in a limited number of kinematic variables, which constrains the achievable parametrisation and leads to both statistical limitations from sparsely populated bins and systematic uncertainties associated with missing variable dependencies. The method assumes that the misidentification probability factorises between these variables and a separate set of variables used to define the analysis categories, implicitly neglecting potential correlations with other event-level or object-level quantities. As analyses increasingly exploit multivariate information, these assumptions can become limiting factors in achieving an optimal background modelling accuracy. Residual mismodelling may arise in regions where the assumptions of the F_{F} method do not hold. In such cases, additional non-closure (i.e. discrepancies between predicted and observed background in control regions) or extrapolation corrections are often required, together with associated systematic uncertainties. Moreover, the need to define multiple parametrisations and correction steps can lead to complex workflows that are difficult to maintain, reproduce, and validate consistently. This method can lead to reduced precision and, in some cases, limit the sensitivity of analyses involving τ_{h} candidates.

Advances in machine learning (ML) techniques provide an opportunity to generalise the F_{F} paradigm by learning multidimensional reweighting functions directly from observed data and simulation. In this paper, MUltivariate Fake-Factor INference (MUFFIN), an ML-based alternative to the F_{F} method based on boosted decision tree (BDT) reweighting [23], is presented.

The MUFFIN method replaces explicit low-dimensional parametrisations with per-object event weights that capture correlations between multiple kinematic and event-level variables, reducing the reliance on factorisation assumptions. At the same time, this novel procedure retains the fully data-driven nature of the background estimation strategy and provides a more unified and reproducible background estimation workflow, developed and demonstrated here using proton-proton (pp) collision data collected with the CMS detector. It is applicable to all analysis channels involving τ_h final states, and is demonstrated explicitly in the fully hadronic $\tau_h\tau_h$ and in the semileptonic $\tau_\mu\tau_h$ channel, where τ_μ denotes a τ lepton decaying to a muon. Although the method is demonstrated using the DEEPTAU [24, 25] algorithm for τ_h identification, the approach does not depend on the specific choice of identification algorithm and can be readily adapted as identification methods evolve. The jet $\to \tau_h$ background constitutes a significantly larger fraction of the total background in the $\tau_h\tau_h$ channel than in the $\tau_\mu\tau_h$ channel. For the inclusive SR selections considered in this paper, defined in Section 5, it accounts for approximately 75% of the total background in the $\tau_h\tau_h$ channel, compared to approximately 35% in the $\tau_\mu\tau_h$ channel. Consequently, improvements in the jet $\to \tau_h$ background modelling are expected to have a larger impact on the overall background estimation in the $\tau_h\tau_h$ channel, while still providing benefits in the $\tau_\mu\tau_h$ channel. Throughout this paper, the F_F method is used as the reference baseline against which the MUFFIN method is compared.

This paper is organised as follows. Section 2 describes the CMS detector and the event reconstruction algorithms. Sections 3 and 4 outline the data and simulated samples used in this analysis, and the event reconstruction process, respectively. Section 5 details the event selection criteria applied to define the SRs for the $\tau_h\tau_h$ and $\tau_\mu\tau_h$ channels. Section 6 introduces the MUFFIN method and its implementation in the context of the jet $\to \tau_h$ background estimation. Section 7 compares the performance of the MUFFIN method with that of the F_F method, as implemented in Ref. [12]. This is followed by a description of the systematic uncertainties associated with the MUFFIN method in Section 8. Section 9 presents the application of the method to events with two τ candidates selected with typical SR selections used in analyses targeting Higgs boson decays to τ lepton pairs. Finally, Section 10 summarises the findings and discusses potential future applications of the MUFFIN method.

2 The CMS detector

The CMS apparatus [26, 27] is a multipurpose, nearly hermetic detector, designed to trigger on [28–30] and identify [31–33] electrons, muons, photons, and (charged and neutral) hadrons. Its central feature is a superconducting solenoid of 6 m internal diameter, providing a magnetic field of 3.8 T. Within the solenoid volume are a silicon pixel and strip tracker, a lead tungstate crystal electromagnetic calorimeter (ECAL), and a brass and scintillator hadron calorimeter (HCAL), each composed of a barrel and two endcap sections. Forward calorimeters extend the pseudorapidity (η) coverage of the barrel and endcap detectors. Muons are reconstructed using gas-ionisation detectors embedded in the steel flux-return yoke outside the solenoid.

Events of interest are selected using a two-tiered trigger system. The first level, composed of custom hardware processors, uses information from the calorimeters and muon detectors to select events at a rate of around 100 kHz within a fixed latency of about 4 μs [28]. The second level, known as the high-level trigger, consists of a farm of processors running a version of the full event reconstruction software optimised for fast processing, and reduces the event rate to a few kHz before data storage [29, 30].

A more detailed description of the CMS detector, together with a definition of the coordinate system used and the relevant kinematic variables, can be found in Refs. [26, 27].

3 Data and simulated samples

The data set analysed in this work was recorded with the CMS detector during 2022–2023 and corresponds to an integrated luminosity of 62.4 fb^{-1} of pp collisions at a centre-of-mass energy of 13.6 TeV [34].

Production of $\text{Z}/\gamma^* + \text{jets}$ and $\text{W} + \text{jets}$ events is simulated with MADGRAPH5_aMC@NLO (Version 2.9.13) [35]. For the $\text{Z}/\gamma^* + \text{jets}$ process, next-to-leading order (NLO) QCD matrix elements with up to two additional partons are employed, with different parton multiplicities merged via the FxFx prescription [36]. The $\text{W} + \text{jets}$ process is modelled at leading order (LO) in QCD, retaining matrix elements with up to four additional partons, combined through the MLM jet-matching scheme [37]. Diboson production is simulated at LO using PYTHIA (Version 8.306) [38]. The predicted yields for the $\text{Z}/\gamma^* + \text{jets}$, $\text{W} + \text{jets}$, and diboson processes are normalised to theoretical cross sections computed at next-to-next-to-leading order (NNLO) in QCD with NLO electroweak corrections applied [39, 40].

Top quark pair ($\text{t}\bar{\text{t}}$) and single top quark production, including the t-channel and tW associated production modes, are modelled at NLO in QCD using the POWHEG 2.0 generator [41–44]. The $\text{t}\bar{\text{t}}$ and t-channel single top quark processes are normalised to cross sections from NNLO QCD calculations [45, 46], while the tW process is normalised to an NLO QCD cross section [47].

All simulated samples use the NNPDF3.1 NNLO parton distribution functions [48]. Parton showering, hadronisation, and τ lepton decays are modelled by PYTHIA, with the underlying event tuned to the CP5 parameter set [49]. The response of the CMS detector is evaluated with a full simulation based on GEANT4 [50], and all simulated events are reconstructed using the same algorithms as applied to data. The effects of additional pp interactions within the same or nearby bunch crossings (pileup) are included by overlaying minimum bias collisions simulated with PYTHIA, and the pileup distribution in simulation is reweighted to match that observed in data.

4 Event reconstruction

Events recorded by the CMS detector are reconstructed using the particle-flow (PF) algorithm [51], which combines information from the tracking system, calorimeters, and muon detectors to identify and reconstruct individual particles produced in pp collisions. The PF algorithm classifies reconstructed particles as charged or neutral hadrons, photons, electrons, or muons, and provides a global and consistent description of the event.

The energy of photons is obtained directly from measurements in the ECAL. Electron momenta are reconstructed by combining the momentum measured in the silicon tracker with the energy deposited in the ECAL, including contributions from bremsstrahlung photons associated with the electron track. Muon momenta are determined from the curvature of tracks reconstructed using information from the silicon tracker and the muon system. The energies of charged hadrons are reconstructed from a combination of the track momentum and the associated calorimetric energy deposits, corrected for the calorimeter response to hadronic showers. Neutral hadron energies are obtained from corrected ECAL and HCAL measurements.

For each event, hadronic jets are clustered from these reconstructed particles using the infrared and collinear safe anti-k_T algorithm [52, 53] with a distance parameter of 0.4. Jet momentum is determined as the vectorial sum of all particle momenta in the jet, and is found from simulation to be, on average, within 5–10% of the true momentum over the whole p_T spectrum and detector acceptance. Jet energy corrections are derived from simulation to bring the mea-

sured response of jets to that of particle level jets on average. In situ measurements of the momentum balance in dijet, photon + jet, Z + jet, and multijet events are used to account for any residual differences in the jet energy scale between data and simulation [54]. The jet energy resolution amounts typically to 15–20% at 30 GeV and 10% at 100 GeV [54]. Additional selection criteria are applied to each jet to remove jets potentially dominated by anomalous contributions from the readout of various detector components or reconstruction failures. The DEEPJET algorithm [55] is used for b jet identification. The algorithm produces a continuous discriminant score for each jet, and a working point is defined by placing a fixed threshold on this score, yielding a binary b jet selection. The medium working point is used, corresponding to an identification efficiency for b jets of approximately 70% and a misidentification rate for charm, light-flavour quark, and gluon jets of about 1% [55]. Scale factors derived from data are applied to simulated events to correct for differences in b-tagging efficiency between data and simulation. The b-tagging requirements are used to define dedicated control regions enriched in $\mathrm{t\bar{t}}$ events, as described in Section 6, and to suppress $\mathrm{t\bar{t}}$ contributions in the SRs by vetoing events containing b-tagged jets.

Interaction vertices are reconstructed by clustering tracks along the beam axis and fitting each cluster with an adaptive vertex fitting algorithm [33]. The primary vertex (PV) is selected as the vertex with the largest value of the squared p_T sum of associated physics objects, constructed from anti-k_T track jets, remaining tracks including identified leptons, and a track-based transverse momentum imbalance [33].

Pileup can contribute extra tracks and calorimetric energy depositions to the jet momentum. The pileup-per-particle identification algorithm (PUPPI) [56, 57] is used to mitigate the effect of pileup at the reconstructed-particle level, making use of local shape information, event pileup properties, and tracking information. A local shape variable is defined, which distinguishes between collinear and soft diffuse distributions of other particles surrounding the particle under consideration. Collinear distributions are attributed to particles originating from the hard scatter, whereas soft diffuse distributions are attributed to particles originating from pileup interactions. Charged particles identified to be originating from pileup vertices are discarded. For each neutral particle, a local shape variable is computed from nearby particles. Within the tracker acceptance ($|\eta| < 2.5$), only charged particles compatible with the PV are considered. Outside the tracker coverage, both charged and neutral particles are used. The momenta of the neutral particles are then rescaled according to their probability to originate from the PV, deduced from the local shape variable, superseding the need for jet-based pileup corrections [56].

The missing transverse momentum vector $\vec{p}_\mathrm{T}^{\,\mathrm{miss}}$ is computed as the negative vector p_T sum of all the PF candidates in an event, and its magnitude is denoted as $p_\mathrm{T}^{\mathrm{miss}}$ [58]. The $\vec{p}_\mathrm{T}^{\,\mathrm{miss}}$ is corrected for the energy scale of the reconstructed jets in the event. The PUPPI algorithm is applied to reduce the pileup dependence of the $\vec{p}_\mathrm{T}^{\,\mathrm{miss}}$ observable. The $\vec{p}_\mathrm{T}^{\,\mathrm{miss}}$ is computed from the PF candidates weighted by their probability of originating from the PV [58].

Muons are reconstructed within $|\eta| < 2.4$ using information from the muon detectors and the silicon tracker. The reconstruction and identification efficiency for muons exceeds 96% over the full acceptance, with p_T resolutions of about 1% in the barrel and 3% in the endcap regions for muons with $p_\mathrm{T} < 100$ GeV [32].

Electrons are reconstructed by matching tracks in the silicon tracker to energy clusters in the ECAL. Their momentum resolution depends on the detector region and the amount of bremsstrahlung radiation emitted in the tracker material, and is approximately 1.6–5.0% for electrons with p_T around 45 GeV from $\mathrm{Z} \to \mathrm{ee}$ decays [31, 59].

The reconstruction of τ_h leptons is performed from anti-k_T jets using the hadrons-plus-strips (HPS) algorithm [24, 60]. The reconstruction is based on PF candidates and targets the characteristic low-multiplicity decay topologies of τ_h decays. Charged hadrons reconstructed by the PF algorithm are combined with electromagnetic PF candidates consistent with neutral pion decays. Neutral pions are identified through their $\pi^0 \to \gamma\gamma$ decay, including cases affected by photon conversions, by clustering nearby photons and electrons into elongated structures in the η-ϕ plane, referred to as strips. The strip size is dynamically adjusted as a function of the p_T of the associated electromagnetic candidates to account for the collimation of the decay products at high momentum.

The four-momentum of each reconstructed neutral pion candidate is constructed by summing the energies of all PF photons and electrons clustered into the strip as a scalar sum, exploiting the superior energy resolution of the ECAL. Its direction is defined by the leading electromagnetic constituent, which in most cases is a photon, as it carries the dominant fraction of the strip energy and therefore provides the most reliable directional estimate. The photon direction is reconstructed by extrapolating the associated ECAL clusters back to the PV, and the invariant mass of the strip is fixed to the known neutral pion mass. The τ_h candidates are then formed by combining these neutral pion strips with one or three charged hadrons within the jet, yielding decay mode hypotheses corresponding to the dominant τ_h decay channels.

Based on the reconstructed charged-particle and strip multiplicities, τ_h candidates are categorised into specific decay modes, including the 1-prong, 1-prong+1-strip, 3-prong, and 3-prong+1-strip topologies. These categories correspond to the most prevalent τ_h decay modes and are used throughout the analysis. To suppress backgrounds from quark- and gluon-initiated jets, as well as from electrons and muons misidentified as τ_h, the DEEPTAU v2.5 algorithm is employed. This deep neural network combines information from individual PF candidates in the vicinity of the τ_h axis with the global properties of the τ_h candidate and the event. The combined HPS and DEEPTAU v2.5 reconstruction achieves an efficiency of approximately 45% for genuine τ_h candidates with $p_T > 20\,\text{GeV}$, while reducing the jet misidentification probability to the level of $\mathcal{O}(10^{-3})$ [24, 25].

5 Event selection

In both channels, events with a pair of oppositely charged τ lepton candidates are selected. Events are required to pass the selection imposed by the CMS trigger system. In the $\tau_\mu\tau_h$ channel, events are selected using both a single-muon trigger and a cross trigger. The cross trigger is specifically designed to identify events containing a muon in association with a τ_h candidate [61]. In the $\tau_h\tau_h$ channel, a combination of a di-τ_h trigger, a di-τ_h plus jet trigger, and a single-τ_h trigger is employed. The thresholds applied during data acquisition (online) and those used in the subsequent event selection (offline) are set such that the selected events lie on the efficiency plateau of the trigger turn-on curve. The trigger configuration and thresholds remained unchanged throughout the full 2022–2023 data-taking period [61]. The trigger and analysis selection thresholds for each channel are summarised in Table 1.

In both channels, a pair of oppositely charged τ leptons with a separation of $\Delta R > 0.5$ is required, where $\Delta R = \sqrt{(\Delta\eta)^2 + (\Delta\phi)^2}$ is the distance in the η–ϕ plane between the two candidates. Each offline-reconstructed object must be geometrically matched to the corresponding trigger object within $\Delta R < 0.5$. A veto on events containing additional loosely identified electrons or muons is applied in both channels to suppress contributions from processes with higher lepton multiplicities. Here, loosely identified electrons and muons refer to objects pass-

Table 1: Online trigger and offline selection requirements applied in the $\tau_\mu\tau_h$ and $\tau_h\tau_h$ channels. All p_T values are given in GeV. Online trigger thresholds are indicated in parentheses.

Channel	Trigger	p_T [GeV]	$\lvert\eta\rvert$
$\tau_h\tau_h$	di-τ_h	$p_T^{\tau_h} > 40\ (35)$, $p_T^{\tau_h} > 40\ (35)$	< 2.1
	di-τ_h +jet	$p_T^{\tau_h} > 35\ (30)$, $p_T^{\tau_h} > 35\ (30)$, $p_T^{\text{jet}} > 60\ (60)$	< 2.1
	single-τ_h	$p_T^{\tau_h} > 190\ (180)$	< 2.1
$\tau_\mu\tau_h$	single-μ	$p_T^{\mu} > 26\ (24)$	$\lvert\eta_\mu\rvert < 2.4$
	μ-τ_h cross trigger	$21\ (20) < p_T^{\mu} < 26$, $p_T^{\tau_h} > 32\ (27)$	$\lvert\eta_\mu\rvert < 2.1$, $\lvert\eta_{\tau_h}\rvert < 2.1$

ing minimal preselection criteria: $p_T > 10\,\text{GeV}$ and $|\eta| < 2.5$ for electrons (with a loose identification requirement [31]), and $p_T > 10\,\text{GeV}$ and $|\eta| < 2.4$ for muons (with a loose isolation requirement [32]). When multiple τ lepton pair candidates are present in an event, candidates of each object type entering the pair are first ranked independently by decreasing isolation, using p_T as a tie-breaker; for τ_h candidates, the raw DEEPTAU D_{jet} score is used as the ranking discriminant. All combinations satisfying the pair-level requirements described above are then formed from these ranked candidate collections, and the highest-ranked pair is retained.

5.1 The $\tau_h\tau_h$ channel

Both τ_h candidates are required to be reconstructed in one of the decay modes described in Section 4, and to satisfy the kinematic and identification criteria summarised in Table 2. A minimum visible mass of $m_{\text{vis}} > 40\,\text{GeV}$, defined as the invariant mass of the visible decay products of the lepton pair, is required for the $\tau_h\tau_h$ pair. To suppress backgrounds from quark- and gluon-initiated jets, electrons, and muons misidentified as τ_h candidates, both τ_h candidates are required to pass the DEEPTAU working points also listed in Table 2. There, the labels D_{jet}, D_e, and D_μ denote the DEEPTAU discriminator decisions against jets, electrons, and muons, respectively, with the working point names (e.g. VVLoose, Medium, Tight) corresponding to fixed thresholds on the discriminator score, as defined in Ref. [24].

5.2 The $\tau_\mu\tau_h$ channel

The muon is required to satisfy a relative isolation $I_{\text{rel}} < 0.15$, defined as

$$I_{\text{rel}} = \frac{\sum_{\text{charged}} p_T + \max\left(\sum_{\text{neutral}} E_T + \sum_\gamma E_T - \Delta\beta \sum_{\text{charged,PU}} p_T,\ 0\right)}{p_T^\mu}, \tag{1}$$

where the sums run over photons, charged and neutral hadrons within a cone of $\Delta R = 0.4$ around the muon direction. Pileup contributions are corrected for using the $\Delta\beta$ method [32], in which the neutral pileup component is estimated as $\Delta\beta = 0.5$ times the scalar p_T sum of charged pileup particles within the isolation cone, reflecting the assumed 2:1 ratio of charged to neutral pileup activity. A minimum visible mass of $m_{\text{vis}} > 40\,\text{GeV}$ is also required for the $\tau_\mu\tau_h$ pair. The τ_h candidate must satisfy the DEEPTAU working points summarised in Table 2. The selection requirements for both objects are summarised in Table 2.

To suppress the otherwise large W + jets background, the transverse mass (m_T) of the muon-

$\vec{p}_{\mathrm{T}}^{\,\mathrm{miss}}$ system is required to satisfy $m_{\mathrm{T}} < 65\,\mathrm{GeV}$, where m_{T} is defined as

$$m_{\mathrm{T}} \equiv \sqrt{2\, p_{\mathrm{T}}^{\mu}\, p_{\mathrm{T}}^{\mathrm{miss}}\, [1 - \cos(\Delta\phi)]}, \tag{2}$$

where $\Delta\phi$ is the azimuthal angle between the muon momentum direction and $\vec{p}_{\mathrm{T}}^{\,\mathrm{miss}}$.

The longitudinal and transverse impact parameters of the muon are required to satisfy $|d_z| < 0.2\,\mathrm{cm}$ and $|d_{xy}| < 0.045\,\mathrm{cm}$, consistent with the muon originating from the PV. For the τ_{h} candidate, only the requirement $|d_z| < 0.2\,\mathrm{cm}$ is imposed, in order to avoid a significant loss in the selection efficiency due to a relatively long τ lepton lifetime.

Table 2: Offline selection requirements in the $\tau_{\mathrm{h}}\tau_{\mathrm{h}}$ and $\tau_{\mu}\tau_{\mathrm{h}}$ channels. A dash indicates that the requirement is not applied in that channel.

Variable	$\tau_{\mathrm{h}}\tau_{\mathrm{h}}$	$\tau_{\mu}\tau_{\mathrm{h}}$
Muon p_{T}	—	$>26\,\mathrm{GeV}$
Muon $\lvert\eta\rvert$	—	<2.4
Muon isolation I_{rel}	—	<0.15
Muon $\lvert d_{xy}\rvert$	—	$<0.045\,\mathrm{cm}$
Muon $\lvert d_z\rvert$	—	$<0.2\,\mathrm{cm}$
τ_{h} p_{T}	$>35\,\mathrm{GeV}$	$>32\,\mathrm{GeV}$
τ_{h} $\lvert\eta\rvert$	<2.1	<2.1
τ_{h} $\lvert d_z\rvert$	$<0.2\,\mathrm{cm}$	$<0.2\,\mathrm{cm}$
DEEPTAU D_{jet}	Medium	Medium
DEEPTAU D_{e}	VVLoose	VVLoose
DEEPTAU D_{μ}	Tight	Tight
Pair m_{vis}	$>40\,\mathrm{GeV}$	$>40\,\mathrm{GeV}$
Pair m_{T}	—	$<65\,\mathrm{GeV}$

6 The MUFFIN method

6.1 Conceptual overview of MUFFIN

The F_{F} method [12] estimates the contribution of backgrounds due to quark- or gluon-initiated jets misidentified as τ_{h} decays using TFs defined as

$$F_{\mathrm{F}}(\mathbf{x}) = \frac{N_{\mathrm{pass}}(\mathbf{x})}{N_{\mathrm{fail}}(\mathbf{x})}, \tag{3}$$

where N_{pass} and N_{fail} denote the number of τ_{h} candidates passing and failing the nominal τ_{h} identification requirements, respectively, measured in DRs as functions of a limited set of kinematic variables $\mathbf{x}$. These TFs are applied to events in the ARs to predict the misidentified background in the SRs.

The MUFFIN method generalises this approach with multidimensional per-object reweighting. A BDT is trained in background-enriched DRs to distinguish failing (fail D_{jet} Medium but

pass VVVLoose DEEPTAU working point) from passing (pass D_{jet} Medium DEEPTAU working point) τ_{h} candidates. The calibrated outputs of the BDT are interpreted as class probabilities (see Section 6.6), which are then used to construct continuous TFs in the full feature space.

After calibration, the model outputs $P_{\text{pass}}(\mathbf{z})$ and $P_{\text{fail}}(\mathbf{z})$ for input features $\mathbf{z}$. Their ratio,

$$w_{\text{MUFFIN}}(\mathbf{z}) \equiv \frac{P_{\text{pass}}(\mathbf{z})}{P_{\text{fail}}(\mathbf{z})}, \tag{4}$$

plays the role of a continuous multidimensional TF, replacing binned $F_{\text{F}}(\mathbf{x})$. The precise definition of P_{pass} and P_{fail} from the calibrated four-class BDT outputs is given in Section 6.6; the BDT is trained separately for each analysis channel and background process, as described in Sections 6.2–6.6. The DRs in Fig. 1 define where this mapping is learned, and the resulting per-object weights are applied in SR-like regions to predict the jet $\rightarrow \tau_{\text{h}}$ background. Dedicated validation regions (VRs), orthogonal to the DRs and SRs, are used to assess the modelling performance of the method. Figure 1 illustrates the region definitions and their role in the method for both the $\tau_{\text{h}}\tau_{\text{h}}$ channel and, generically, semileptonic $\tau_{\ell}\tau_{\text{h}}$ channels (ℓ = electron or muon), although only the $\tau_{\mu}\tau_{\text{h}}$ channel is shown in this paper.

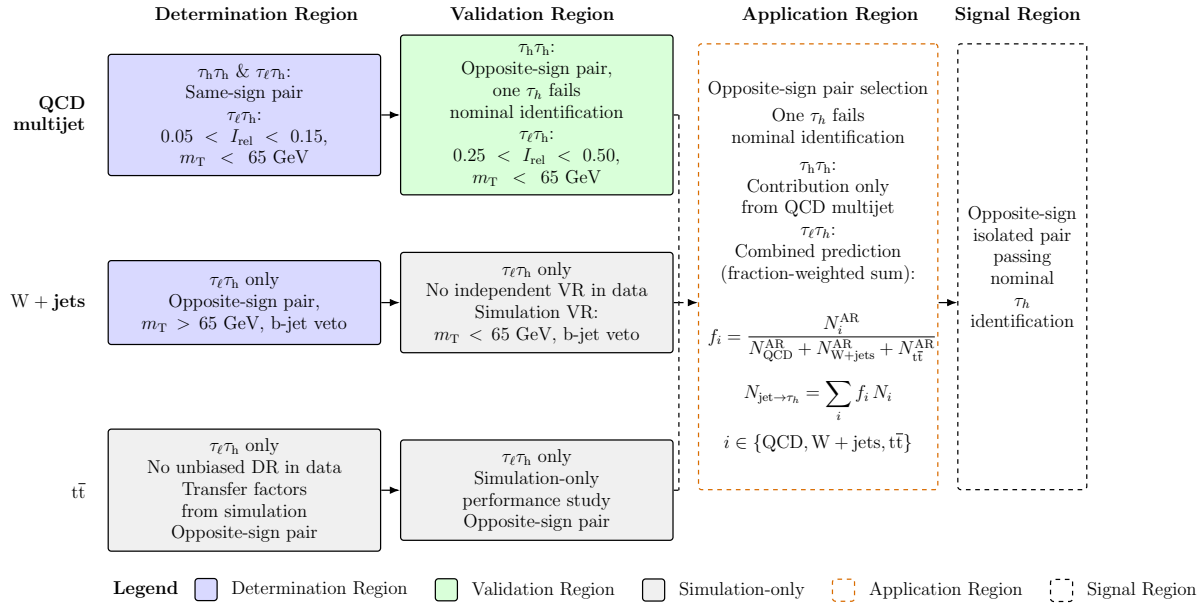

Figure 1: Schematic overview of the DRs, VRs, AR, and SR used in the estimation of the jet $\rightarrow \tau_{\text{h}}$ backgrounds. For each process, TFs are derived in dedicated DRs enriched in jets misidentified as τ_{h} candidates. The performance of the method is assessed in VRs, where available, or through simulation-based studies in cases without an unbiased DR. The prediction is then applied in a common AR, defined by opposite-sign events with one τ_{h} candidate failing the nominal identification requirement. In the $\tau_{\text{h}}\tau_{\text{h}}$ channel, the AR is dominated by QCD multijet events, while in the $\tau_{\mu}\tau_{\text{h}}$ channel a combined prediction is constructed from QCD multijet, W + jets, and $\text{t}\bar{\text{t}}$ contributions using relative fractions derived in the AR. The final estimate is obtained in the SR, defined by opposite-sign isolated events passing the nominal τ_{h} identification requirements.

6.2 Construction of determination and application regions

The TFs are measured separately for each dominant source of jets misidentified as τ_{h} leptons: QCD multijet, W + jets, and $\text{t}\bar{\text{t}}$ production in the $\tau_{\mu}\tau_{\text{h}}$ channel, and QCD multijet production

in the $\tau_h\tau_h$ channel. For each process and channel, dedicated DRs are defined to enrich the corresponding background contribution while suppressing processes with genuine τ leptons. Where appropriate, orthogonal VRs are constructed to assess the modelling performance of the method. In all cases, the DRs are defined by requiring one τ_h candidate to fail the nominal identification criterion, while passing a looser τ_h identification working point (D_{jet} VVVLoose), as defined in Ref. [24]. Additional selections on charge sign requirements, lepton isolation, m_T, and b-tagged jet multiplicity are applied to enhance the purity of the targeted background process. The DRs and ARs are common to both the F_F and MUFFIN methods. The final background estimate in each channel is then obtained by combining the weighted contributions from the relevant sources of misidentified τ_h candidates. A schematic overview of the region definitions and their role in the method is shown in Fig. 1. The resulting background estimate from the MUFFIN method in a signal-like region of phase space is discussed in Section 9.1.

For the estimation of the QCD multijet background, same-sign charge requirements are used in all channels to suppress electroweak and top quark processes, which are predominantly opposite-sign. In the $\tau_\mu\tau_h$ channel, the nominal muon isolation requirement ($I_{rel} < 0.15$) and m_T selection ($m_T < 65\,\text{GeV}$) are retained to ensure the DR remains kinematically representative of the SR, while the same-sign requirement provides the primary QCD multijet enrichment by suppressing $W + \text{jets}$ and $Z/\gamma^* + \text{jets}$ contributions. In the $\tau_h\tau_h$ channel, a VR is defined by requiring one of the τ_h candidates to fail the nominal τ_h identification requirement while passing a looser working point, and by requiring the two τ_h candidates to have opposite signs. In the $\tau_\mu\tau_h$ channel the VR is defined by modifying the muon isolation requirement ($0.25 < I_{rel} < 0.5$). These VRs provide independent samples for testing the performance of the method, while maintaining a high purity of the targeted background process.

The $W + \text{jets}$ DR is defined in the $\tau_\mu\tau_h$ channel by requiring opposite-sign events with $m_T > 65\,\text{GeV}$. To suppress contamination from $t\bar{t}$ events, a veto on b-tagged jets is applied. As the inversion of the large m_T requirement would lead to overlap with the SR, no independent VR is defined for this background; instead, the performance is assessed using a dedicated simulation-only training and validation procedure. To this end, MUFFIN is trained on simulated $W + \text{jets}$ events using the same DR selections as for the data (i.e. $m_T > 65\,\text{GeV}$) and this is validated by applying the methods to simulated events with $m_T < 65\,\text{GeV}$. Likewise, the F_F method derives the TFs in high-m_T events and applies them in low-m_T events.

The $t\bar{t}$ TFs are measured from simulated events. This is necessary as it is not possible to define a DR in data that is sufficiently pure in $t\bar{t}$ jet $\to \tau_h$ events without applying selections that bias the measured TFs. In particular, selections that substantially enhance the $t\bar{t}$ purity (e.g. requirements on b-tagged jets and/or specific lepton flavour configurations) can modify the flavour composition and kinematics of the jets that are misidentified as τ_h candidates, thereby distorting the jet $\to \tau_h$ misidentification probability. As a result, the performance of the method for $t\bar{t}$ is assessed using simulation-only studies, where the true composition of the sample is known and the impact of the method can be reliably evaluated. The uncertainty model for the $t\bar{t}$ background estimation is designed to account for potential mismodelling of the $t\bar{t}$ jet $\to \tau_h$ TFs in simulation.

6.3 Training inputs

The data are split into independent training (70%) and evaluation (30%) samples to ensure stable training and unbiased performance evaluation. The VR, defined in Section 6.2, serves as a fully blind test set, as it is a separate physics region whose data never enters the training or hyperparameter optimisation. The training is performed separately for each analysis channel and

background process to capture channel-specific kinematic properties and event topologies. For each targeted process, the training is performed on data events in the corresponding DR. However, the data sample contains small contributions ($\mathcal{O}(1\%)$) from other background processes with genuine τ_h candidates (e.g. $t\bar{t}$, $Z/\gamma^* + \text{jets}$). To isolate the jet $\rightarrow \tau_h$ misidentification TF, these genuine τ_h contributions enter the training as a source of contamination that is subtracted from the data components in the final weight definition (Section 6.6). Crucially, no simulation of the targeted jet $\rightarrow \tau_h$ process itself is used at any stage: e.g. when deriving the $W + \text{jets}$ TFs, no $W + \text{jets}$ simulation enters either the training or the subtraction, ensuring that the method is entirely data-driven for the targeted jet $\rightarrow \tau_h$ component. For dedicated simulation-only studies, a binary setup with two classes (pass and fail) is used.

The input feature set is chosen to capture both object-level properties of the τ_h candidate and aspects of the global event environment that influence the jet $\rightarrow \tau_h$ misidentification probability. Local variables include the reconstructed decay mode of the τ_h candidate (the specific decay channel of the τ_h as determined by the HPS algorithm), its p_T, η, and azimuthal angle ϕ, as well as the ratio of the p_T of the jet from which the τ_h candidate is reconstructed to that of the τ_h candidate. This ratio provides sensitivity to differences in energy sharing between the reconstructed τ_h decay products and the other jet constituents. In genuine τ_h decays, the visible decay products typically carry a large fraction of the momentum of the original τ lepton and are more collimated, leading to a reconstructed τ_h candidate whose p_T closely matches that of the associated jet. In contrast, jets misidentified as τ_h candidates often arise from broader hadronic activity, where only a subset of the jet constituents is selected by the τ_h reconstruction algorithm. As a result, the p_T of the reconstructed τ_h candidate tends to represent a smaller and more variable fraction of the full jet momentum, making this ratio a powerful discriminant between the two cases.

In addition to local quantities, a small number of global event-level variables are included in the training. These variables, such as the total number of reconstructed jets and the number of b-tagged jets in the event, encode information about the overall hadronic activity and event topology. Although they are not directly associated with the τ_h candidate, they can impact the composition and kinematic properties of the jet $\rightarrow \tau_h$ background and therefore improve the modelling of the misidentification rate. This is not dissimilar to how, in the F_F method, similar variables are used to define separate F_F parametrisations in different analysis categories. Lastly, an explicit data-taking period label is included as an input feature to account for potential variations in detector conditions and performance across different data-taking periods. The relative importance of the input variables, as determined by feature importance studies, can be ranked as follows:

1. Decay mode of the τ_h candidate (most important);
2. Ratio of jet p_T to τ_h p_T;
3. The p_T of the τ_h candidate;
4. Total number of reconstructed jets in the event;
5. Number of b-tagged jets in the event;
6. The η of the τ_h candidate;
7. The ϕ of the τ_h candidate;
8. An explicit data-taking period label (subdominant but non-negligible).

Feature importance is evaluated using the built-in XGBOOST [62] metrics "weight", "gain", and "cover", which respectively quantify the number of times a feature is used to split the data, the average improvement in accuracy brought by a feature, and the relative coverage of samples affected by a feature. These metrics are extracted from the trained BDT and visualised to assess the contribution of each input variable. These studies help to validate the choice of input features and provide insights into the physical properties that govern the jet $\rightarrow \tau_{\mathrm{h}}$ misidentification rates. Across all channels and processes, the BDT models consistently identify the decay mode and jet-to-τ_{h} kinematics such as the ratio of jet p_{T} to τ_{h} p_{T} as the most important features. Angular variables and event-level quantities are found to have a secondary but non-negligible impact, highlighting the benefit of including global event information in the training. Another important conclusion from these studies is that the relative importance of the explicit data-taking period label (as an input feature) is found to be non-negligible but subdominant compared to the main kinematic features, indicating that while there are some differences in the detector performance across data-taking periods that can lead to heightened/reduced misidentification rates, the core physics properties driving the misidentification rates remain consistent.

6.4 The BDT architecture

The ML models used for the reweighting are based on BDT classifiers implemented using the XGBOOST framework. The model architecture and training hyperparameters are optimised using the OPTUNA toolkit [63], which performs an automated search of the hyperparameter space using a Bayesian optimisation strategy [64]. The objective of the optimisation is to minimise the loss evaluated on an independent evaluation data set, thereby ensuring good generalisation performance and stable behaviour across the phase space relevant to the analysis.

The hyperparameter search includes variations of the maximum tree depth, the learning rate, the fraction of events and features used at each boosting iteration, and regularisation parameters controlling the complexity of the model. In particular, parameters governing tree depth and minimum node population are used to limit overfitting, while regularisation terms are introduced to penalise overly complex decision boundaries: a sparsity penalty that encourages the model to rely on fewer features per tree, and a weight-decay penalty that prevents individual node weights from becoming too large. This choice of hyperparameters allows the model to capture non-linear dependencies between input variables, while maintaining robustness against statistical fluctuations in the training data.

For each optimisation trial, a BDT model is trained with a maximum number of boosting iterations of 1000, and early stopping is employed based on the evaluation loss to determine the optimal number of trees. Training stops when the evaluation loss fails to improve by more than 0.1% in absolute value for 10 consecutive boosting iterations. The optimisation is performed over a fixed number of trials ($N = 50$), after which the hyperparameter configuration yielding the best evaluation performance is selected for the final training. This procedure, illustrated in Fig. 2, provides a reproducible and data-driven approach to selecting the model architecture, reducing sensitivity to manual tuning and ensuring consistent performance across analysis channels and data-taking periods.

6.5 Training performance

The performance and stability of the BDT training are evaluated using independent training and evaluation data sets. The evolution of the loss function as a function of the boosting iteration is monitored to assess convergence and to identify potential overtraining. The training

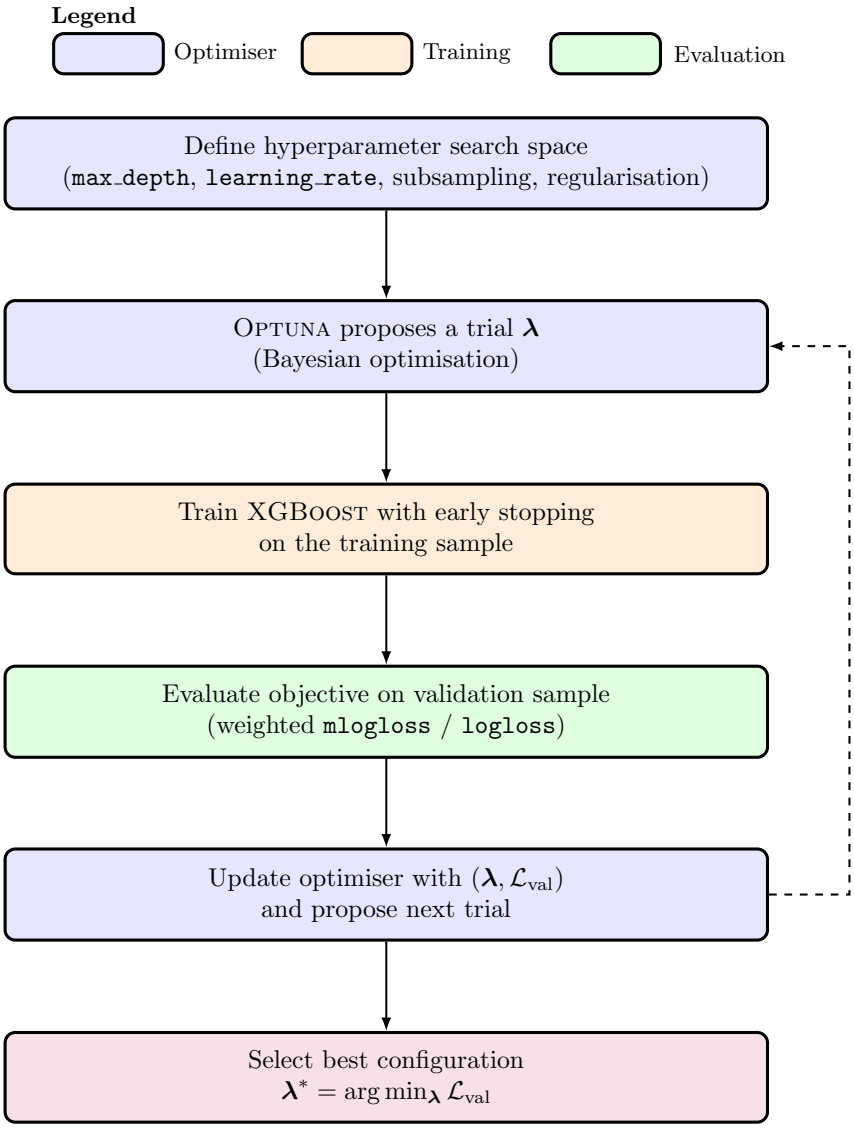

Figure 2: Schematic overview of the hyperparameter optimisation procedure used to configure the BDT models. For each trial, OPTUNA proposes a hyperparameter set, the model is trained with early stopping, and the evaluation loss is used as the optimisation objective.

minimises the cross-entropy loss,

$$\mathcal{L} = -\frac{1}{N}\sum_{i=1}^{N}\sum_{k=1}^{K} y_{ik}\log \hat{p}_{ik}, \tag{5}$$

where $y_{ik} \in \{0,1\}$ is the true-class indicator ($y_{ik} = 1$ if candidate i belongs to class k, and $y_{ik} = 0$ otherwise), $\hat{p}_{ik}$ is the corresponding predicted class probability, and K is the number of classes. In the nominal subtraction-based training, $K = 4$ (data pass, data fail, simulation pass, and simulation fail). In dedicated simulation-only studies, a binary setup with $K = 2$ is used. The initial loss therefore differs between configurations: $\ln 4 \approx 1.386$ for the four-class channels and $\ln 2 \approx 0.693$ for the binary simulation-only channels, explaining the lower starting loss observed for the simulation-based W + jets and $t\bar{t}$ models. The simulation-based W + jets model requires more boosting iterations to converge, reflecting the greater complexity of the learned TF for this process. In all channels, the training and evaluation losses are observed to decrease smoothly and to stabilise at similar values, indicating good generalisation performance.

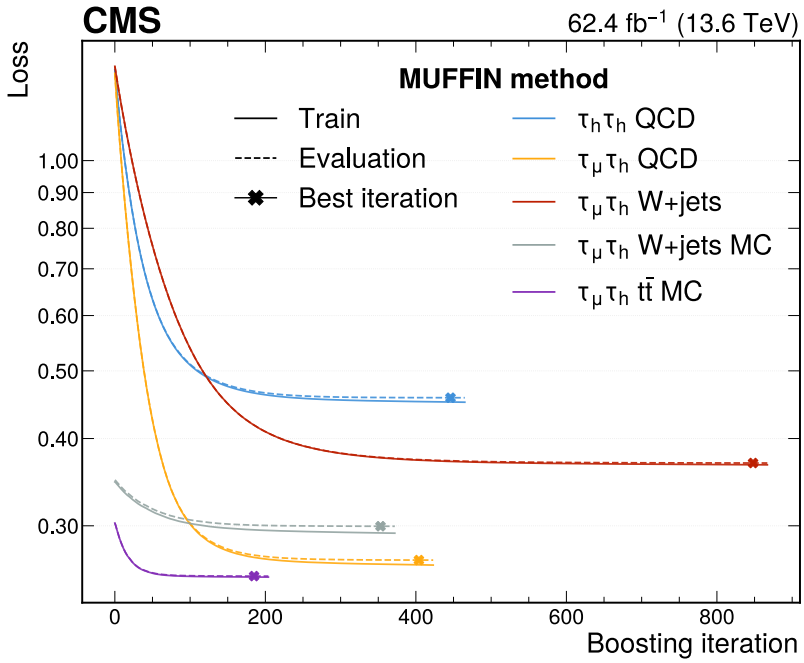

Figure 3: Cross-entropy loss (Eq. (5)) versus boosting iteration for all BDT models in the $\tau_h\tau_h$ and $\tau_\mu\tau_h$ channels, with the loss axis shown on a logarithmic scale. Solid (dashed) lines correspond to the training (evaluation) loss. Cross markers indicate the best (saved) iteration; curves extend up to 10 iterations beyond this point, corresponding to the early stopping window. The lower initial loss of the simulation-only (W + jets, $t\bar{t}$) models reflects the binary ($K = 2$) classifier setup ($\ln 2 \approx 0.693$) compared to the four-class ($K = 4$) data channels ($\ln 4 \approx 1.386$).

Figure 3 shows representative loss curves for all channels and processes. The cross marker indicates the best iteration, at which the model is saved; the loss curves extend up to 10 iterations beyond this point, corresponding to the early stopping window over which no improvement exceeding 0.1% was observed. A small gap between training and evaluation loss is expected, as the model has seen the training data. Overfitting would manifest as a rising evaluation loss while the training loss continues to fall. The absence of such divergence confirms that the model is not overfitting to statistical fluctuations in the training data, and that it is learning meaningful patterns that generalise well to unseen data. This behaviour is consistent across all

channels and background processes, demonstrating the robustness of the training procedure and the suitability of the chosen hyperparameters for capturing the relevant features of the jet $\rightarrow \tau_h$ misidentification background.

6.6 Calibration of BDT outputs

The BDT output scores are subsequently used to derive per-object weights for the jet $\rightarrow \tau_h$ background. For this purpose, it is important that the classifier output can be interpreted as a well-calibrated probability, such that the predicted score is consistent with the empirical class frequency observed in the evaluation sample. Calibration in this sense is a purely empirical requirement: it does not require prior knowledge of the true class proportions, but rather ensures that a predicted confidence of p corresponds to an observed frequency of p in the held-out data. A post-training calibration of the BDT outputs is therefore performed using temperature scaling [65, 66]. In this approach, the logits $\mathbf{z}$ of the trained classifier are divided by a single global temperature parameter T^*, yielding calibrated class probabilities $\text{softmax}(\mathbf{z}/T^*)$. The optimal T^* is determined by minimising the cross-entropy loss of Eq. (5) on the independent 30% held-out evaluation sample, ensuring the calibration is unbiased with respect to the training. This procedure preserves the ordering of classifier scores and does not alter the decision boundaries of the model, while correcting potential mismatches between predicted probabilities and observed frequencies.

The calibration performance is assessed using reliability diagrams, which verify that the predicted class probability (confidence) matches the empirical fraction of correctly classified events (accuracy) in bins of the classifier output. For a well-calibrated classifier, a predicted confidence of p should correspond to an observed accuracy of p, lying along the diagonal. Here, the confidence is defined as the maximum predicted class probability for each event, while the accuracy corresponds to the event-weight-averaged fraction of correctly classified events within a given confidence bin. Uncertainties on the accuracy are estimated using Wilson score 68% confidence intervals, with the effective sample size $n_{\text{eff}} = (\sum_i w_i)^2 / \sum_i w_i^2$ accounting for the non-uniform event weights.

For the QCD multijet BDT in the $\tau_h\tau_h$ channel, the optimal temperature parameter is found to be $T^* = 0.999 \approx 1$, meaning the BDT outputs require negligible rescaling and are already well-calibrated class probabilities. This confirms the stability of the training and that the BDT class probabilities are directly suitable for use in the weight formula introduced below. Figure 4 shows the reliability diagram after calibration for the QCD multijet BDT in the $\tau_h\tau_h$ channel. Similar behaviour is observed across other channels and background processes ($T^* \in [0.990, 1.001]$). Given the small magnitude of the calibration correction in all cases, temperature scaling is primarily employed as a validation step to ensure probabilistic interpretability of the classifier output, rather than as a substantial modification of the model predictions.

The calibrated BDT output scores are then used to derive per-object weights for the background reweighting, following the same logic as the F_F method. The weights are defined as

$$w_{\text{MUFFIN}}(\mathbf{z}) = \frac{P^{\text{data}}_{\text{pass}}(\mathbf{z}) - P^{\tau_{\text{sim}}}_{\text{pass}}(\mathbf{z})}{P^{\text{data}}_{\text{fail}}(\mathbf{z}) - P^{\tau_{\text{sim}}}_{\text{fail}}(\mathbf{z})}. \tag{6}$$

Here, the calibrated BDT output provides four class probabilities for a given set of input features $\mathbf{z}$: $P^{\text{data}}_{\text{pass}}$ and $P^{\text{data}}_{\text{fail}}$ are the probabilities for an object in data to pass or fail the τ_h identification, containing contributions from both genuine τ leptons and jet $\rightarrow \tau_h$; $P^{\tau_{\text{sim}}}_{\text{pass}}$ and $P^{\tau_{\text{sim}}}_{\text{fail}}$ are the corresponding probabilities for simulated genuine τ leptons only. The subtraction of

the genuine τ simulation contributions serves to remove any residual genuine τ contamination in the DRs, ensuring that the weights capture only the jet $\rightarrow \tau_h$ misidentification rates. Importantly, no simulation of the targeted jet $\rightarrow \tau_h$ process itself (e.g. QCD, W + jets, or $t\bar{t}$ when treated as the target) is used in this subtraction, preserving the fully data-driven nature of the method. This explicit use of the BDT output probabilities is a key feature of the ML-based method, enabling a continuous, multidimensional reweighting that generalises the F_F method. In the simulation-only configurations for $t\bar{t}$ and W + jets, the data class probabilities are set to zero, ($P^{data}_{pass}(\mathbf{z}) = P^{data}_{fail}(\mathbf{z}) = 0$), so the subtraction-based expression simplifies to the ratio of the genuine τ simulation probabilities. Since w_{MUFFIN} depends on the ratio of class probabilities, any dependence on the class proportions π_k assumed during training enters only as a global multiplicative constant, leaving the shape of the weight function invariant to assumptions about these proportions. The overall normalisation of the background estimate is independently constrained by the observed data yield in the AR, ensuring robustness with respect to the training class balance.

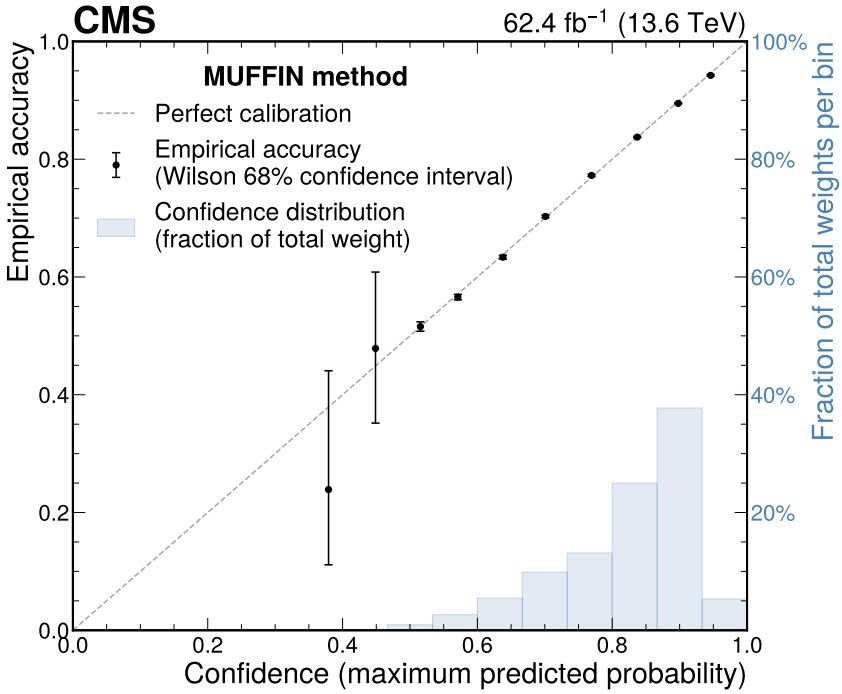

Figure 4: Reliability diagram for the QCD multijet BDT in the $\tau_h\tau_h$ channel after temperature scaling ($T^* = 0.999$), shown on the evaluation data set. Each point is placed at the weighted mean confidence of events in the bin (not the geometric bin centre) and shows the event-weight-averaged fraction of correctly classified events (accuracy), with Wilson score 68% confidence intervals using the effective sample size $n_{eff} = (\sum_i w_i)^2 / \sum_i w_i^2$. The dashed diagonal indicates perfect calibration. The shaded histogram (right axis) shows the weighted confidence-score distribution. The model is well calibrated across the full range, with most events (>30% per bin) at high confidence (>0.8); the larger uncertainties at low confidence reflect the correspondingly small event counts there.

In the limit of reduced input dimensionality, this approach naturally converges to the F_F method. The incorporation of ML techniques enables a more flexible multidimensional reweighting that captures correlations between input variables that are not explicitly modelled in the F_F method. Owing to their per-object definition and evaluation in a high-dimensional feature space, the BDT-derived weights can be applied consistently across different analysis categories and regions of phase space. This reduces the reliance on additional corrections and uncertainties that

account for missing variable dependencies, and simplifies the overall background estimation workflow.

7 Performance comparison

The performance of the MUFFIN method is benchmarked directly against the F_{F} method using a series of closure tests performed in the respective VRs for each process. These regions are designed to be kinematically similar to the SRs while remaining orthogonal to the regions used for the derivation of the background estimates, thereby providing an unbiased assessment of the predictive power of each method. In the $\tau_\mu\tau_{\mathrm{h}}$ channel the performance is also assessed in a dedicated simulation-only validation procedure for the W + jets background, as described in Section 6.

For each method, the predicted distribution of jet $\to \tau_{\mathrm{h}}$ background events is compared to the data in the VRs for a range of key observables. The level of agreement is quantified by the mean absolute per-bin Poisson pull, $\langle|z|\rangle$ [67, 68], where lower values indicate improved agreement and larger values signal worse residual mismodelling. The metric is defined as:

$$\langle|z|\rangle = \frac{1}{N}\sum_{i=1}^{N}|z_i|, \qquad z_i = \frac{N_i^{\mathrm{obs}} - N_i^{\mathrm{pred}}}{\sqrt{N_i^{\mathrm{pred}}}}, \tag{7}$$

where N_i^{obs} and N_i^{pred} are the observed and predicted yields in bin i, N is the total number of bins, and z_i is the per-bin Poisson pull. The metric has no free parameters, and its denominator is independent of the degree of closure, ensuring that methods with worse agreement are not artificially favoured.

The set of observables considered is representative of the kinematic and topological quantities commonly used in analyses involving τ_{h} decays. These variables probe both the overall event kinematics and the properties of the reconstructed τ_{h} candidates, and are therefore sensitive to potential mismodelling of the jet $\to \tau_{\mathrm{h}}$ background. The distributions examined include the total transverse mass [12, 69],

$$m_{\mathrm{T}}^{\mathrm{total}} = \sqrt{m_{\mathrm{T}}^2(\tau_1,\tau_2) + m_{\mathrm{T}}^2(\tau_1,\vec{p}_{\mathrm{T}}^{\,\mathrm{miss}}) + m_{\mathrm{T}}^2(\tau_2,\vec{p}_{\mathrm{T}}^{\,\mathrm{miss}})}, \tag{8}$$

where τ_1 and τ_2 denote the two τ lepton candidates, $\vec{p}_{\mathrm{T}}^{\,\mathrm{miss}}$ is the missing transverse momentum vector, and $m_{\mathrm{T}}(a,b)$ is the pairwise transverse mass defined in Eq. (2), and the visible invariant mass m_{vis}, both of which are key discriminating variables in measurements and searches and are particularly sensitive to mismodelling of the jet $\to \tau_{\mathrm{h}}$ background. Kinematic properties of the reconstructed τ_{h} candidates are also probed through their p_{T} and η, as well as the angular separation between the decay products, quantified by ΔR. These variables test the modelling of both the object-level properties of the τ_{h} candidates and their correlations with the surrounding event topology. Finally, the reconstructed decay mode of the τ_{h} candidates is examined to validate the modelling across different τ_{h} topologies. Together, this set of observables provides a broad test of the background estimation performance across the kinematic and topological phase space relevant for physics analyses, ensuring that improvements observed in closure tests translate into robust modelling in SRs.

A notable limitation of the reference F_{F} method is its treatment of observables not directly used in the derivation of the TFs, such as the τ_{h} η and decay mode. In practice, the F_{F} TFs are derived as averages over observables such as η and decay mode, effectively marginalising over

any dependence these variables may have on the jet $\rightarrow \tau_h$ misidentification probability. The choice of variables to average over is often driven by practical considerations, and is dependent on the specific analysis and the available data sample size in the DRs. While this is a pragmatic choice that yields acceptable modelling of the primary fit observables, it introduces a residual mismodelling whenever the distributions of these averaged-over variables differ between the DR and the SR. This condition is generally not guaranteed by the region definitions and can vary across analysis categories. Since these marginalised observables enter downstream discriminants and feed directly into the signal-over-background separation, even small shape differences can translate into increased systematic uncertainties on the background estimate. The MUFFIN method avoids this limitation by learning the full multidimensional dependence of the misidentification probability from data, incorporating η, decay mode, and other correlated observables as continuous inputs to the BDT. This allows the method to implicitly capture the dependence of the jet $\rightarrow \tau_h$ misidentification probability on these variables without requiring explicit binning, and therefore provides improved modelling even for observables that the F_F method cannot efficiently parametrise. The improvement is clearly visible in the closure tests presented below, where pronounced gains relative to the F_F method are consistently observed in the η and decay mode distributions.

7.1 Performance in the $\tau_h\tau_h$ channel

The performance of the MUFFIN method in the $\tau_h\tau_h$ channel is evaluated using the dedicated VR defined following Section 6.2. In this channel, the jet $\rightarrow \tau_h$ background arises primarily from the QCD multijet process, with smaller contributions from $W+$jets and $t\bar{t}$ production. Figures 5 and 6 show representative comparisons between distributions obtained with the MUFFIN and F_F methods for the key observables described above. The ratio panels include the $\langle|z|\rangle$ metric values for each method, allowing a quantitative comparison of their performance.

The MUFFIN method is observed to significantly improve the modelling of all distributions compared to the F_F method. This demonstrates that the MUFFIN method provides improved modelling of the jet $\rightarrow \tau_h$ background in the $\tau_h\tau_h$ channel, supporting its use in physics analyses targeting this final state.

7.2 Performance in the $\tau_\mu\tau_h$ channel

The performance of the MUFFIN method is also evaluated in the $\tau_\mu\tau_h$ channel using dedicated VRs defined following Section 6.2 and simulated $W+$jets and $t\bar{t}$ events. In this channel, the jet $\rightarrow \tau_h$ background modelling is assessed for QCD multijet, $W+$jets, and $t\bar{t}$ production modes in turn.

Figures 7–10 show representative comparisons between distributions obtained with the MUFFIN and F_F methods for the key observables described at the beginning of this section. For brevity, the η and m_{vis} distributions are not shown here, but similar improvements with the MUFFIN method are observed as in the $\tau_h\tau_h$ channel.

Figure 7 shows comparisons between distributions obtained with the MUFFIN and F_F methods in a representative VR for the QCD multijet background. The MUFFIN method provides improved modelling across a wide range of observables, particularly in the ΔR and decay mode distributions, with the remaining observables also showing improved modelling with the MUFFIN method.

Figure 8 shows comparisons between distributions obtained with the MUFFIN and F_F methods in the $W+$jets DR. This contains the same events that are used to train MUFFIN and derive

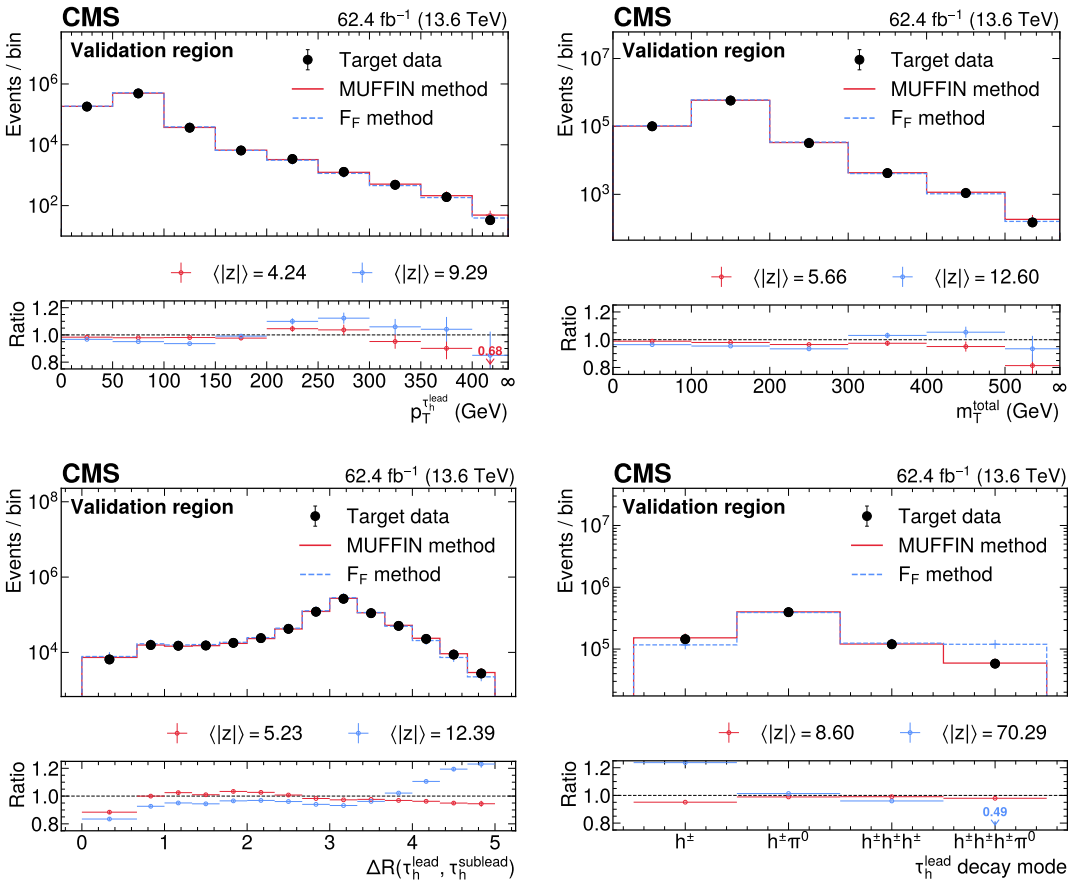

Figure 5: Distributions of representative observables in the $\tau_h\tau_h$ AR comparing the MUFFIN prediction (red) and F_F estimate (blue, dashed) to the target distribution (black markers) for $p_T^{\tau_h}$, m_T^{total}, ΔR, and decay mode. Vertical bars on the points indicate the statistical uncertainty. The ratio panels display the target-to-prediction ratio, with the corresponding $\langle|z|\rangle$ values quoted in each panel. Arrows indicate bins outside the plotted range. Overflow is included in the final bin (∞), where applicable.

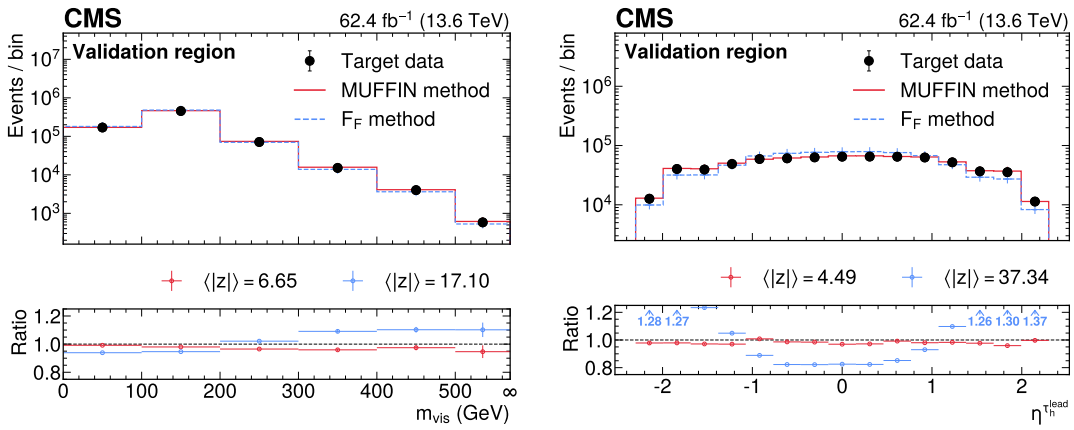

Figure 6: Comparison of the visible mass m_{vis} and η distributions in the same $\tau_{\text{h}}\tau_{\text{h}}$ AR with the MUFFIN (red) and F_{F} (blue, dashed) predictions. Vertical bars on the points indicate the statistical uncertainty. The ratio panels highlight residual deviations and the corresponding $\langle|z|\rangle$ metric values. Arrows indicate bins outside the plotted range. Overflow is included in the final bin (∞), where applicable.

the F_{F} TFs, so good agreement is expected. Nevertheless, the MUFFIN method again provides improved modelling across all observables considered. Figure 9 shows additional comparisons between distributions obtained in a dedicated simulation-only validation procedure for the W + jets background, defined by applying the methods trained in the high-m_{T} DR to simulated events with low m_{T}. The MUFFIN method again demonstrates improved modelling across all observables.

Finally, Fig. 10 shows comparisons between distributions obtained with the MUFFIN and F_{F} methods in simulated $\text{t}\bar{\text{t}}$ events. The MUFFIN method provides improved modelling across all observables considered.

These results demonstrate that the MUFFIN method provides enhanced modelling of the jet $\to \tau_{\text{h}}$ background in the $\tau_{\mu}\tau_{\text{h}}$ channel as well, supporting its broader applicability across different analysis channels. This is particularly evident at the high end of the τ_{h} p_{T} spectrum, where the MUFFIN method better captures the kinematic dependencies of the misidentification rates, leading to improved background estimates in high-p_{T} regions critical for new physics searches, as further demonstrated in Section 9. This resonates with the findings in the $\tau_{\text{h}}\tau_{\text{h}}$ channel, highlighting the robustness and versatility of the MUFFIN method in addressing the challenges associated with jet $\to \tau_{\text{h}}$ background estimation, especially in kinematic regions with limited event yields. A residual shape dependence remains in the ΔR distributions in the $\tau_{\mu}\tau_{\text{h}}$ channel, more pronounced than in the $\tau_{\text{h}}\tau_{\text{h}}$ channel and qualitatively similar to that seen with the F_{F} method. As ΔR is deliberately excluded from the BDT training to serve as an independent closure test (Section 8.2), this points to an additional phase space dependence that could be captured via the addition of a suitable variable to an extended input variable list for the MUFFIN method.

8 Uncertainty model

The uncertainties associated with the MUFFIN method are categorised into statistical and systematic components. The uncertainty model is designed to provide a systematic treatment of the dominant sources of variation affecting the BDT-based reweighting procedure and its ap-

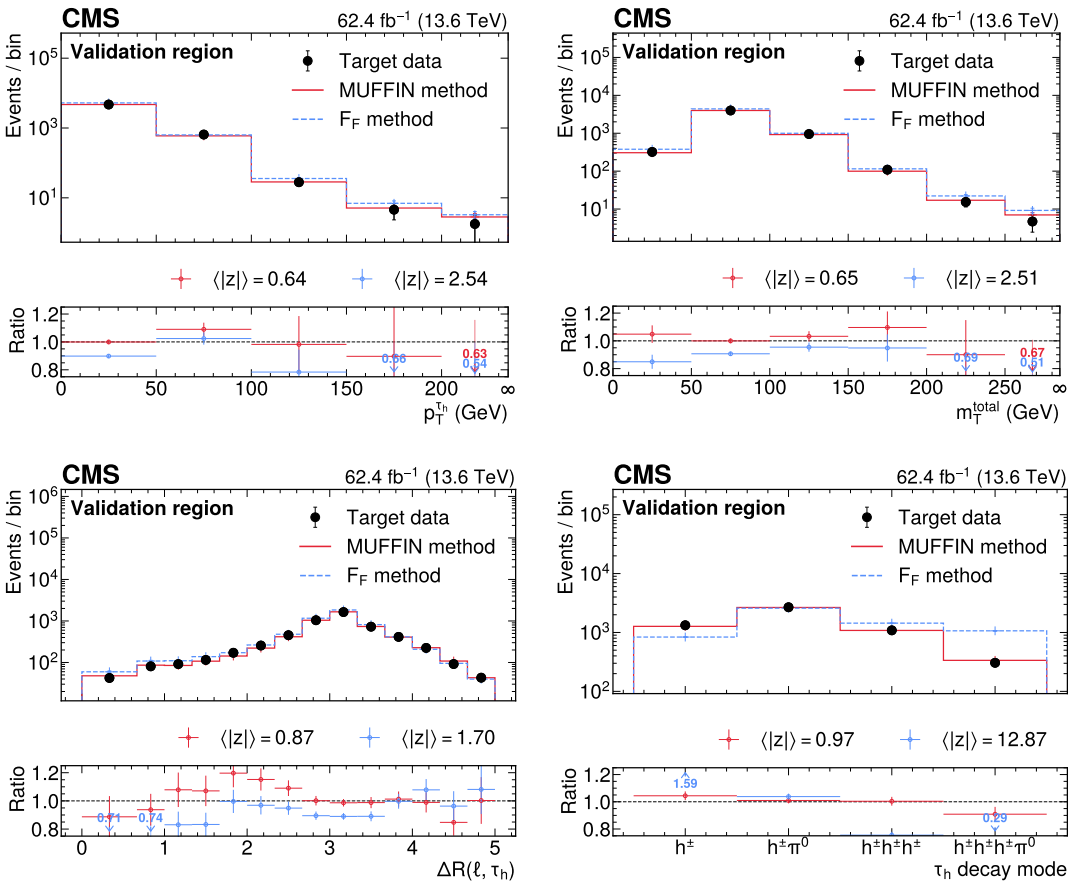

Figure 7: Validation of the QCD multijet background modelling in the $\tau_\mu\tau_h$ VR. Predictions from MUFFIN (red) and F_F (blue, dashed) are compared to data for $p_T^{\tau_h}$, m_T^{total}, ΔR, and τ_h decay mode. Vertical bars on the points indicate the statistical uncertainty. The lower panels show the data-to-prediction ratio, with $\langle|z|\rangle$ values indicating the overall level of agreement. Arrows indicate bins outside the plotted range. Overflow is included in the final bin (∞), where applicable.

plication from determination to analysis phase space.

8.1 Statistical uncertainties

The statistical uncertainty of the MUFFIN method arises primarily from the finite size of the training data set used to derive the BDT reweighting factors. To propagate this uncertainty to the final background prediction, an ensemble approach based on bootstrap resampling is employed. An ensemble of 50 BDT models is trained using independent bootstrapped replicas of the training data. This choice provides a practical balance between computational cost and the stability of the bootstrap-based uncertainty estimate, for which further increases in the number of replicas were found to have only a small impact on the resulting uncertainty. For each model, the full reweighting procedure is applied, yielding a set of alternative predictions. The spread of these predictions is interpreted as the statistical uncertainty associated with the reweighting factors and is propagated to all observables used in the analysis.

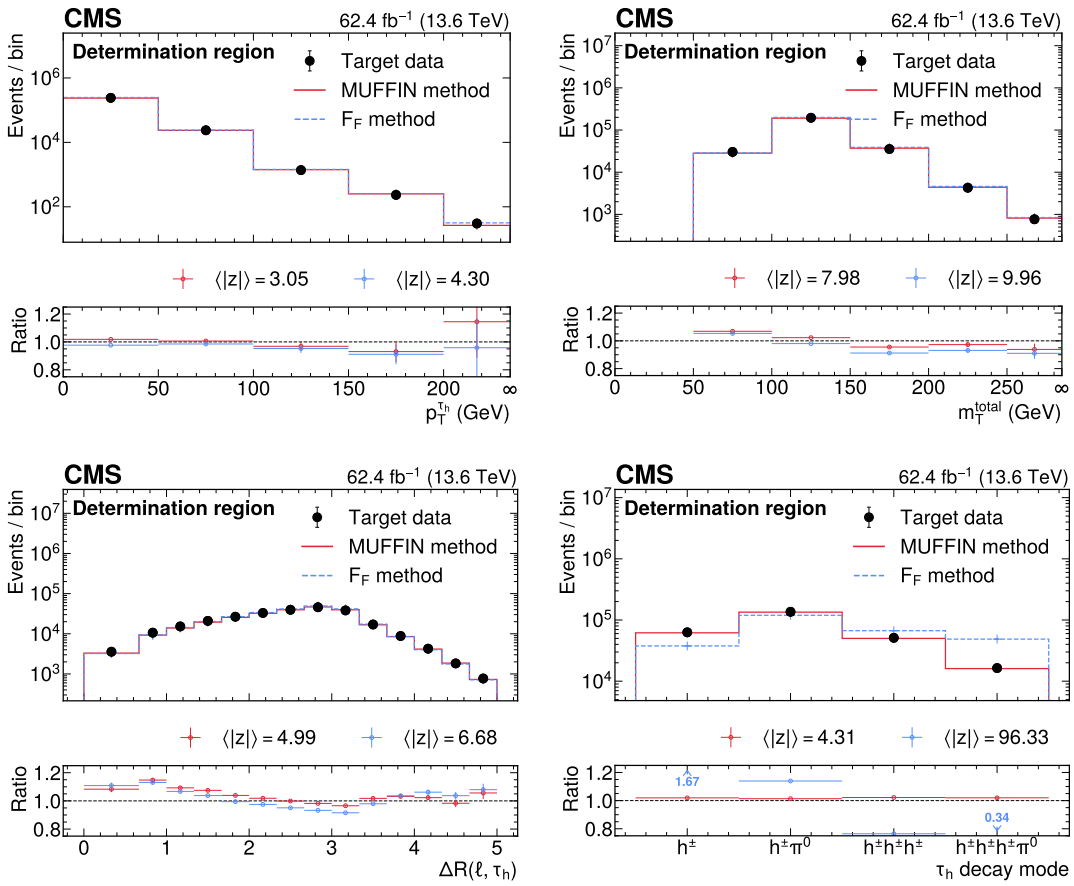

Figure 8: Comparison of $p_{\mathrm{T}}^{\tau_{\mathrm{h}}}$, $m_{\mathrm{T}}^{\mathrm{total}}$, ΔR, and τ_{h} decay mode in the W + jets DR of the $\tau_\mu\tau_{\mathrm{h}}$ channel, showing MUFFIN (red) and F_{F} (blue, dashed). Vertical bars on the points indicate the statistical uncertainty. The ratio panels report the $\langle|z|\rangle$ values for each method; arrows mark bins outside the plotted range. Overflow is included in the final bin (∞), where applicable.

8.2 Systematic uncertainties

Systematic uncertainties associated with the MUFFIN method are assigned to account for potential mismodelling in the BDT reweighting procedure and its extrapolation from DR to SR. These uncertainties are grouped into four categories, corresponding to distinct sources of potential bias.

8.2.1 Non-closure uncertainty

Residual mismodelling can arise in observables that are not explicitly constrained by the BDT training. These include variables orthogonal to the input feature set, such as ΔR and $p_{\mathrm{T}}^{\mathrm{miss}}$, which are not included as training inputs and therefore provide an independent test of the modelling performance. The non-closure is evaluated using Eq. (9) as the bin-by-bin ratio of observed to predicted yields in the VR. A flat uncertainty of 5% is assigned based on the typical level of residual non-closure observed in these orthogonal observables. This uncertainty covers mismodelling in variables not seen during training and potential non-closure in trained variables when extrapolating from the DR to the SR phase space is separately addressed by the extrapolation uncertainty described in Section 8.2.2. This uncertainty is significantly smaller than the non-closures of up to 20% or more that can be observed with the F_{F} method, which often necessitate explicit closure corrections.

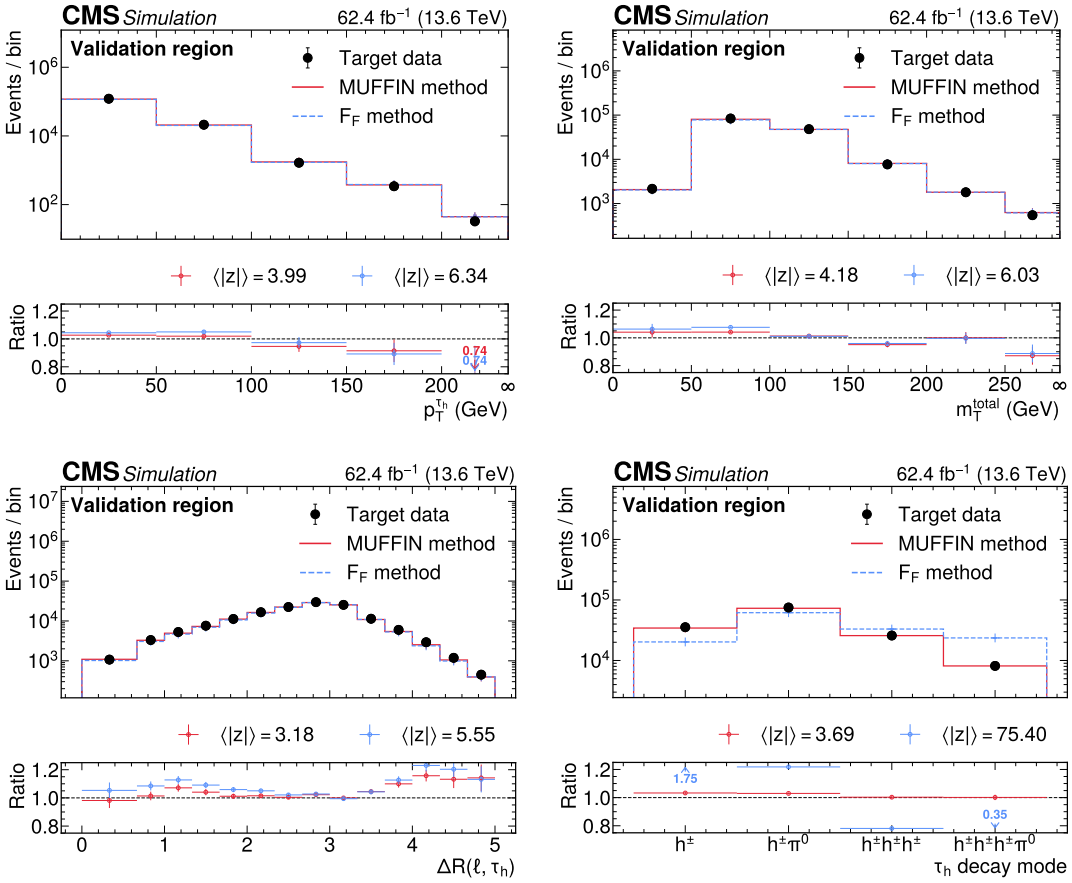

Figure 9: Comparison of $p_{\mathrm{T}}^{\tau_{\mathrm{h}}}$, $m_{\mathrm{T}}^{\mathrm{total}}$, ΔR, and τ_{h} decay mode for MUFFIN (red) and F_{F} (blue, dashed) using simulated W + jets events. Vertical bars on the points indicate the statistical uncertainty. Ratio panels show agreement with respect to the simulated target and report the corresponding $\langle|z|\rangle$ values. Arrows indicate bins outside the plotted range. Overflow is included in the final bin (∞), where applicable.

8.2.2 Extrapolation uncertainty

The BDT model is trained in DRs enriched in misidentified jets and subsequently applied in VRs. Differences in phase space between these regions can introduce residual biases that are not fully constrained by the training. To quantify this effect, the level of non-closure in a key analysis observable is evaluated, as described in Section 9.2. For QCD-enriched DRs such as those considered in Section 9.2, the resulting uncertainty was found to remain within approximately 10%, and is significantly smaller over most of the accessible phase space, particularly in regions dominated by non-jet $\rightarrow \tau_{\mathrm{h}}$ backgrounds. Since this uncertainty is derived from the non-closure evaluated in a VR, the VR must be chosen to adequately capture the phase space difference between the DR and the SR, so that the resulting non-closure provides a reliable estimate of the extrapolation uncertainty. Therefore, both the choice of VR and the resulting magnitude of the uncertainty are analysis dependent.

8.2.3 Modelling uncertainty

Potential biases related to the ML model itself are assessed by varying the training configuration. These variations include changes to the set of input features, hyperparameter choices, and the inclusion of different combinations of global event variables. For each variation, the

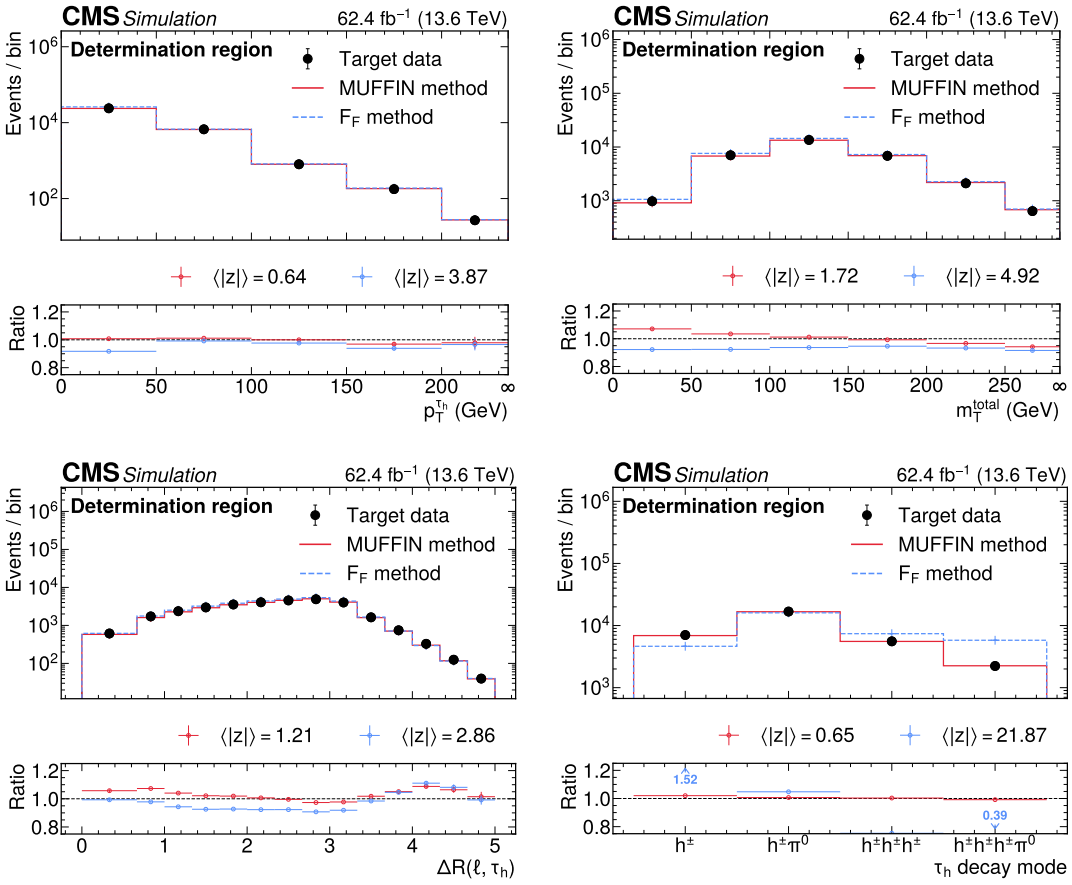

Figure 10: Comparison of $p_{\mathrm{T}}^{\tau_{\mathrm{h}}}$, $m_{\mathrm{T}}^{\mathrm{total}}$, ΔR, and τ_{h} decay mode for MUFFIN (red) and F_{F} (blue, dashed) in simulated $\mathrm{t\bar{t}}$ for the $\tau_{\mu}\tau_{\mathrm{h}}$ channel. Vertical bars on the points indicate the statistical uncertainty. The ratio panels show agreement with respect to the simulated target and report the corresponding $\langle|z|\rangle$ values. Arrows indicate bins outside the plotted range. Overflow is included in the final bin (∞), where applicable.

full training and reweighting procedure is repeated, and the resulting differences in the predictions are propagated as a systematic uncertainty. This uncertainty is treated as dependent on the analysis channel and background process, reflecting the differing sensitivities of each category to modelling choices. The magnitude of this uncertainty is typically at the level of 2% or less, indicating a robust performance of the BDT-based reweighting procedure against variations in the training configuration.

8.2.4 Background subtraction uncertainty

The subtraction of genuine-τ_h contributions in the DRs introduces an associated uncertainty on the estimated TFs. This is propagated by varying the subtracted backgrounds by $\pm 20\%$ for the QCD multijet process and $\pm 10\%$ for the W + jets process, reflecting the typical uncertainty in the genuine-τ_h contamination in the respective DRs. The variation is applied in both the numerator and denominator of the weight formula, and the full reweighting procedure is repeated for each variation to propagate the effect to the final background estimate. In rare cases, statistical fluctuations in sparsely populated bins can yield negative TFs; the method remains well-defined in this limit; when the nominal TF is negative, the unsubtracted ratio $w_{\text{MUFFIN}}(\mathbf{z}) = (P^{\text{data}}_{\text{pass}}(\mathbf{z}))/(P^{\text{data}}_{\text{fail}}(\mathbf{z}))$ is used as both the nominal prediction and the uncertainty bound, ensuring no negative event weights enter the final prediction. The bootstrap ensemble naturally captures the impact of such fluctuations on the final background prediction. This uncertainty is not applicable to simulation-based derivations (W + jets and $t\bar{t}$), where there is no genuine-τ_h contamination.

Together, these uncertainty components provide a comprehensive treatment of the statistical and systematic effects associated with the MUFFIN method, ensuring robust coverage of residual mismodelling, extrapolation effects, and training-related variations. The total relative uncertainty in the jet $\rightarrow \tau_h$ background yield in representative inclusive SR selections for each channel is summarised in Table 3. In both channels, the extrapolation uncertainty is the single largest source of systematic uncertainty, while all other components remain well below the 2% level.

Table 3: Total relative uncertainty in the jet $\rightarrow \tau_h$ background yield in representative inclusive SR selections for each channel.

Channel	Dominant background	Total relative uncertainty
$\tau_h\tau_h$	QCD multijet	6%
$\tau_\mu\tau_h$	QCD multijet, W + jets, $t\bar{t}$	5%

9 Performance in physics analyses

9.1 Application of the MUFFIN method to signal regions

In this section we present the application of the MUFFIN method in physics analyses at CMS involving τ_h leptons. The results shown correspond to baseline SR selections as described in Section 5, without additional categorisation beyond the nominal event selection. The MUFFIN method is used to estimate the dominant backgrounds arising from jets misidentified as τ_h candidates, encompassing contributions from QCD multijet, W + jets, and $t\bar{t}$ processes. In the $\tau_h\tau_h$ channel, the method is applied to estimate the jet $\rightarrow \tau_h$ background from the QCD multijet process.

In the $\tau_\mu\tau_h$ channel, the method is applied to estimate the combined jet $\rightarrow \tau_h$ background from all relevant processes. This is done by calculating process-specific reweighting factors and

combining them according to their relative contributions in the respective analysis categories. The resulting m_{vis} distributions in the $\tau_h\tau_h$ and $\tau_\mu\tau_h$ channels are shown for the SRs in Fig. 11, where the MUFFIN-based prediction is found to be in good agreement with the observed data; the corresponding improvement relative to the F_F method is demonstrated in Sections 7 and 9.2.

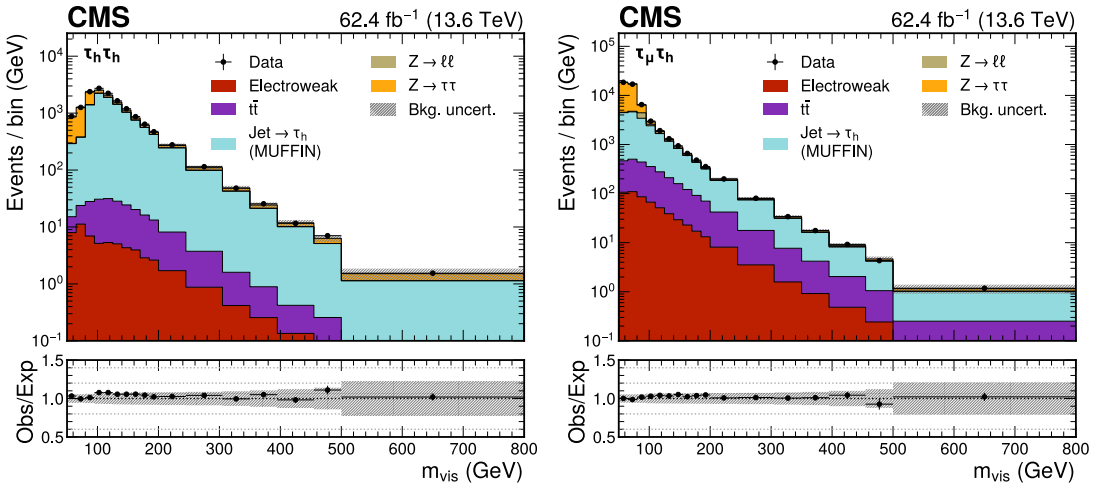

Figure 11: Distributions of the visible mass in the $\tau_h\tau_h$ (left) and the $\tau_\mu\tau_h$ (right) channels in the SRs, as defined in Section 5, of physics analyses targeting Higgs boson decays to τ lepton pairs. The MUFFIN method is used to estimate the jet $\to \tau_h$ background contributions. Vertical bars represent the statistical uncertainty on the data points. The lower panels show the ratio of data to the total background prediction, with shaded bands representing the combined statistical and systematic uncertainties from the MUFFIN method.

When the MUFFIN method is applied to SRs, agreement within uncertainties between the predicted background and the observed data is found in the m_{vis} distributions. A χ^2 goodness-of-fit test [67], computed using statistical uncertainties only, yields $\chi^2/\text{dof} = 11.42/17$ ($p = 0.834$) in the $\tau_h\tau_h$ channel and $\chi^2/\text{dof} = 7.14/17$ ($p = 0.982$) in the $\tau_\mu\tau_h$ channel, where dof is the number of degrees of freedom, confirming compatibility between the observed data and the prediction. The non-closure systematic uncertainties derived from the VRs, as quantified in Sections 9.2 and 8, are excluded from the χ^2 denominator to avoid circularity, and are shown separately as the shaded band in Fig. 11.

9.2 Comparison of MUFFIN and F_F methods in categorised and multivariate analyses

While overall agreement in the total distribution of a primary fit observable is a necessary validation, it may not fully capture the impact of jet $\to \tau_h$ modelling once analyses probe extreme kinematics, categorise events into jet multiplicity or high-p_T bins, and/or use multivariate discriminants built from many correlated inputs. To address this, additional closure tests are performed in VRs that are orthogonal to both the DRs used to derive the MUFFIN reweighting and the SRs used to evaluate the final analysis sensitivity, but are kinematically representative of the SRs. In these VRs, the predicted jet $\to \tau_h$ background is compared to the observed data distribution in a relevant analysis observable, and the resulting residual differences between predicted and observed yields are used directly to estimate the systematic uncertainty associated with the jet $\to \tau_h$ background estimation with each method. For each analysis setup, the non-closure in the VR is evaluated as a function of the relevant analysis observable.

The performance of the MUFFIN and F_{F} methods is evaluated using the non-closure

$$r(\vec{z}) \equiv \frac{N_{\mathrm{obs}}(\vec{z})}{N_{\mathrm{pred}}(\vec{z})}, \tag{9}$$

where $\vec{z}$ denotes a bin in the (possibly multidimensional) space of relevant observables, N_{obs} is the observed yield in the signal-like VR, and N_{pred} is the corresponding method prediction, computed across the full distribution. The bin-by-bin non-closure is taken directly as the systematic uncertainty in the jet $\to \tau_{\mathrm{h}}$ background estimate in that bin. In sparsely populated regions where statistical precision does not support fine binning, a constant is fit to the ratio above a threshold, yielding r_{tail}, which is then used as the systematic uncertainty in that region.

The corresponding total uncertainty per bin is constructed as

$$\text{Total uncertainty} = \sqrt{(1-r)^2 + \sigma_r^2}, \tag{10}$$

which combines the statistical component σ_r with the observed deviation from unity. Crucially, by evaluating these non-closures in a VR that is kinematically representative of the SR, the resulting per-bin uncertainties provide a data-driven estimate of the residual modelling uncertainty that would be assigned in an actual analysis. A smaller non-closure therefore translates directly into a smaller systematic uncertainty in the jet $\to \tau_{\mathrm{h}}$ background estimate, and hence improved sensitivity.

Three representative analysis setups are studied, spanning some of the most commonly used cases for jet $\to \tau_{\mathrm{h}}$ background estimation in analyses involving τ_{h} decays at CMS. The first setup targets Higgs boson $\mathrm{H}(125) \to \tau\tau$ decays in a *CP*-structure measurement [4, 70], where a multivariate discriminant is used to enhance signal purity by separating Higgs boson events from background. The second one focuses on differential cross section measurements in the simplified template cross section (STXS) framework [5]. The third setup searches for new heavy resonances decaying to $\tau_{\mathrm{h}}\tau_{\mathrm{h}}$ and $\tau_\mu\tau_{\mathrm{h}}$ final states at high mass [12]. Together, these cover a representative range of analysis strategies, from inclusive SRs to finely categorised and multivariate-discriminant-based selections, and allow the systematic uncertainty reduction achievable with the MUFFIN method to be quantified in each context.

9.2.1 The *CP* structure in $\mathrm{H}(125) \to \tau\tau$ decays: multivariate discriminant-based analysis

To probe whether improved modelling propagates to multivariate analyses, closure tests are performed directly on the output of a signal-versus-background BDT discriminator $D(\vec{x})$ used in the $\mathrm{H}(125) \to \tau\tau$ *CP* analysis. The bin-by-bin non-closure and integrated bias,

$$b \equiv \frac{\sum_i N_i^{\mathrm{pred}} - \sum_i N_i^{\mathrm{obs}}}{\sum_i N_i^{\mathrm{obs}}}, \tag{11}$$

are evaluated across the full BDT score range, with particular attention to the signal-enriched high-score region where modelling quality has the largest impact on sensitivity.

In the illustrated $\mathrm{H}(125) \to \tau\tau$ BDT example in Fig. 12, the root-mean-square of the bin-by-bin residuals improves from $\sim$6.6% (F_{F}) to $\sim$3.4% (MUFFIN), and the integrated bias improves from $\sim$6.5% to $\sim$3.3%, demonstrating substantially reduced systematic uncertainties in the signal-enriched (high-score) region. Complementary results in a W + jets enriched VR in the $\tau_\mu\tau_{\mathrm{h}}$ channel are shown in Fig. 13. In this case the non-closure evaluation is statistically limited

at high BDT scores, where the signal-enriched bins are sparsely populated, and the resulting systematic uncertainties are dominated by their statistical component. The non-closure values obtained with both methods are therefore comparable within current statistical precision, and the systematic component is expected to become better constrained as larger data sets become available.

9.2.2 Differential cross section STXS measurements: jet multiplicity and high-p_{T} categories

A second robustness check targets the STXS measurement framework, which is widely used in Higgs boson measurements. In this approach, the phase space is divided into exclusive categories based on jet multiplicity and event topology (e.g. 0-jet, 1-jet, $\geq$2-jet, and high-p_{T} regions), in order to probe different Higgs boson production mechanisms. These categories introduce strong kinematic and topological constraints, making them particularly sensitive to mismodelling of backgrounds. Neither method is explicitly tuned to STXS definitions (as provided in Ref. [5]); both are applied without category-specific optimisation to probe robustness under aggressive phase space slicing. The non-closure is evaluated per STXS category by comparing predicted-to-observed yields in a fixed FASTMTT mass [71] window, which provides an approximate reconstruction of the di-τ invariant mass in the presence of neutrinos from τ decays, with the category-level non-closures, as defined in Eq. (10), used to estimate the per-category systematic uncertainty in the jet $\to \tau_{\mathrm{h}}$ background.

In a $\tau_{\mathrm{h}}\tau_{\mathrm{h}}$ QCD multijet-dominated VR, the MUFFIN method achieves $\chi^2 = 8.39$ ($p = 0.818$) across all STXS categories, compared to $\chi^2 = 10.64$ ($p = 0.641$) for the F_{F} method, with the largest improvements observed in the high-p_{T} and multi-jet categories where the F_{F} method is most challenged by its inability to capture correlations between jet activity and the jet $\to \tau_{\mathrm{h}}$ misidentification probability. In a $\tau_\mu\tau_{\mathrm{h}}$ W + jets-dominated test, MUFFIN achieves $\chi^2 = 7.21$ ($p = 0.781$) compared to $\chi^2 = 8.51$ ($p = 0.667$) for the F_{F} method. Categories for which the available sample size is insufficient to obtain a statistically meaningful non-closure estimate are excluded from the comparison. In the majority of categories where a reliable comparison is possible, MUFFIN achieves smaller or comparable deviations from unity than the F_{F} method, demonstrating that the improvement is systematic and not confined to particular phase space regions. In a small number of individual categories the central non-closure value for MUFFIN is marginally larger than for F_{F}, but in all such cases the difference is well within the statistical uncertainties of the two methods. Figure 14 shows the category-by-category yield closure and derived systematic uncertainties for both VRs, illustrating the improved per-category agreement and the reduced systematic uncertainties achievable with the MUFFIN method, particularly in the high-p_{T} and multijet categories. In statistically limited categories, both methods perform comparably, with the non-closure values dominated by their statistical component. As larger data sets become available, the improved modelling of the MUFFIN method is expected to translate into significantly reduced systematic uncertainties in these categories as well.

9.2.3 High-mass resonance searches: kinematic tails sensitive regions

For searches targeting BSM heavy resonances decaying to $\tau_{\mathrm{h}}\tau_{\mathrm{h}}$ and $\tau_\mu\tau_{\mathrm{h}}$ final states, sensitivity often comes from the high-p_{T} tails of the τ_{h} kinematic distributions, where the jet $\to \tau_{\mathrm{h}}$ background systematic uncertainty is typically the limiting factor. The non-closure in these tail regions is evaluated by fitting a constant to the residuals above a τ_{h} p_{T} threshold ($p_{\mathrm{T}}^{\tau_{\mathrm{h}}} > 200\,\mathrm{GeV}$ in $\tau_{\mathrm{h}}\tau_{\mathrm{h}}$ and $p_{\mathrm{T}}^{\tau_{\mathrm{h}}} > 100\,\mathrm{GeV}$ in $\tau_\mu\tau_{\mathrm{h}}$), yielding r_{tail} and the corresponding tail systematic uncertainty σ^{tail} as defined in Eq. (10).

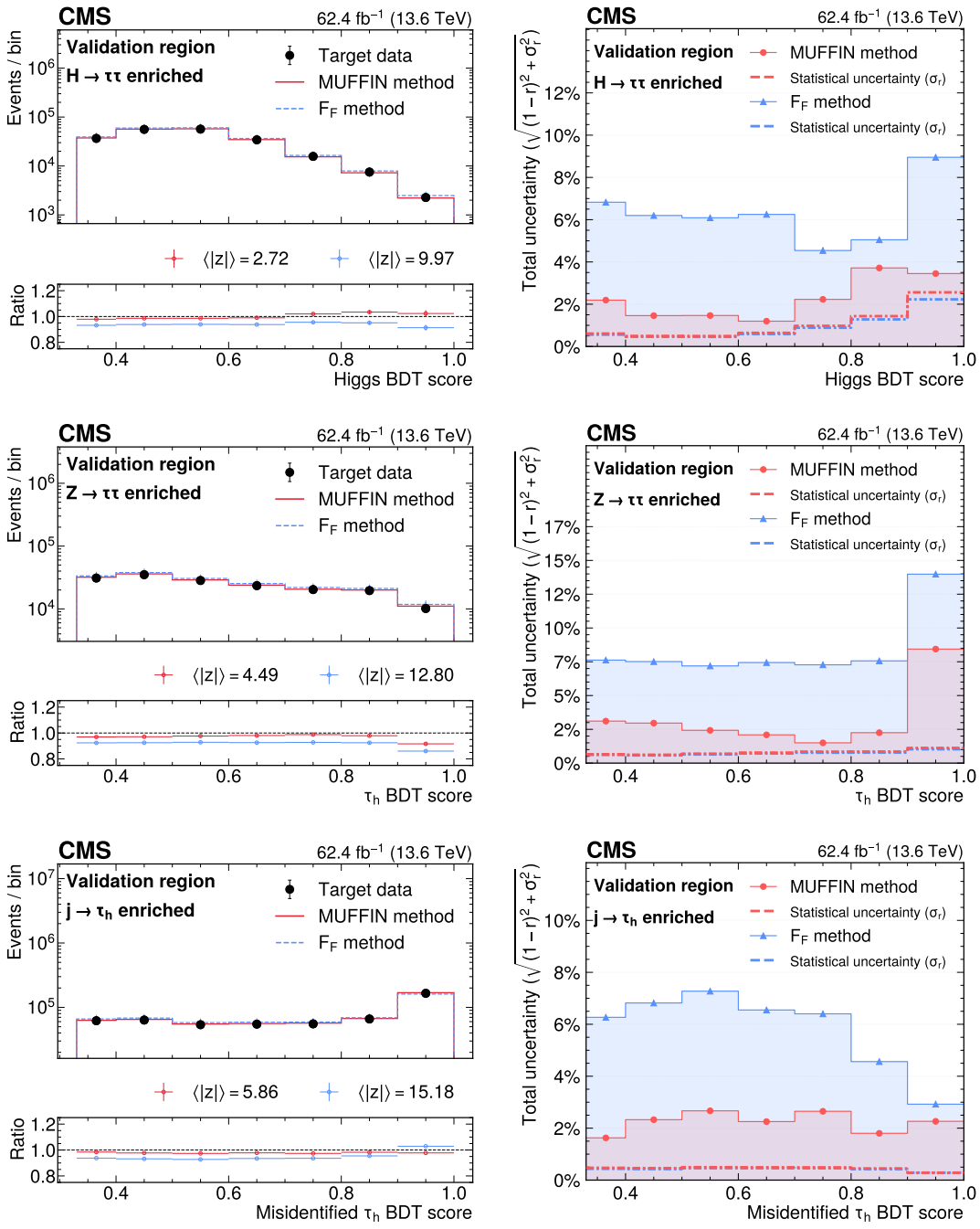

Figure 12: The BDT score validation in a $H(125) \rightarrow \tau\tau$ *CP* VR in the $\tau_h\tau_h$ channel for the Higgs boson enriched, Z boson enriched, and misidentified jet enriched categories. MUFFIN (red) and F_F (blue, dashed) predictions are compared at the distribution level (left) and through the corresponding non-closure evaluation (right). The statistical uncertainty is indicated by the vertical bars on the data points. In the right panels, the hatched bars indicate the statistical component of the total uncertainty.

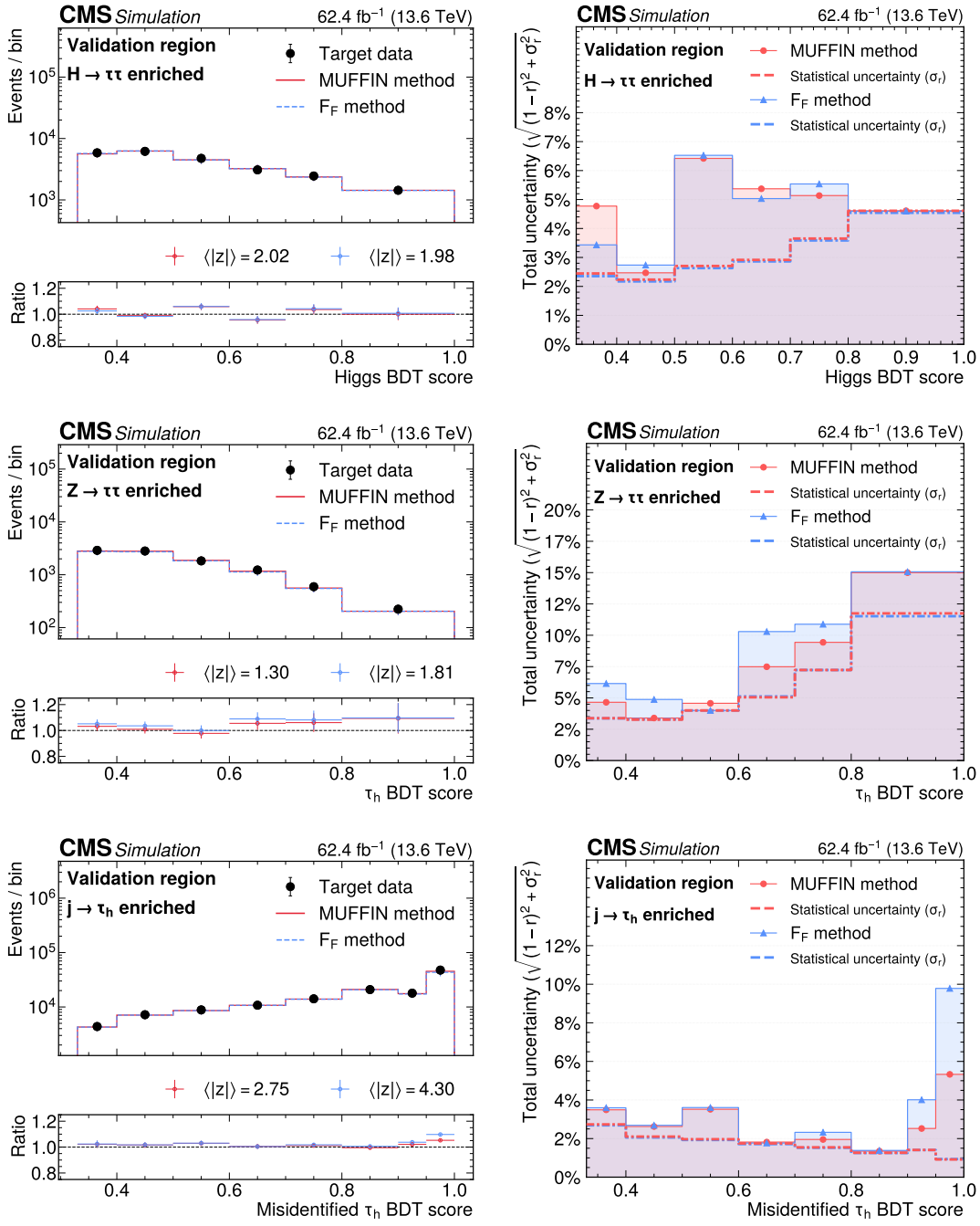

Figure 13: The BDT score validation in a W + jets-enriched VR in the $\tau_\mu\tau_h$ channel for the Higgs boson enriched, Z boson enriched, and misidentified jet enriched categories. MUFFIN (red) and F_F (blue, dashed) predictions are compared at the distribution level (left) and through the corresponding non-closure evaluation (right). The statistical uncertainty is indicated by the vertical bars on the data points. In the right panels, the hatched bars indicate the statistical component of the total uncertainty.

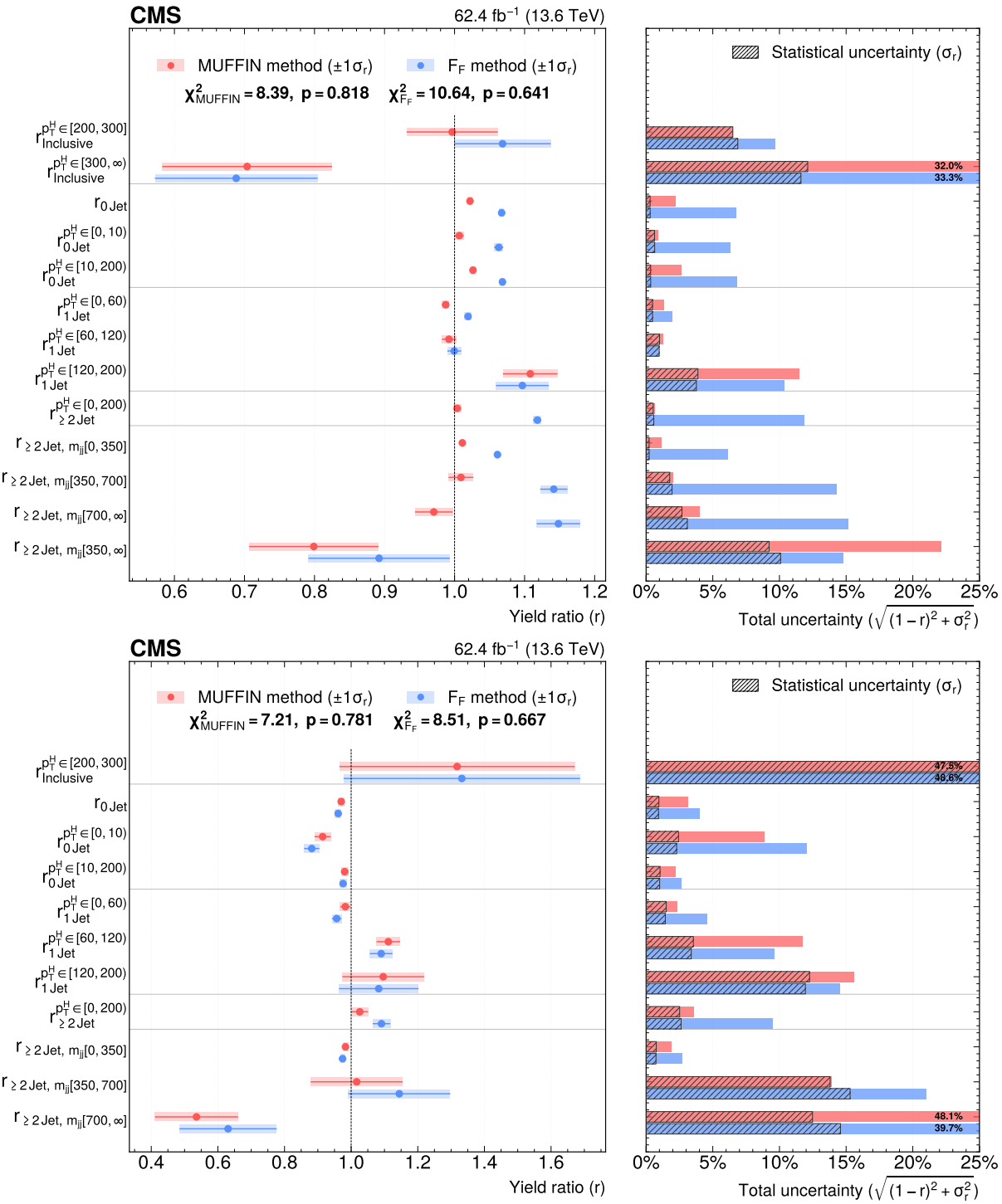

Figure 14: The STXS-inspired category-by-category yield closure for a $\tau_h\tau_h$ (upper) and $\tau_\mu\tau_h$ (lower) VR. Points show the ratio of observed to predicted yields per STXS category (non-closure), for the MUFFIN (red) and F_F (blue) methods, where deviations from unity are interpreted as systematic uncertainties in the jet $\rightarrow \tau_h$ background estimate. The right panel shows the total uncertainty per category, with the hatched grey bars indicating the statistical component. Only statistical uncertainties are shown in the left panel; the observed non-closure along with the statistical uncertainty define the systematic uncertainty that would be assigned in a real analysis.

In the $\tau_h\tau_h$ QCD multijet-dominated VR, the fitted tail residuals are $r_{\text{tail}}^{F_F} = 1.095 \pm 0.018$ and $r_{\text{tail}}^{\text{MUFFIN}} = 1.021 \pm 0.018$ for the τ_h p_T tail, corresponding to tail systematic uncertainties of $\sigma_{F_F}^{\text{tail}} = 9.7\%$ and $\sigma_{\text{MUFFIN}}^{\text{tail}} = 2.7\%$, as shown in Fig. 15. In the $\tau_\mu\tau_h$ W + jets-dominated VR, the fitted tail residuals are $r_{\text{tail}}^{F_F} = 0.873 \pm 0.074$ and $r_{\text{tail}}^{\text{MUFFIN}} = 0.890 \pm 0.075$, corresponding to tail systematic uncertainties of $\sigma_{F_F}^{\text{tail}} = 14.7\%$ and $\sigma_{\text{MUFFIN}}^{\text{tail}} = 13.3\%$. This corresponds to a reduction of $\sim$70% in the $\tau_h\tau_h$ channel. In the $\tau_\mu\tau_h$ channel, where the evaluation is limited by the available event yields, a modest improvement of $\sim$10% is observed, with both methods yielding comparable uncertainties within statistical precision. These reductions directly translate into reduced systematic uncertainties in the jet $\to \tau_h$ background estimate in the high-mass SR, and hence into improved sensitivity for BSM physics searches.

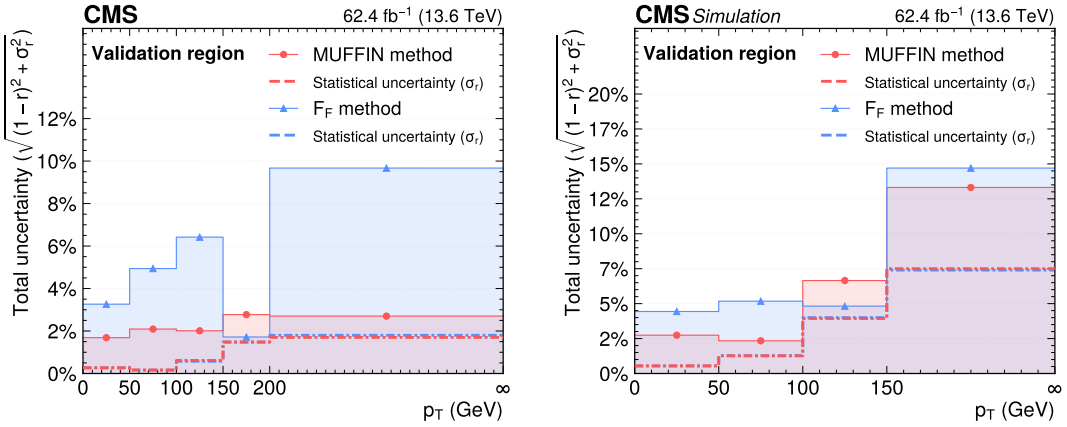

Figure 15: Closure in the high-p_T tails of the kinematic distributions for a $\tau_h\tau_h$ QCD multijet-dominated (left) and $\tau_\mu\tau_h$ W + jets (right) VRs. The dashed lines indicate the statistical component of the uncertainty. The ratio in each bin reflects the non-closure, and the fitted constant (solid horizontal line) is derived by fitting over all events above the p_T threshold, providing a more statistically robust estimate of the aggregate tail closure than any individual bin. The MUFFIN method achieves significantly improved agreement in both tails, leading to substantially reduced systematic uncertainties for the $\tau_h\tau_h$ channel and moderate improvements in the $\tau_\mu\tau_h$ channel. Overflow is included in the final bin (∞).

Taken together, the three case studies above demonstrate that the improvements in inclusive modelling observed in Section 7 translate directly into reduced systematic uncertainties across all major analysis strategies. The MUFFIN method consistently achieves smaller non-closures in BDT score distributions, STXS categories, and kinematic tails, without introducing instabilities in well-modelled regions. The resulting reduction in jet $\to \tau_h$ systematic uncertainties is most pronounced in the phase space regions of greatest sensitivity to new physics and differential measurements, where the F_F method is most limited by its inability to capture the full multidimensional dependence of the misidentification probability.

10 Summary and outlook

In this paper, a machine-learning-based alternative to the "Fake Factor" (F_F) method for estimating backgrounds from jets misidentified as hadronically decaying τ leptons (τ_h) is presented, referred to as MUltivariate Fake-Factor INference (MUFFIN). This method is a generalisation of the previous F_F method by replacing low-dimensional transfer factors with multidimensional, per-object reweighting functions learned directly from observed data, while pre-

serving the fully data-driven nature of the background estimation.

The method has been developed and validated using CMS data collected in 2022–2023 and is benchmarked against the F_F method using a series of closure tests. Across the analysis channels and observables considered, the MUFFIN method has demonstrated improved modelling performance, increased stability in regions sensitive to correlations between multiple variables, and a reduced reliance on additional non-closure corrections. At the same time, the method has provided a more unified and reproducible workflow for background estimation, leading to a reduction of up to 70% in the associated systematic uncertainty (Section 9.2).

These results indicate that MUFFIN constitutes a robust method for future analyses involving hadronically decaying τ leptons. As analyses increasingly exploit fine-grained categorisation and multidimensional phase space information, the method presented here provides a natural framework to improve background modelling precision and to enhance the sensitivity of measurements and searches involving τ_h final states.

Looking forward, further improvement in the performance of the MUFFIN method is expected as larger data sets become available. Training on larger, combined data sets therefore offers a natural path to increasing statistical precision while maintaining robustness against changing experimental conditions. The method also does not depend on the specific τ_h identification algorithm and can be readily deployed with future algorithm developments. More broadly, the general nature of the MUFFIN method makes it readily applicable to other data-driven background estimation problems involving misidentified or non-prompt objects, beyond τ_h candidates.

Acknowledgments

We congratulate our colleagues in the CERN accelerator departments for the excellent performance of the LHC and thank the technical and administrative staffs at CERN and at other CMS institutes for their contributions to the success of the CMS effort. In addition, we gratefully acknowledge the computing centres and personnel of the Worldwide LHC Computing Grid and other centres for delivering so effectively the computing infrastructure essential to our analyses. Finally, we acknowledge the enduring support for the construction and operation of the LHC, the CMS detector, and the supporting computing infrastructure provided by the following funding agencies: SC (Armenia), BMFWF and FWF (Austria); FNRS and FWO (Belgium); CNPq, CAPES, FAPERJ, FAPERGS, and FAPESP (Brazil); MES and BNSF (Bulgaria); CERN; CAS, MoST, and NSFC (China); MINCIENCIAS (Colombia); MSES and CSF (Croatia); RIF (Cyprus); SENESCYT (Ecuador); ERC PRG and PSG, TARISTU24-TK10 and MoER TK202 (Estonia); Academy of Finland, MEC, and HIP (Finland); CEA and CNRS/IN2P3 (France); SRNSF (Georgia); BMFTR, DFG, and HGF (Germany); GSRI (Greece); MATE and NKFIH (Hungary); DAE and DST (India); IPM (Iran); SFI (Ireland); INFN (Italy); MSIT and NRF (Republic of Korea); MES (Latvia); LMTLT (Lithuania); MOE and UM (Malaysia); BUAP, CINVESTAV, CONACYT, LNS, SEP, and UASLP-FAI (Mexico); MOS (Montenegro); MBIE (New Zealand); PAEC (Pakistan); MSHE, NSC, and NAWA (Poland); FCT (Portugal); MESTD (Serbia); MICIU/AEI and PCTI (Spain); MOSTR (Sri Lanka); Swiss Funding Agencies (Switzerland); NSTC (Taiwan); MHESI (Thailand); TUBITAK and TENMAK (Türkiye); NASU (Ukraine); STFC (United Kingdom); DOE and NSF (USA).

Individuals have received support from the Marie-Curie programme and the European Research Council and Horizon 2020 Grant, contract Nos. 675440, 724704, 752730, 758316, 765710, 824093, 101115353, 101002207, 101001205, and COST Action CA16108 (European Union); the

Leventis Foundation; the Alfred P. Sloan Foundation; the Alexander von Humboldt Foundation; the Science Committee, project no. 22rl-037 (Armenia); the Fonds pour la Formation à la Recherche dans l'Industrie et dans l'Agriculture (FRIA) and Fonds voor Wetenschappelijk Onderzoek contract No. 1228724N (Belgium); the Beijing Municipal Science & Technology Commission, No. Z191100007219010, the Fundamental Research Funds for the Central Universities, the Ministry of Science and Technology of China under Grant No. 2023YFA1605804, the Natural Science Foundation of China under Grant No. 12535004, and USTC Research Funds of the Double First-Class Initiative No. YD2030002017 (China); the Ministry of Education, Youth and Sports (MEYS) of the Czech Republic; the Shota Rustaveli National Science Foundation (Georgia); the Deutsche Forschungsgemeinschaft (DFG), among others, under Germany's Excellence Strategy – EXC 2121 "Quantum Universe" – 390833306, and under project number 400140256 - GRK2497; the Hellenic Foundation for Research and Innovation (HFRI), Project Number 2288 (Greece); the Hungarian Academy of Sciences, the New National Excellence Program - ÚNKP, the NKFIH research grants K 131991, K 138136, K 143460, K 143477, K 147557, K 146913, K 146914, K 147048, TKP2021-NKTA-64, 2026-4.1.1-MISSZIÓK-2026-00005 and 2025-1.1.5-NEMZ_KI-2025-00004, and MATE KKP and KKPCs Research Excellence and Flagship Research Groups grants (Hungary); the Council of Science and Industrial Research, India; ICSC – National Research Centre for High Performance Computing, Big Data and Quantum Computing, FAIR – Future Artificial Intelligence Research, and CUP I53D23001070006 (Mission 4 Component 1), funded by the NextGenerationEU program, the Italian Ministry of University and Research (MUR) under Bando PRIN 2022 – CUP I53C24002390006, PRIN PRIMULA 2022RBYK7T (Italy); the Latvian Council of Science; the Ministry of Science and Higher Education, project no. 2022/WK/14, and the National Science Centre, contracts Opus 2021/41/B/ST2/01369, 2021/43/B/ST2/01552, 2023/49/B/ST2/03273, and the NAWA contract BPN/PPO/2021/1/00011 (Poland); the Fundação para a Ciência e a Tecnologia (Portugal); the National Priorities Research Program by Qatar National Research Fund; MICIU/AEI/10.13039/501100011033, ERDF/EU, "European Union NextGenerationEU/PRTR", projects PID2022-142604OB-C21, PID2022-139519OB-C21, PID2023-147706NB-I00, PID2023-148896NB-I00, PID2023-146983NB-I00, PID2023-147115NB-I00, PID2023-148418NB-C41, PID2023-148418NB-C42, PID2023-148418NB-C43, PID2023-148418NB-C44, PID2024-158190NB-C22, RYC2021-033305-I, RYC2024-048719-I, CNS2023-144781, CNS2024-154769 and Plan de Ciencia, Tecnología e Innovación de Asturias, Spain; the Chulalongkorn Academic into Its 2nd Century Project Advancement Project, the National Science, Research and Innovation Fund program IND_FF_68_369_2300_097, and the Program Management Unit for Human Resources & Institutional Development, Research and Innovation, grant B39G680009 (Thailand); the Eric & Wendy Schmidt Fund for Strategic Innovation through the CERN Next Generation Triggers project under grant agreement number SIF-2023-004; the Kavli Foundation; the Nvidia Corporation; the SuperMicro Corporation; the Welch Foundation, contract C-1845; and the Weston Havens Foundation (USA).

Data availability

Release and preservation of data used by the CMS Collaboration as the basis for publications is guided by the CMS data preservation, re-use and open access policy.

References

[1] CMS Collaboration, "Observation of the Higgs boson decay to a pair of τ leptons with the CMS detector", *Phys. Lett. B* **779** (2018) 283,

doi:10.1016/j.physletb.2018.02.004, arXiv:1708.00373.

[2] ATLAS Collaboration, "Cross-section measurements of the Higgs boson decaying into a pair of τ-leptons in proton-proton collisions at $\sqrt{s} = 13$ TeV with the ATLAS detector", *Phys. Rev. D* **99** (2019) 072001, doi:10.1103/PhysRevD.99.072001, arXiv:1811.08856.

[3] CMS Collaboration, "Search for nonresonant Higgs boson pair production in final state with two bottom quarks and two tau leptons in proton-proton collisions at $\sqrt{s} = 13$ TeV", *Phys. Lett. B* **842** (2023) 137531, doi:10.1016/j.physletb.2022.137531, arXiv:2206.09401.

[4] CMS Collaboration, "Analysis of the CP structure of the Yukawa coupling between the Higgs boson and τ leptons in proton-proton collisions at $\sqrt{s} = 13$ TeV", *JHEP* **06** (2022) 012, doi:10.1007/jhep06(2022)012, arXiv:2110.04836.

[5] CMS Collaboration, "Measurements of Higgs boson production in the decay channel with a pair of τ leptons in proton–proton collisions at $\sqrt{s} = 13$ TeV", *Eur. Phys. J. C* **83** (2023) 562, doi:10.1140/epjc/s10052-023-11452-8, arXiv:2204.12957.

[6] CMS Collaboration, "Constraints on anomalous Higgs boson couplings to vector bosons and fermions from the production of Higgs bosons using the $\tau\tau$ final state", *Phys. Rev. D* **108** (2023) 032013, doi:10.1103/PhysRevD.108.032013, arXiv:2205.05120.

[7] ATLAS Collaboration, "Measurement of the CP properties of Higgs boson interactions with τ-leptons with the ATLAS detector", *Eur. Phys. J. C* **83** (2023) 563, doi:10.1140/epjc/s10052-023-11583-y, arXiv:2212.05833.

[8] ATLAS Collaboration, "Search for the nonresonant production of Higgs boson pairs via gluon fusion and vector-boson fusion in the $b\bar{b}\tau^+\tau^-$ final state in proton-proton collisions at $\sqrt{s} = 13$ TeV with the ATLAS detector", *Phys. Rev. D* **110** (2024) 032012, doi:10.1103/PhysRevD.110.032012, arXiv:2404.12660.

[9] ATLAS Collaboration, "Differential cross-section measurements of Higgs boson production in the $h \to \tau^+\tau^-$ decay channel in pp collisions at $\sqrt{s} = 13$ TeV with the ATLAS detector", *JHEP* **03** (2025) 010, doi:10.1007/JHEP03(2025)010, arXiv:2407.16320.

[10] ATLAS Collaboration, "Probing the Higgs boson CP properties in vector-boson fusion production in the $h \to \tau^+\tau^-$ channel with the ATLAS detector", *JHEP* **10** (2025) 092, doi:10.1007/JHEP10(2025)092, arXiv:2506.19395.

[11] CMS Collaboration, "Search for heavy neutral resonances decaying to tau lepton pairs in proton-proton collisions at $\sqrt{s} = 13$ TeV", *Phys. Rev. D* **111** (2025) 112004, doi:10.1103/PhysRevD.111.112004, arXiv:2412.04357.

[12] CMS Collaboration, "Searches for additional Higgs bosons and for vector leptoquarks in $\tau\tau$ final states in proton-proton collisions at $\sqrt{s} = 13$ TeV", *JHEP* **07** (2023) 073, doi:10.1007/JHEP07(2023)073, arXiv:2208.02717.

[13] ATLAS Collaboration, "Search for heavy Higgs bosons decaying into two tau leptons with the ATLAS detector using pp collisions at $\sqrt{s} = 13$ TeV", *Phys. Rev. Lett.* **125** (2020) 051801, doi:10.1103/PhysRevLett.125.051801, arXiv:2002.12223.

[14] CMS Collaboration, "Search for a third-generation leptoquark coupled to a τ lepton and a b quark through single, pair, and nonresonant production in proton-proton collisions at $\sqrt{s}$ = 13 TeV", *JHEP* **05** (2024) 311, doi:10.1007/JHEP05(2024)311, arXiv:2308.07826.

[15] ATLAS Collaboration, "Search for pair-produced scalar and vector leptoquarks decaying into third-generation quarks and first- or second-generation leptons in pp collisions with the ATLAS detector", *JHEP* **06** (2023) 188, doi:10.1007/JHEP06(2023)188, arXiv:2210.04517.

[16] CMS Collaboration, "Search for singly and pair-produced leptoquarks coupling to third-generation fermions in proton-proton collisions at $\sqrt{s} = 13$ TeV", *Phys. Lett. B* **819** (2021) 136446, doi:10.1016/j.physletb.2021.136446, arXiv:2012.04178.

[17] CMS Collaboration, "Search for the pair production of long-lived supersymmetric partners of the tau lepton in proton-proton collisions at $\sqrt{s} = 13$ TeV", *Submitted to JHEP* (2026) doi:10.48550/arXiv.2601.17576, arXiv:2601.17576.

[18] ATLAS Collaboration, "Search for direct stau production in events with two hadronic τ-leptons in $\sqrt{s} = 13$ TeV pp collisions with the ATLAS detector", *Phys. Rev. D* **101** (2020) 032009, doi:10.1103/PhysRevD.101.032009, arXiv:1911.06660.

[19] ATLAS Collaboration, "Search for lepton-flavour violation in high-mass dilepton final states using 139 fb^{-1} of pp collisions at $\sqrt{s}$ = 13 TeV with the ATLAS detector", *JHEP* **23** (2020) 082, doi:10.1007/JHEP10(2023)082, arXiv:2307.08567.

[20] ATLAS Collaboration, "Estimation of backgrounds from jets misidentified as τ-leptons using the Universal Fake Factor method with the ATLAS detector", *Eur. Phys. J. C* **85** (2025) 1441, doi:10.1140/epjc/s10052-025-14916-1, arXiv:2502.04156.

[21] CMS Collaboration, "Measurement of the $Z\gamma^* \to \tau\tau$ cross section in pp collisions at $\sqrt{s} = 13$ TeV and validation of τ lepton analysis techniques", *Eur. Phys. J. C* **78** (2018) 708, doi:10.1140/epjc/s10052-018-6146-9, arXiv:1801.03535.

[22] CMS Collaboration, "Search for additional neutral MSSM Higgs bosons in the $\tau\tau$ final state in proton-proton collisions at $\sqrt{s} = 13$ TeV", *JHEP* **09** (2018) 007, doi:10.1007/JHEP09(2018)007, arXiv:1803.06553.

[23] A. Rogozhnikov, "Reweighting with Boosted Decision Trees", *J. Phys. Conf. Ser.* **762** (2016) 012036, doi:10.1088/1742-6596/762/1/012036, arXiv:1608.05806.

[24] CMS Collaboration, "Identification of hadronic tau lepton decays using a deep neural network", *JINST* **17** (2022) P07023, doi:10.1088/1748-0221/17/07/P07023, arXiv:2201.08458.

[25] CMS Collaboration, "Identification of tau leptons using a convolutional neural network with domain adaptation", *JINST* **20** (2025) P12032, doi:10.1088/1748-0221/20/12/P12032, arXiv:2511.05468.

[26] CMS Collaboration, "The CMS experiment at the CERN LHC", *JINST* **3** (2008) S08004, doi:10.1088/1748-0221/3/08/S08004.

[27] CMS Collaboration, "Development of the CMS detector for the CERN LHC Run 3", *JINST* **19** (2024) P05064, doi:10.1088/1748-0221/19/05/P05064, arXiv:2309.05466.

[28] CMS Collaboration, "Performance of the CMS Level-1 trigger in proton-proton collisions at $\sqrt{s} = 13\,\text{TeV}$", *JINST* **15** (2020) P10017, doi:10.1088/1748-0221/15/10/P10017, arXiv:2006.10165.

[29] CMS Collaboration, "The CMS trigger system", *JINST* **12** (2017) P01020, doi:10.1088/1748-0221/12/01/P01020, arXiv:1609.02366.

[30] CMS Collaboration, "Performance of the CMS high-level trigger during LHC Run 2", *JINST* **19** (2024) P11021, doi:10.1088/1748-0221/19/11/P11021, arXiv:2410.17038.

[31] CMS Collaboration, "Electron and photon reconstruction and identification with the CMS experiment at the CERN LHC", *JINST* **16** (2021) P05014, doi:10.1088/1748-0221/16/05/P05014, arXiv:2012.06888.

[32] CMS Collaboration, "Performance of the CMS muon detector and muon reconstruction with proton-proton collisions at $\sqrt{s} = 13$ TeV", *JINST* **13** (2018) P06015, doi:10.1088/1748-0221/13/06/P06015, arXiv:1804.04528.

[33] CMS Collaboration, "Description and performance of track and primary-vertex reconstruction with the CMS tracker", *JINST* **9** (2014) P10009, doi:10.1088/1748-0221/9/10/P10009, arXiv:1405.6569.

[34] CMS Collaboration, "Luminosity measurement in proton-proton collisions at 13.6 TeV in 2022 at CMS", CMS Physics Analysis Summary CMS-PAS-LUM-22-001, 2024.

[35] J. Alwall et al., "The automated computation of tree-level and next-to-leading order differential cross sections, and their matching to parton shower simulations", *JHEP* **07** (2014) 079, doi:10.1007/JHEP07(2014)079, arXiv:1405.0301.

[36] R. Frederix and S. Frixione, "Merging meets matching in MC@NLO", *JHEP* **12** (2012) 061, doi:10.1007/JHEP12(2012)061, arXiv:1209.6215.

[37] J. Alwall et al., "Comparative study of various algorithms for the merging of parton showers and matrix elements in hadronic collisions", *Eur. Phys. J. C* **53** (2008) 473, doi:10.1140/epjc/s10052-007-0490-5, arXiv:0706.2569.

[38] C. Bierlich et al., "A comprehensive guide to the physics and usage of PYTHIA 8.3", *SciPost Phys. Codeb.* **2022** (2022) 8, doi:10.21468/SciPostPhysCodeb.8, arXiv:2203.11601.

[39] M. Grazzini, S. Kallweit, and M. Wiesemann, "Fully differential NNLO computations with MATRIX", *Eur. Phys. J. C* **78** (2018) 537, doi:10.1140/epjc/s10052-018-5771-7, arXiv:1711.06631.

[40] M. Grazzini et al., "NNLO QCD + NLO EW with Matrix+OpenLoops: precise predictions for vector-boson pair production", *JHEP* **02** (2020) 087, doi:10.1007/JHEP02(2020)087, arXiv:1912.00068.

[41] S. Alioli, P. Nason, C. Oleari, and E. Re, "A general framework for implementing NLO calculations in shower Monte Carlo programs: the POWHEG BOX", *JHEP* **06** (2010) 043, doi:10.1007/JHEP06(2010)043, arXiv:1002.2581.

[42] S. Alioli, S.-O. Moch, and P. Uwer, "Hadronic top-quark pair-production with one jet and parton showering", *JHEP* **01** (2012) 137, doi:10.1007/JHEP01(2012)137, arXiv:1110.5251.

[43] E. Re, "Single-top *Wt*-channel production matched with parton showers using the POWHEG method", *Eur. Phys. J. C* **71** (2011) 1547, doi:10.1140/epjc/s10052-011-1547-z, arXiv:1009.2450.

[44] R. Frederix, E. Re, and P. Torrielli, "Single-top *t*-channel hadroproduction in the four-flavour scheme with POWHEG and MC@NLO", *JHEP* **09** (2012) 130, doi:10.1007/JHEP09(2012)130, arXiv:1207.5391.

[45] M. Czakon and A. Mitov, "Top++: A program for the calculation of the top-pair cross-section at hadron colliders", *Comput. Phys. Commun.* **185** (2014) 2930, doi:10.1016/j.cpc.2014.06.021, arXiv:1112.5675.

[46] J. Campbell, T. Neumann, and Z. Sullivan, "Single-top-quark production in the *t*-channel at NNLO", *JHEP* **02** (2021) 040, doi:10.1007/JHEP02(2021)040, arXiv:2012.01574.

[47] N. Kidonakis and N. Yamanaka, "Higher-order corrections for *tW* production at high-energy hadron colliders", *JHEP* **05** (2021) 278, doi:10.1007/JHEP05(2021)278, arXiv:2102.11300.

[48] NNPDF Collaboration, "Parton distributions from high-precision collider data", *Eur. Phys. J. C* **77** (2017) 663, doi:10.1140/epjc/s10052-017-5199-5, arXiv:1706.00428.

[49] CMS Collaboration, "Extraction and validation of a new set of CMS PYTHIA8 tunes from underlying-event measurements", *Eur. Phys. J. C* **80** (2020) 4, doi:10.1140/epjc/s10052-019-7499-4, arXiv:1903.12179.

[50] GEANT4 Collaboration, "GEANT4—a simulation toolkit", *Nucl. Instrum. Meth. A* **506** (2003) 250, doi:10.1016/S0168-9002(03)01368-8.

[51] CMS Collaboration, "Particle-flow reconstruction and global event description with the CMS detector", *JINST* **12** (2017) P10003, doi:10.1088/1748-0221/12/10/P10003, arXiv:1706.04965.

[52] M. Cacciari, G. P. Salam, and G. Soyez, "The anti-k_{T} jet clustering algorithm", *JHEP* **04** (2008) 063, doi:10.1088/1126-6708/2008/04/063, arXiv:0802.1189.

[53] M. Cacciari, G. P. Salam, and G. Soyez, "FastJet user manual", *Eur. Phys. J. C* **72** (2012) 1896, doi:10.1140/epjc/s10052-012-1896-2, arXiv:1111.6097.

[54] CMS Collaboration, "Jet energy scale and resolution in the CMS experiment in pp collisions at 8 TeV", *JINST* **12** (2017) P02014, doi:10.1088/1748-0221/12/02/P02014, arXiv:1607.03663.

[55] E. Bols et al., "Jet flavour classification using DeepJet", *JINST* **15** (2020) P12012, doi:10.1088/1748-0221/15/12/P12012, arXiv:2008.10519.

[56] CMS Collaboration, "Pileup mitigation at CMS in 13 TeV data", *JINST* **15** (2020) P09018, doi:10.1088/1748-0221/15/09/p09018, arXiv:2003.00503.

[57] D. Bertolini, P. Harris, M. Low, and N. Tran, "Pileup per particle identification", *JHEP* **10** (2014) 059, doi:10.1007/JHEP10(2014)059, arXiv:1407.6013.

[58] CMS Collaboration, "Performance of missing transverse momentum reconstruction in proton-proton collisions at $\sqrt{s} = 13$ TeV using the CMS detector", *JINST* **14** (2019) P07004, doi:10.1088/1748-0221/14/07/P07004, arXiv:1903.06078.

[59] CMS Collaboration, "ECAL 2016 refined calibration and Run2 summary plots", CMS Detector Performance Summary CERN-CMS-DP-2020-021, 2020.

[60] CMS Collaboration, "Performance of reconstruction and identification of τ leptons decaying to hadrons and ν_τ in pp collisions at $\sqrt{s} = 13$ TeV", *JINST* **13** (2018) P10005, doi:10.1088/1748-0221/13/10/P10005, arXiv:1809.02816.

[61] CMS Collaboration, "High-level hadronic tau lepton triggers of the CMS experiment in proton-proton collisions at $\sqrt{s}$ = 13.6 TeV", *JINST* **21** (2026) P04002, doi:10.1088/1748-0221/21/04/P04002, arXiv:2602.11359.

[62] T. Chen and C. Guestrin, "XGBoost: A scalable tree boosting system", in *Proc. 22nd ACM SIGKDD Int. Conf. on Knowledge Discovery and Data Mining*, p. 785. 2016. doi:10.1145/2939672.2939785.

[63] T. Akiba et al., "Optuna: A next-generation hyperparameter optimization framework", in *Proc. 25th ACM SIGKDD Int. Conf. on Knowledge Discovery and Data Mining*, p. 2623. 2019. arXiv:1907.10902. doi:10.1145/3292500.3330701.

[64] J. Bergstra, R. Bardenet, Y. Bengio, and B. Kégl, "Algorithms for hyper-parameter optimization", in *Advances in Neural Information Processing Systems*, J. Shawe-Taylor et al., eds., volume 24. Curran Associates, Inc., 2011.

[65] C. Guo, G. Pleiss, Y. Sun, and K. Q. Weinberger, "On calibration of modern neural networks", in *Proc. 34th Int. Conf. on Machine Learning*, p. 1321. 2017. arXiv:1706.04599.

[66] J. C. Platt, "Probabilistic outputs for support vector machines and comparisons to regularized likelihood methods", in *Advances in Large Margin Classifiers*, A. J. Smola, P. Bartlett, B. Schölkopf, and D. Schuurmans, eds., p. 61. MIT Press, Cambridge, MA, 1999.

[67] G. Cowan, "Statistical data analysis". Oxford University Press, Oxford, 1998. ISBN 978-0-19-850560-5.

[68] Particle Data Group, F. Takahashi et al., "Review of particle physics", *Int. J. Mod. Phys. A* **41** (2026) 2630011, doi:10.1142/S0217751X26300115.

[69] ATLAS Collaboration, "Search for neutral Higgs bosons of the minimal supersymmetric standard model in pp collisions at $\sqrt{s}$ = 8 TeV with the ATLAS detector", *JHEP* **11** (2014) 056, doi:10.1007/JHEP11(2014)056, arXiv:1409.6064.

[70] CMS Collaboration, "Analysis of the CP structure of the Yukawa coupling between the Higgs boson and tau leptons in proton-proton collisions at $\sqrt{s} = 13.6$ TeV", *JHEP* **10** (2026) 084, arXiv:2606.03510.

[71] A. Kalinowski and W. Matyszkiewicz, "Efficient tau-pair invariant mass reconstruction with simplified matrix element techniques", *Nucl. Instrum. Meth. A* **1086** (2026) 171318, doi:10.1016/j.nima.2026.171318, arXiv:2509.26069.

A The CMS Collaboration

Yerevan Physics Institute, Yerevan, Armenia
A. Gevorgyan, A. Hayrapetyan, V. Makarenko, A. Tumasyan[1]

Marietta Blau Institute for Particle Physics, Vienna, Austria
W. Adam, L. Benato, T. Bergauer, M. Dragicevic, S. Gundacker, A.K. Guven, P.S. Hussain, M. Jeitler[2], N. Krammer, A. Li, D. Liko, M. Matthewman, J. Schieck[2], R. Schöfbeck[2], M. Shooshtari, M. Sonawane, N. Van Den Bossche, W. Waltenberger, C.E. Wulz[2]

Universiteit Antwerpen, Antwerpen, Belgium
T. Janssen, D. Ocampo Henao, T. Van Laer, P. Van Mechelen

Vrije Universiteit Brussel, Brussel, Belgium
D. Ahmadi, J. Bierkens, N. Breugelmans, S. Dansana, A. De Moor, M. Delcourt, S. Duponcheel, C. Gupta, F. Heyen, Y. Hong, K. Kang, P. Kashko, S. Lowette, I. Makarenko, S. Nandakumar, J. Niedziela, S. Tavernier, M. Tytgat[3], G.P. Van Onsem, S. Van Putte, T. Wybouw

Université Libre de Bruxelles, Bruxelles, Belgium
A. Beshr, B. Bilin, F. Caviglia Roman, B. Clerbaux, A.K. Das, I. De Bruyn, G. De Lentdecker, E. Ducarme, H. Evard, L. Favart, I. Kalaitzidou, A. Khalilzadeh, A. Malara, A. Potrebko, M.A. Shahzad, L. Thomas, M. Vanden Bemden, C. Vander Velde, P. Vanlaer, C. Yuan, F. Zhang

Ghent University, Ghent, Belgium
A. Cauwels, M. De Coen, D. Dobur[4], C. Giordano, G. Gokbulut, K. Kaspar, D. Kavtaradze, D. Marckx, A. Mehta, K. Skovpen, A.M. Tomaru, J. van der Linden, J. Vandenbroeck

Université Catholique de Louvain, Louvain-la-Neuve, Belgium
H. Aarup Petersen, A. Benecke, A. Bethani, G. Bruno, A. Cappati, J. De Favereau De Jeneret, C. Delaere, F. Gameiro Casalinho, A. Giammanco, A.O. Guzel, M. Hussain, Z. Lawrence, V. Lemaitre, J. Lidrych, P. Malek, S. Turkcapar

Centro Brasileiro de Pesquisas Fisicas, Rio de Janeiro, Brazil
G. Alves, E. Coelho, M.V. Gonçalves Sales, C. Hensel, D. Matos Figueiredo, T. Menezes De Oliveira, C. Mora Herrera, P. Rebello Teles, M. Soeiro, E.J. Tonelli Manganote[5], A. Vilela Pereira

Universidade do Estado do Rio de Janeiro, Rio de Janeiro, Brazil
W.L. Aldá Júnior, M. Barroso Ferreira Filho, H. Brandao Malbouisson, W. Carvalho, J. Chinellato[6], G. Correia Silva, M. Costa Reis, E.M. Da Costa, D. Da Silva Dalto, G.G. Da Silveira[7], D. De Jesus Damiao, S. Fonseca De Souza, R. Gomes De Souza, S. Jesus, T. Laux Kuhn[7], K. Maslova Gioseffi Defante, K. Mota Amarilo, L. Mundim, H. Nogima, J.P. Pinheiro, A. Santoro, A. Sznajder, M. Thiel, F. Torres Da Silva De Araujo[8], D. Torres Machado

Universidade Estadual Paulista (a), Universidade Federal do ABC (b), São Paulo, Brazil
C.A. Bernardes, L. Calligaris, J. Carvalho Leite, F. Damas, E. De Moraes Gregores, B. Lopes Da Costa, I. Maietto Silverio, P.G. Mercadante, S.F. Novaes, S. Padula, M. Pereira Coelho, V. Scheurer, T. Tomei

Institute for Nuclear Research and Nuclear Energy, Bulgarian Academy of Sciences, Sofia,

Bulgaria
A. Aleksandrov, G. Antchev, P. Danev, R. Hadjiiska, P. Iaydjiev, M. Shopova, G. Sultanov

University of Sofia, Sofia, Bulgaria
A. Dimitrov, L. Litov, B. Pavlov, P. Petkov, A. Petrov

Instituto de Alta Investigación, Universidad de Tarapacá, Arica, Chile
S. Keshri, D.N. Laroze Navarrete, M. Meena, S. Thakur

Universidad Técnica Federico Santa María, Valparaiso, Chile
W. Brooks

Beihang University, Beijing, China
T. Cheng, L. Tan, L. Wang, L. Yuan

Department of Physics, Tsinghua University, Beijing, China
J. Gu, Z. Hu, Z. Liang, J. Liu, Y. Wang, H. Yang, S. Zhang, Y. Zhao

Institute of High Energy Physics, Beijing, China
N. Bi[9], G.M. Chen[9], H.S. Chen[9], M. Chen[9], Y. Chen, B. Hou[9], Q. Hou, F. Iemmi, C.H. Jiang, P.z. Lai, H. Liao, G. Liu, Z. Liu[10], S. Song[9], J. Tao, C. Wang[9], J. Wang, A. Zada[9], H. Zhang, J. Zhao

State Key Laboratory of Nuclear Physics and Technology, Peking University, Beijing, China
Y. Ban, A. Carvalho Antunes De Oliveira, S. Deng, X. Geng, B. Guo, Q. Guo, Z. He, C. Jiang, A. Levin, C. Li, L. Li, Q. Li, Y. Mao, S. Qian, S.J. Qian, X. Qin, C. Quaranta, X. Sun, D. Wang, J. Wang, T. Yang, M. Zhang, M. Zhang, Y. Zhao, C. Zhou

State Key Laboratory of Nuclear Physics and Technology, Institute of Quantum Matter, South China Normal University, Guangzhou, China, Guangzhou, China
X. Hua, S. Yang

Sun Yat-Sen University, Guangzhou, China
Z. You

University of Science and Technology of China, Hefei, China
N. Lu

Nanjing Normal University, Nanjing, China
G. Bauer[11,12], L. Chen, Z. Cui[12], B. Li[13], H. Wang, X. Wang, K. Yi[14], J. Zhang, F. Zhu

Institute of Frontier and Interdisciplinary Science, Shandong University, Qingdao, China
C. Li

Institute of Modern Physics and Key Laboratory of Nuclear Physics and Ion-beam Application (MOE) - Fudan University, Shanghai, China
Y. Li, Z. Wang, Y. Zhou[15]

Zhejiang University - Department of Physics, Zhejiang, China
Z. Lin, C. Lu, M. Xiao[16]

Universidad de Los Andes, Bogota, Colombia
C. Avila, A. Cabrera, C. Florez, J.A. Reyes Vega

Universidad de Antioquia, Medellin, Colombia

C. Rendón, M. Rodriguez, A.A. Ruales Barbosa, J.D. Ruiz Alvarez

University of Split, Faculty of Electrical Engineering, Mechanical Engineering and Naval Architecture, Split, Croatia
N. Godinovic, D. Lelas, I. Puljak, A. Sculac

University of Split, Faculty of Science, Split, Croatia
M. Kovac, A. Petkovic, T. Sculac

Institute Rudjer Boskovic, Zagreb, Croatia
P. Bargassa, V. Brigljevic, D. Ferencek, K. Jakovcic, A. Starodumov, T. Susa

University of Cyprus, Nicosia, Cyprus
A. Attikis, S. Konstantinou, C. Leonidou, L. Paizanos, F. Ptochos, P.A. Razis, H. Saka, A. Stepennov

Charles University, Prague, Czech Republic
M. Finger Jr., A. Kveton

Escuela Politecnica Nacional, Quito, Ecuador
E. Acurio

Universidad San Francisco de Quito, Quito, Ecuador
E. Carrera Jarrin

Academy of Scientific Research and Technology of the Arab Republic of Egypt, Egyptian Network of High Energy Physics, Cairo, Egypt
A.A. Abdelalim[17,18], S. Khalil[18], E. Salama[19,20]

Center for High Energy Physics (CHEP-FU), Fayoum University, El-Fayoum, Egypt
A. Lotfy, M. Mahmoud, H. Mohammed, Y. Mohammed

National Institute of Chemical Physics and Biophysics, Tallinn, Estonia
K. Jaffel, M. Kadastik, T. Lange, C. Nielsen, J. Pata, M. Raidal, N. Seeba, L. Tani

Department of Physics, University of Helsinki, Helsinki, Finland
E. Brücken, A. Milieva, K. Osterberg, M. Voutilainen

Helsinki Institute of Physics, Helsinki, Finland
F.I. Garcia Fuentes, T. Hilden, P. Inkaew, K.T.S. Kallonen, R. Kumar Verma, T. Lampén, K. Lassila-Perini, B. Lehtela, S. Lehti, T. Lindén, N.R. Mancilla Xinto, M. Myllymäki, M.m. Rantanen, S. Saariokari, N.T. Toikka, J. Tuominiemi, E. Veikkola

Lappeenranta-Lahti University of Technology, Lappeenranta, Finland
N. Bin Norjoharuddeen, H. Kirschenmann, P.R. Luukka, H. Petrow

IRFU, CEA, Université Paris-Saclay, Gif-sur-Yvette, France
M. Besancon, F. Couderc, M. Dejardin, D. Denegri, P. Devouge, J.L. Faure, F. Ferri, P. Gaigne, S. Ganjour, P. Gras, F. Guilloux, G. Hamel de Monchenault, M. Kumar, V. Lohezic, Y. Maidannyk, J. Malcles, F. Orlandi, L. Portales, S. Ronchi, M.Ö. Sahin, P. Simkina, M. Titov

Laboratoire Leprince-Ringuet, CNRS/IN2P3, Ecole Polytechnique, Institut Polytechnique de Paris, Palaiseau, France
R. Amella Ranz, F. Beaudette, K. Biriukov, P. Busson, F. Cetorelli, C. Charlot, M. Chiusi, T.D. Cuisset, O. Davignon, A. De Wit, T. Debnath, I.T. Ehle,

S. Ghosh, A. Gilbert, R. Granier de Cassagnac, M. Manoni, M. Nguyen, S. Obraztsov, C. Ochando, L.m. Rabour, R. Salerno, J.B. Sauvan, Y. Sirois, G. Sokmen, Y. Song, L. Urda Gómez, B. Voirin, A. Zabi, A. Zghiche

Institut Pluridisciplinaire Hubert Curien (IPHC), Université de Strasbourg, CNRS/IN2P3, Strasbourg, France
J.L. Agram[21], J. Andrea, D. Bloch, E.C. Chabert, C. Collard, G. Coulon, C. Eschenlauer, S. Falke, U. Goerlach, A.C. Le Bihan, G. Saha, A. Savoy-Navarro[22], P. Vaucelle

Centre de Calcul de l'Institut National de Physique Nucleaire et de Physique des Particules, CNRS/IN2P3, Villeurbanne, France
A. Di Florio, G. Mauceri, B. Orzari

Institut de Physique des 2 Infinis de Lyon (IP2I), Villeurbanne, France
D. Amram, S. Beauceron, B. Blancon, G. Boudoul, N. Chanon, D. Contardo, J. Daniel, P. Depasse, H. El Mamouni, J. Fay, E. Fillaudeau, S. Gascon, M. Gouzevitch, C. Greenberg, B. Ille, E. Jourd'Huy, M. Lethuillier, K. Long, B. Massoteau, L. Mirabito, A. Purohit, M. Vander Donckt, C. Verollet

Georgian Technical University, Tbilisi, Georgia
D. Chokheli, I. Lomidze, Z. Tsamalaidze[23]

RWTH Aachen University, I. Physikalisches Institut, Aachen, Germany
K.F. Adamowicz, V. Botta, S. Consuegra Rodríguez, L. Feld, K. Klein, M. Lipinski, P. Nattland, V. Oppenländer, A. Pauls, D. Pérez Adán

RWTH Aachen University, III. Physikalisches Institut A, Aachen, Germany
C. Daumann, S. Diekmann, E. Ehlert, N. Eich, D. Eliseev, F. Engelke, J. Erdmann, M. Erdmann, M.Z. Farkas, B. Fischer, T. Hebbeker, K. Hoepfner, A. Jung, N. Kumar, F. Mausolf, M. Merschmeyer, A. Meyer, A. Pozdnyakov, H. Reithler, U. Sarkar, V. Sarkisovi, A. Schmidt, J.G. Schulz, C. Seth, A. Sharma, J.L. Spah, V. Vaulin, U. Willemsen, S. Zaleski, F.P. Zinn

RWTH Aachen University, III. Physikalisches Institut B, Aachen, Germany
M.R. Beckers, G. Flügge, N. Hoeflich, T. Kress, A. Nowack, O. Pooth, A. Stahl

University of Hamburg, Hamburg, Germany
A.R. Alves Andrade, M. Antonello, S. Bollweg, M. Bonanomi, L. Ebeling, K. El Morabit, Y. Fischer, M. Frahm, P.P. Gadow, E. Garutti, A. Grohsjean, A.A. Guvenli, J. Haller, D. Hundhausen, M. Jalalvandi, G. Kasieczka, P. Keicher, R. Klanner, W. Korcari, T. Kramer, C.c. Kuo, J. Lange, M.y. Lee, A. Lobanov, J. Matthiesen, L. Moureaux, K. Nikolopoulos, K.J. Pena Rodriguez, N. Prouvost, B. Raciti, M. Rieger, D. Savoiu, P. Schleper, M. Schröder, J. Schwandt, M. Sommerhalder, H. Stadie, G. Steinbrück, J. Sun, T. von Schwartz, R. Ward, B. Wiederspan, M. Wolf, C. Yede

Deutsches Elektronen-Synchrotron, Hamburg, Germany
A. Abel, A. Akhil, M. Aldaya Martin, J. Alimena, Y. An, I. Andreev, J. Bach, S. Baxter, H. Becerril Gonzalez, O. Behnke, F. Blekman[24], K. Borras[25], L. Braga Da Rosa, A. Campbell, C. Cazzaniga, S. Chatterjee, L.X. Coll Saravia, G. Eckerlin, D. Eckstein, E. Gallo[24], A. Geiser, M. Guthoff, A. Hinzmann, U. Husemann, M. Kasemann, C. Kleinwort, R. Kogler, M. Komm, D. Krücker, F. Labe, W. Lange, D. Leyva Pernia, J.h. Li, K.y. Lin, K. Lipka[26], W. Lohmann[27], J. Mal-

vaso, R. Mankel, I.A. Melzer-Pellmann, M. Mendizabal Morentin, A.B. Meyer, G. Milella, M.N.J. Momed, K. Moral Figueroa, A. Mussgiller, L.P. Nair, A. Nürnberg, J. Park, F. Preau, E. Ranken, A. Raspereza, D. Rastorguev, L. Rygaard, M. Scham[28,25], C. Schwanenberger[24], D. Schwarz, P. Schütze, D. Selivanova, K. Sharko, M. Shchedrolosiev, A. Sritharan, D. Stafford, M. Torkian, S. Vashishtha, R. Walsh, D. Wang, Q. Wang, K. Wichmann, C. Wissing, S. Zakharov, A. Zimermmane Castro Santos

Institut für Experimentelle Teilchenphysik, Karlsruhe, Germany
J. Ahäuser, A. Brusamolino, E. Butz, Y.M. Chen, T. Chwalek, A. Dierlamm, G.G. Dincer, U. Elicabuk, N. Faltermann, M. Giffels, A. Gottmann, F. Hartmann[29], F. Hummer, J. Kieseler, M. Klute, H.A. Krause, R. Kunnilan Muhammed Rafeek, O. Lavoryk, J.M. Lawhorn, S. Maier, N. Meenamthuruthil Radhakrishnan, T. Mehner, M. Molch, A.A. Monsch, M. Mormile, T. Müller, M. Presilla, G. Quast, K. Rabbertz, B. Regnery, R. Schmieder, T. Selezneva, N. Shadskiy, L. Sowa, L. Stockmeier, M. Toms, B. Topko, N. Trevisani, C. Verstege, T. Voigtländer, R.F. Von Cube, J. Von Den Driesch, J.H. Voss, C. Winter, R. Wolf, W.D. Zeuner, X. Zuo

Institute of Nuclear and Particle Physics (INPP), NCSR Demokritos, Aghia Paraskevi, Greece
G. Anagnostou, G. Daskalakis, A. Kyriakis

National and Kapodistrian University of Athens, Athens, Greece
P. Iosifidou, P. Katris, M. Kotsarini, G. Melachroinos, Z. Painesis, N. Plastiras, N. Saoulidou, K. Theofilatos, E. Tzovara, K. Vellidis, I. Zisopoulos

National Technical University of Athens, Athens, Greece
T. Chatzistavrou, G. Karapostoli, K. Kousouris, K. Paschos, L.P. Rouseliotaki, E. Siamarkou, A. Taxeidi, G. Tsipolitis

University of Ioánnina, Ioánnina, Greece
I. Evangelou, C. Foudas, P. Katsoulis, P. Kokkas, P.G. Kosmoglou Kioseoglou, N. Manthos, I. Papadopoulos, J. Strologas

Department of Physics, School of Sciences Democritus, University of Thrace, Kavala, Greece
E. Tziaferi

HUN-REN Wigner Research Centre for Physics, Budapest, Hungary
C. Hajdu, D. Horvath[30,31], Á. Kadlecsik, C. Lee, K. Márton, A.J. Rádl[32], F. Sikler, V. Veszpremi

MTA-ELTE Lendület CMS Particle and Nuclear Physics Group, Eötvös Loránd University, Budapest, Hungary
G. Balint, M. Csanad, K. Farkas, A. Fehérkuti[33], M.M.A. Gadallah[34], M. León Coello, G. Pasztor, G.I. Veres

Faculty of Informatics, University of Debrecen, Debrecen, Hungary, Debrecen, Hungary
B. Ujvari, G. Zilizi

HUN-REN ATOMKI - Institute of Nuclear Research, Debrecen, Hungary
G. Bencze, S. Czellar, J. Molnar, Z. Szillasi

Karoly Robert Campus, MATE Institute of Technology, Gyongyos, Hungary
T.F. Csorgo[33], F. Nemes[33], T. Novak, I. Szanyi[35]

Indian Institute of Science (IISC), Bangalore, India
J.R. Komaragiri

Indian Institute of Technology Bhubaneswar, Bhubaneswar, India
S. Bahinipati, R. Raturi

Panjab University, Chandigarh, India
S. Bansal, V. Bhatnagar, B. Chauhan, S. Chauhan, N. Dhingra[36], A. Kaur, H. Kaur, S. Kumar, T. Sheokand, A. Singla, K. Verma

University of Delhi, Delhi, India
A. Bhardwaj, A. Chhetri, B.C. Choudhary, A. Kumar, A. Kumar, M. Naimuddin, S. Phor, C. Prakash, K. Ranjan, M.K. Saini

Indian Institute of Technology Mandi (IIT-Mandi), Himachal Pradesh, India
M. Kumari, N. Neeraj, P. Palni, S. Rana, A. Rathore, A. Sarkar

University of Hyderabad, Hyderabad, India
S. Acharya[37], B. Gomber, S.K. Satapathy

Indian Institute of Technology Kanpur, Kanpur, India
S. Mukherjee

Saha Institute of Nuclear Physics, HBNI, Kolkata, India
S. Bhattacharya, S. Das Gupta, S. Dutta, S. Dutta, S. Sarkar

Indian Institute of Technology Madras, Madras, India
M.M. Ameen, P.K. Behera, S. Chatterjee, G. Dash, A. Dattamunsi, P. Jana, P. Kalbhor, S. Kamble, P.R. Pujahari, A.K. Sikdar, R.K. Singh, A. Swain, P. Verma, S. Verma, A. Vijay

Indian lnstitute of Science Education and Research Mohali, Mohali, India
A. Chauhan, S. Nayak, H. Rajpoot, B.K. Sirasva

Tata Institute of Fundamental Research-A, Mumbai, India
L. Bhatt, S. Dugad, T. Mishra, G.B. Mohanty, M. Shelake, P. Suryadevara

Tata Institute of Fundamental Research-B, Mumbai, India
A. Bala, S. Banerjee, S. Barman[38], R.M. Chatterjee, J. Chhikara, M. Guchait, S. Jain, A. Jaiswal, S. Kumar, M. Maity[38], G. Majumder, K. Mazumdar, L. Panwar[39], R. Pramanik, R. Saxena, P. Sharma, A. Thachayath

National Institute of Science Education and Research, Jatni, Khorda, Odisha 752050, India Homi Bhabha National Institute, Training School Complex, Anushakti Nagar, Mumbai 400094, India, Odisha, India
R. Kumar Agrawal, D. Maity[40], P. Mal, K. Naskar[40], A. Nayak[40], K. Pal, P. Sadangi, S. Shuchi, S.K. Swain, S. Varghese[40], D. Vats[40]

Indian Institute of Science Education and Research (IISER), Pune, India
S. Dube, P. Hazarika, A. Laha, R. Sharma, S. Sharma, K.Y. Vaish

Indian Institute of Technology Hyderabad, Telangana, India
C. Agrawal, B. Babu, S. Ghosh

Isfahan University of Technology, Isfahan, Iran
H. Bakhshiansohi[41], A. Jafari[42], V. Sedighzadeh Dalavi, M. Zeinali[43]

Institute for Research in Fundamental Sciences (IPM), Tehran, Iran
S. Bashiri, S. Chenarani[44], S.M. Etesami, Y. Hosseini, M. Khakzad, E. Khazaie, M. Mohammadi Najafabadi, M. Nourbakhsh, S. Tizchang[45]

University College Dublin, Dublin, Ireland
M. Felcini, M. Grunewald

INFN Sezione di Bari[a], Università di Bari[b], Politecnico di Bari[c], Bari, Italy
M. Abbrescia[a,b], M. Buonsante[a,b], A. Colaleo[a,b], D. Creanza[a,c], N. De Filippis[a,c], M. De Palma[a,b], W. Elmetenawee[a,b,17], N. Ferrara[a,c], L. Fiore[a], L. Generoso[a,b], L. Longo[a], M. Louka[a,b], G. Maggi[a,c], M. Maggi[a], S. My[a,b], F. Nenna[a,b], S. Nuzzo[a,b], A. Pellecchia[a,b], A. Pompili[a,b], F.M. Procacci[a,b], G. Pugliese[a,c], R. Radogna[a,b], D. Ramos[a], A. Ranieri[a], L. Silvestris[a], F.M. Simone[a,b], A. Stamerra[a,b], Ü. Sözbilir[a,46], F. Tenchini[a,b], D. Troiano[a,b], R. Venditti[a,b], P. Verwilligen[a], A. Zaza[a,b]

INFN Sezione di Bologna[a], Università di Bologna[b], Bologna, Italy
S. Balducci[a,b], C. Battilana[a,b], D. Bonacorsi[a,b], P. Capiluppi[a,b], F.R. Cavallo[a], M. Cruciani[a,b], M. Cuffiani[a,b], G.M. Dallavalle[a], T. Diotalevi[a,b], F. Fabbri[a], A. Fanfani[a,b], R. Farinelli[a], D. Fasanella[a], L. Ferragina[a,b], P. Giacomelli[a], C. Grandi[a], L. Guiducci[a,b], M. Lorusso[a,b], L. Lunerti[a], G. Masetti[a], F. Navarria[a,b], G. Paggi[a,b], A. Perrotta[a], A. Rossi[a,b], S. Rossi Tisbeni[a,b], T. Rovelli[a,b], G.P. Siroli[a,b]

INFN Sezione di Catania[a], Università di Catania[b], Catania, Italy
S. Costa[a,b,47], A. Di Mattia[a], A. Lapertosa[a], R. Potenza[a,b], A. Tricomi[a,b,47]

INFN Sezione di Firenze[a], Università di Firenze[b], Firenze, Italy
J. Altork[a,b], G. Barbagli[a], A. Calandri[a,b], B. Camaiani[a,b], A. Cassese[a], R. Ceccarelli[a], V. Ciulli[a,b], C. Civinini[a], R. D'Alessandro[a,b], L. Damenti[a,b], E. Focardi[a,b], T. Kello[a], G. Latino[a,b], P. Lenzi[a,b], M. Lizzo[a], M. Meschini[a], S. Paoletti[a], A. Papanastassiou[a,b], G. Sguazzoni[a], L. Viliani[a]

INFN Laboratori Nazionali di Frascati, Frascati, Italy
L. Benussi, S. Colafranceschi[48], S. Meola[49], D. Piccolo

INFN Sezione di Genova[a], Università di Genova[b], Genova, Italy
M. Alves Gallo Pereira[a], F. Ferro[a], E. Robutti[a], S. Tosi[a,b]

INFN Sezione di Milano-Bicocca[a], Università di Milano-Bicocca, Milano[b], Milano-Bicocca, Italy
A. Benaglia[a], F. Brivio[a], V. Camagni[a,b], F. De Guio[a,b], M.E. Dinardo[a,b], P. Dini[a], S. Gennai[a], R. Gerosa[a,b], A. Ghezzi[a,b], P. Govoni[a,b], L. Guzzi[a], G. Lavizzari[a,b], M.T. Lucchini[a,b], M. Malberti[a], S. Malvezzi[a], A. Massironi[a], L. Moroni[a], M. Paganoni[a,b], S. Palluotto[a,b], D. Pedrini[a], A. Perego[a,b], T. Tabarelli de Fatis[a,b]

INFN Sezione di Napoli[a], Università di Napoli 'Federico II'[b], Università della Basilicata (Potenza)[c], Scuola Superiore Meridionale (SSM)[d], Napoli, Italy
S. Buontempo[a], F. Confortini[a,b], C. Di Fraia[a,b], F. Fabozzi[a,c], A.O.M. Iorio[a,b], L. Lista[a,b,50], P. Paolucci[a,29], B. Rossi[a]

INFN Sezione di Padova[a], Università di Padova[b], Universita degli Studi di Cagliari[c], Padova, Italy
P. Azzi[a], N. Bacchetta[a,51], D. Bisello[a,b], L. Borella[a], P. Bortignon[a,c],

G. Bortolato[a,b], A.C.M. Bulla[a,c], R. Carlin[a,b], P. Checchia[a], T. Dorigo[a,52], F. Gasparini[a,b], U. Gasparini[a,b], P. Grutta[a], N. Lai[a], E. Lusiani[a], M. Margoni[a,b], A.T. Meneguzzo[a,b], M. Missiroli[a], J. Pazzini[a,b], F. Primavera[a,b], P. Ronchese[a,b], R. Rossin[a,b], F. Simonetto[a,b], M. Toffano[a], M. Tosi[a,b], A. Triossi[a,b], S. Ventura[a], M. Zanetti[a,b], P. Zotto[a,b], A. Zucchetta[a,b], G. Zumerle[a,b]

INFN Sezione di Pavia[a], Università di Pavia[b], Pavia, Italy
S. A. AbuZeid[a,20], C. Aimè[a], A. Braghieri[a], M. Brunoldi[a,b], P. Montagna[a,b], M. Pelliccioni[a,b], V. Re[a], C. Riccardi[a,b], P. Salvini[a], I. Vai[a,b], P. Vitulo[a,b]

INFN Sezione di Perugia[a], Università di Perugia[b], Perugia, Italy
S. Ajmal[a,b], M.E. Ascioti[a,b], G.M. Bilei[a], W.D. Buitrago Ceballos[a,b], C. Carrivale[a,b], D. Ciangottini[a,b], L. Della Penna[a,b], L. Fanò[a,b], V. Mariani[a,b], M. Menichelli[a], F. Moscatelli[a,53], F. Napolitano[a], A. Rossi[a,b], A. Santocchia[a,b], D. Spiga[a], T. Tedeschi[a,b]

INFN Sezione di Pisa[a], Università di Pisa[b], Scuola Normale Superiore di Pisa[c], Università di Siena[d], Pisa, Italy
C.A. Alexe[a,c], P. Asenov[a,b], P. Azzurri[a], G. Bagliesi[a], L. Bianchini[a,b], T. Boccali[a], E. Bossini[a], D. Bruschini[a,c], R. Castaldi[a], F. Cattafesta[a,c], M.A. Ciocci[a,d], M. Cipriani[a,b], R. Dell'Orso[a], S. Dhani[a,d], S. Donato[a,b], A. Feliziani[a,d], R. Forti[a,b], A. Giassi[a], F. Ligabue[a,c], A.C. Marini[a,b], A. Messineo[a,b], S. Mishra[a], V.K. Muraleedharan Nair Bindhu[a,b], S. Nandan[a], F. Palla[a], M. Riggirello[a,c], A. Rizzi[a,b], G. Rolandi[a,c], A. Scribano[a], P. Solanki[a,b], P. Spagnolo[a], R. Tenchini[a], G. Tonelli[a,b], N. Turini[a,d], F. Vaselli[a,c], A. Venturi[a], P.G. Verdini[a]

INFN Sezione di Roma[a], Sapienza Università di Roma[b], Roma, Italy
P. Akrap[a,b], S.C. Behera[a], F. Cavallari[a], L. Cunqueiro Mendez[a,b], F. De Riggi[a,b], D. Del Re[a,b], M. Del Vecchio[a,b], E. Di Marco[a], M. Diemoz[a], F. Errico[a], L. Frosina[a,b], R. Gargiulo[a,b], B. Harikrishnan[a,b], F. Lombardi[a,b], L. Martikainen[a,b], G. Organtini[a,b], N. Palmeri[a,b], R. Paramatti[a,b], T. Pauletto[a,b], S. Rahatlou[a,b], C. Rovelli[a], F. Santanastasio[a,b], L. Soffi[a], V. Vladimirov[a,b]

INFN Sezione di Torino[a], Università di Torino[b], Università del Piemonte Orientale (Novara)[c], Torino, Italy
N. Amapane[a,b], R. Arcidiacono[a,c], S. Argiro[a,b], M. Arneodo[a,c], N. Bartosik[a,c], F. Bashir[a,b], R. Bellan[a,b], A. Bellora[a,b], C. Biino[a], C. Borca[a,b], L. Bulaja[a,b], N. Cartiglia[a], M. Costa[a,b], R. Covarelli[a,b], N. Demaria[a], E. Ferrando[a,b], L. Finco[a], M. Grippo[a,b], B. Kiani[a,b], L. Lanteri[a,b], F. Luongo[a,b], C. Mariotti[a,54], S. Maselli[a], A. Mecca[a,b], L. Menzio[a,b], P. Meridiani[a], E. Migliore[a,b], M. Monteno[a], M.M. Obertino[a,b], G. Ortona[a], L. Pacher[a,b], N. Pastrone[a], M. Ruspa[a,c], F. Siviero[a,b], V. Sola[a,b], A. Solano[a,b], A. Staiano[a], C. Tarricone[a,b], M. Tornago[a,b], D. Trocino[a], G. Umoret[a,b], E. Vlasov[b], R. White[a,b]

INFN Sezione di Trieste[a], Università di Trieste[b], Trieste, Italy
J. Babbar[a,b,55], S. Belforte[a], V. Candelise[a,b], M. Casarsa[a], F. Cossutti[a], K. De Leo[a], G. Della Ricca[a,b], R. Delli Gatti[a,b], C. Giraldin[a,b]

Kyungpook National University, Daegu, Korea
S. Dogra, J. Hong, J. Kim, J. Kim, T. Kim, D. Lee, H. Lee, J. Lee, S.W. Lee, C.S. Moon, Y.D. Oh, S. Sekmen, B. Tae, Y.C. Yang

Department of Mathematics and Physics - Gangneung-Wonju National University,

Gangneung, Korea
M.S. Kim

Chonnam National University, Institute for Universe and Elementary Particles, Kwangju, Korea
G. Bak, P. Gwak, H. Kim, H. Lee, S. Lee, D.H. Moon, J. Seo

Department of Physics, Chung-Ang University, Seoul, Korea
K. Lee, Y. Lee

Hanyang University, Seoul, Korea
E. Asilar, F. Carnevali, J. Choi[56], T.J. Kim, Y. Ryou, J. Song, T. Yang

Korea University, Seoul, Korea
S. Ha, B.S. Hong, J. Kim, K. Lee, K. Lee, S. Lee, J. Padmanaban, B.A.N. Putra, J. Yoo

Kyung Hee University, Department of Physics, Seoul, Korea
J. Goh, J. Shin, S. Yang

Sejong University, Seoul, Korea
L. Kalipoliti, Y. Kang, H. Kim, Y. Kim, B. Ko, S. Lee

Seoul National University, Seoul, Korea
J. Choi, J. Choi, W. Jun, H. Kim, J. Kim, J. Kim, T. Kim, Y. Kim, Y.W. Kim, S. Ko, H. Lee, J. Lee, J. Lee, B.H. Oh, J. Shin, U. Yang, I. Yoon

University of Seoul, Seoul, Korea
W. Heo, W. Jang, D. Kim, S. Kim, Y. Roh, I. J. Watson

Yonsei University, Department of Physics, Seoul, Korea
S. Calzaferri, G. Cho, Y. Eo, K. Hwang, H. Jang, B. Kim, D. Kim, S. Kim, J.S.H. Lee, G. Mocellin, H.D. Yoo

Sungkyunkwan University, Suwon, Korea
Y. Lee, I. Yu

College of Engineering and Technology, American University of the Middle East (AUM), Dasman, Kuwait
T. Beyrouthy, Y. Gharbia

Kuwait University - College of Science - Department of Physics, Safat, Kuwait
F. Alazemi

Riga Technical University, Riga, Latvia
K. Dreimanis, O.M. Eberlins, A. Gaile, J.K. Heikkilä, M. Klevs, C. Munoz Diaz, D. Osite, G. Pikurs, R. Plese, M. Seidel, D. Sidiropoulos Kontos

University of Latvia (LU), Riga, Latvia
N.R. Strautnieks

Vilnius University, Vilnius, Lithuania
M. Ambrozas, A. Juodagalvis, S. Nargelas, S. Nayak, G. Tamulaitis

National Centre for Particle Physics, Universiti Malaya, Kuala Lumpur, Malaysia
I. Yusuff[57], Z. Zolkapli

University of Sonora (UNISON), Hermosillo, Mexico

J.P. Barajas Ibarria, J.F. Benitez, A. Castaneda Hernandez, A. Cota Rodriguez, L.E. Cuevas Picos, H.A. Encinas Acosta, L.G. Gallegos Maríñez, J.A. Murillo Quijada, L. Valencia Palomo

Centro de Investigacion y de Estudios Avanzados del IPN, Mexico City, Mexico
H. Castilla-Valdez, H. Crotte Ledesma, R. Lopez-Fernandez, J. Mejia Guisao, R. Reyes-Almanza, A. Sánchez Hernández

Universidad Iberoamericana, Mexico City, Mexico
C. Oropeza Barrera, D.L. Ramirez Guadarrama, M. Ramírez García

Benemerita Universidad Autonoma de Puebla, Puebla, Mexico
I. Bautista, F.E. Neri Huerta, I. Pedraza, H.A. Salazar Ibarguen, C. Uribe Estrada

University of Montenegro, Podgorica, Montenegro
I. Bubanja, J. Mijuskovic, N. Raicevic

National Centre for Physics, Quaid-I-Azam University, Islamabad, Pakistan
A. Ahmad, M.I. Asghar, A. Awais, M.I.M. Awan, W.A. Khan, I. Sohail

AGH University of Krakow, Krakow, Poland
Z. Abdy, V. Avati, L. Forthomme, L. Grzanka, M. Malawski, K. Piotrzkowski

National Centre for Nuclear Research, Swierk, Poland
H. Awedikian, M. Bluj, M. Ghimiray, M. Górski, M. Kazana, M. Szleper, P. Zalewski

Institute of Experimental Physics, Faculty of Physics, University of Warsaw, Warsaw, Poland
K. Bunkowski, K. Doroba, A. Kalinowski, M. Konecki, J. Krolikowski, W. Matyszkiewicz, A. Muhammad, S. Slawinski

Warsaw University of Technology, Warsaw, Poland
P. Fokow, K. Pozniak, W. Zabolotny

Laboratório de Instrumentação e Física Experimental de Partículas, Lisboa, Portugal
M. Araujo, C. Beirão Da Cruz E Silva, A. Boletti, M. Bozzo, T. Camporesi[54,58], G. Da Molin, M. Gallinaro, R. Guitton, J. Hollar, H. Legoinha, N. Leonardo[59], G.B. Marozzo, A. Petrilli, M. Pisano, J. Seixas, J. Varela, J.W. Wulff

Faculty of Physics, University of Belgrade, Belgrade, Serbia
P. Adzic, L. Markovic, P. Milenovic, V. Milosevic

Vinca Institute of Nuclear Science, Belgrade, Serbia
D. Devetak, M. Dordevic, J. Milosevic, L. Nadderd, V. Rekovic, M. Stojanovic

Centro de Investigaciones Energéticas Medioambientales y Tecnológicas (CIEMAT), Madrid, Spain
M. Alcalde Martinez, J. Alcaraz Maestre, J.A. Brochero Cifuentes, M. Cepeda, M. Cerrada, N. Colino, B. De La Cruz, A. Escalante Del Valle, C. Fernandez Bedoya, D. Fernández Del Val, J.P. Fernández Ramos, J. Flix, M.C. Fouz, C. Garcia Sanchez, M. Gonzalez Hernandez, O. Gonzalez Lopez, S. Goy Lopez, J.M. Hernandez, M.I. Josa, J. Llorente Merino, O. Manzanilla, C. Martin Perez, E. Martin Viscasillas, D. Moran, C.M. Morcillo Perez, Á. Navarro Tobar, J. Puerta Pelayo, A.M. Pérez-Calero Yzquierdo, I. Redondo, D.D. Redondo Ferrero, E. Sanchez Berenguer, J. Vazquez Escobar

Universidad Autónoma de Madrid, Madrid, Spain
J.F. de Trocóniz

Universidad de Oviedo, Instituto Universitario de Ciencias y Tecnologías Espaciales de Asturias (ICTEA), Oviedo, Spain
E. Aller Gutierrez, B. Alvarez Gonzalez, J. Ayllon Torresano, A. Cardini, J. Cuevas, J. Del Riego Badas, D. Estrada Acevedo, J. Fernandez Menendez, S. Folgueras, L. Garcia Diaz, I. Gonzalez Caballero, P. Leguina, M. Obeso Menendez, E. Palencia Cortezon, J. Prado Pico, S. Sanchez Cruz, A. Soto Rodríguez, P. Vischia

Instituto de Física de Cantabria (IFCA), CSIC-Universidad de Cantabria, Santander, Spain
S. Blanco Fernández, I.J. Cabrillo, A. Calderon, M. Caserta, J. Duarte Campderros, M. Fernandez, G. Gomez, A. Gomez Carrera, C. Lasaosa García, R. Lopez Ruiz, C. Martinez Rivero, P. Martinez Ruiz del Arbol, F. Matorras, P. Matorras Cuevas, E. Navarrete Ramos, J. Piedra Gomez, C. Quintana San Emeterio, V. Rodriguez, L. Scodellaro, I. Vila, R. Vilar Cortabitarte, J.M. Vizan Garcia

University of Colombo, Colombo, Sri Lanka
B. Kailasapathy[60]

University of Ruhuna, Department of Physics, Matara, Sri Lanka
W.G. Dharmaratna[61], N. Perera

CERN, European Organization for Nuclear Research, Geneva, Switzerland
D. Abbaneo, C. Amendola, R. Ardino, E. Auffray, J. Baechler, G. Bardelli, D. Barney, J. Bendavid, I. Bestintzanos, M. Bianco, A. Bocci, G. Boldrini, L. Borgonovi, C. Botta, A. Bragagnolo, C.E. Brown, C. Caillol, G. Cerminara, P. Connor, K. Cormier, D. D'Enterria, A. Dabrowski, P. Das, A. David Tinoco Mendes, M.M. Defranchis, M. Deile, M. Dobson, L. Favilla, P.J. Fernández Manteca, E. Fialova, B.A. Fontana Santos Alves, E. Fontanesi, W. Funk, A. Gaddi, S. Giani, D. Gigi, K. Gill, S. Giorgetti, F. Glege, M. Glowacki, A. Gruber, J. Hegeman, R. Hofsaess, B. Huber, T. James, P. Janot, L. Jeppe, O. Kaluzinska, O. Karacheban[27], G. Karathanasis, S. Laurila, P. Lecoq, E. Leutgeb, J. León Holgado, C. Lourenco, A.m. Lyon, M. Magherini, L. Malgeri, E. Manca, M. Mannelli, F. Meijers, J.A. Merlin, S. Mersi, E. Meschi, M. Migliorini, F. Monti, F. Moortgat, M.C. Muehlnikel, M. Mulders, M. Musich, I. Neutelings, S. Orfanelli, F. Pantaleo, M. Pari, F. Pereira Carneiro, G. Petrucciani, A. Pfeiffer, M. Pierini, M. Pitt, H. Qu, W. Redjeb, A. Reimers, B. Ribeiro Lopes, F. Riti, P. Rosado, M. Rovere, H. Sakulin, R. Salvatico, S. Scarfi, S.F. Schaefer, M. Selvaggi, P. Silva, P. Sphicas[62], A.G. Stahl Leiton, A. Steen, S. Summers, G. Terragni, D. Treille, P. Tropea, E. Vernazza, M. Vojinovic, J. Wanczyk[63], S. Wuchterl, M. Zarucki, P. Zehetner, P. Zejdl, G. Zevi Della Porta

PSI Center for Neutron and Muon Sciences, Villigen, Switzerland
L. Caminada[64], W. Erdmann, R. Horisberger, Q. Ingram, H.C. Kaestli, D. Kotlinski, C. Lange, U. Langenegger, A. Nigamova, L. Noehte[64], L. Redard-Jacot[64], T. Rohe, A. Samalan

ETH Zurich - Institute for Particle Physics and Astrophysics (IPA), Zurich, Switzerland
T.K. Aarrestad, M. Backhaus, A. Belvedere, T. Bevilacqua[64], G. Bonomelli, K. Datta, P. De Bryas Dexmiers D'Archiacchiac[63], A. De Cosa, G. Dissertori, M. Dittmar, M. Donegà, F. Glessgen, C. Grab, T.G. Harte, N. Härringer, B. Kaynak, M. Koppel, W. Lustermann, M. Malucchi, R.A. Manzoni, L. Marchese,

F. Nessi-Tedaldi, F. Pauss, A.A. Petre, J. Prendi, B. Ristic, S. Rohletter, P.M. Sander, R. Seidita, A. Tarabini, C.Z. Tee, D. Valsecchi, P.H. Wagner, R. Wallny

Universität Zürich, Zurich, Switzerland
C. Amsler[65], F. Bilandzija, P. Bärtschi, M.F. Canelli, G. Celotto, Z. Ghafoor, T.A. Goldschmidt, V. Guglielmi, A. Jofrehei, B. Kilminster, T.H. Kwok, S. Leontsinis, V. Lukashenko, A. Macchiolo, F. Meng, J. Motta, P. Robmann, E. Shokr, F. Stäger, R. Tramontano, P. Viscone

Çukurova University, Adana, Türkiye
D. Agyel, F. Dolek, I. Dumanoglu[66], Y. Guler[67], E. Gurpinar Guler[67], A. Kayis Topaksu, G. Onengut, K. Ozdemir[68], B. Tali[69], U.G. Tok, E. Uslan

Hacettepe University, Ankara, Türkiye
S. Sen

Bogazici University, Istanbul, Türkiye
B. Akgun, I.O. Atakisi[70], E. Gülmez, M. Kaya[71], O. Kaya[72], M.A. Sarkisla[73], S. Tekten[74]

Istanbul Technical University, Istanbul, Türkiye
D. Boncukcu, A. Cakir, K. Cankocak[66,75], M. Gumustekin, A.D. Gungordu

Istanbul University, Istanbul, Türkiye
B. Hacisahinoglu, I. Hos[76], S. Ozkorucuklu, O. Potok, H. Sert, C. Simsek, C. Zorbilmez

Yildiz Technical University, Istanbul, Türkiye
S. Cerci, C. Dozen[77], E. Iren[78], B. Isildak, E. Simsek, D. Sunar Cerci, T. Yetkin[77]

National Central University, Chung-Li, Taiwan
D. Bhowmik, Y.h. Chou, C.M. Kuo, P.K. Rout, S. Taj, P.C. Tiwari[39]

National Taiwan University (NTU), Taipei, Taiwan
L. Ceard, K.F. Chen, Z.g. Chen, A. De Iorio, G.W.S. Hou, H.w. Hsia, T.h. Hsu, S. Karmakar, F. Khuzaimah, G. Kole, Y.y. Li, R.S. Lu, E. Paganis, X.f. Su, J. Thomas-Wilsker, L.s. Tsai, D. Tsionou, H.y. Wu, E. Yazgan

High Energy Physics Research Unit, Department of Physics, Faculty of Science, Chulalongkorn University, Bangkok, Thailand
C. Asawatangtrakuldee, N. Srimanobhas

Tunis El Manar University, Tunis, Tunisia
Y. Maghrbi

Institute for Scintillation Materials of National Academy of Science of Ukraine, Kharkiv, Ukraine
O. Dadazhanova, B. Grynyov

National Science Centre, Kharkiv Institute of Physics and Technology, Kharkiv, Ukraine
K. Klimenko, O. Kurov, L. Levchuk, S. Lukyanenko, A. Pristavka, D. Soroka

University of Bristol, Bristol, United Kingdom
J.J. Brooke, A. Bundock, F.J.J. Bury, E. Clement, D. Cussans, D. Dharmender, H. Flacher, J. Goldstein, H.F. Heath, M.l. Holmberg, A. Karakoulaki, L. Kreczko, S. Paramesvaran, L. Robertshaw, M.S. Sanjrani[41], J. Segal, V.J. Smith

Rutherford Appleton Laboratory, Didcot, United Kingdom
A. Ball, K.W. Bell, A. Belyaev[79], C. Brew, R.M. Brown, D.J. Cockerill, A. Elliot, K.V. Ellis, J. Gajownik, K. Harder, S. Harper, J. Linacre, K. Manolopoulos, M. Moallemi, D.M. Newbold, E. Olaiya, D. Petyt, T. Reis, A.R. Sahasransu, T. Schuh, C. Shepherd-Themistocleous, I.R. Tomalin, K.C. Whalen, T. Williams

Imperial College, London, United Kingdom
I. Andreou, S. Awan, R. Bainbridge, P. Bloch, O. Buchmuller, C.A. Carrillo Montoya, D. Colling, A. Cox, I. Das, P. Dauncey, G. Davies, A. De Roeck, M. Della Negra, S. Fayer, G. Fedi, G. Hall, H.R. Hoorani, A. Howard, G. Iles, C.R. Knight, P. Krueper, J. Langford, K.H. Law, L. Lyons, A.M. Magnan, B. Maier, S. Mallios, A. Mastronikolis, J. Nash[80], M. Pesaresi, P.B. Pradeep, E.V. Protopapa, B.C. Radburn-Smith, A. Richards, A. Rose, T.B. Runting, L. Russell, K. Savva, R. Schmitz, C. Seez, R. Shukla, A. Tapper, T. Travis, K. Uchida, G.P. Uttley, T. Virdee[29], N. Wardle, D. Winterbottom, J. Xiao

Brunel University, Uxbridge, United Kingdom
J. Cole, L. Juckett, A. Khan, P. Kyberd, I. Reid

The University of Alabama, Tuscaloosa, Alabama, USA
B. Bam, A. Buchot Perraguin, S. Campbell, R. Chudasama, S. Cooper, C. Crovella, G. Fidalgo, S.V. Gleyzer, R. Kaur, A. Khukhunaishvili, K. Matchev, E. Pearson, P. Rumerio[81], E. Usai

University of California, Davis, Davis, California, USA
S. Abbott, S. Baradia, B. Barton, R. Breedon, H. Cai, M. Calderon De La Barca Sanchez, E. Cannaert, M. Chertok, M. Citron, J. Conway, P.T. Cox, F. Eble, R. Erbacher, C. Fairchild, O. Kukral, S. Ostrom, I. Salazar Segovia, J.H. Steenis, J.S. Tafoya Vargas, W. Wei, S. Yoo

University of California, San Diego, La Jolla, California, USA
A. Aportela, A. Arora, J.G. Branson, S. Cittolin, B. D'Anzi, D. Diaz, J. Duarte, L. Giannini, Y. Gu, J. Guiang, V. Krutelyov, R. Lee, J. Letts, H. Li, R. Marroquin Solares, M. Masciovecchio, F. Mokhtar, S. Morovic, S. Mukherjee, M. Pieri, D. Primosch, M. Quinnan, V. Sharma, M. Tadel, E. Vourliotis, F. Würthwein, A. Yagil, Z. Zhao

University of California, Los Angeles, California, USA
K. Adamidis, H. Ancelin, M. Bachtis, D. Campos, R. Cousins, S. Crossley, G. Flores Avila, J. Hauser, M. Ignatenko, M.A. Iqbal, T. Lam, Y.f. Lo, A. Nunez Del Prado, D. Saltzberg, V. Valuev

California Institute of Technology, Pasadena, California, USA
A. Albert, S. Bhattacharya, A. Bornheim, O. Cerri, Z. Hao, R. Kansal, L. Mori, H.B. Newman, G. Reales Gutiérrez, T. Sievert, P. Simmerling, E. Sledge, M. Spiropulu, C. Sun, J.R. Vlimant, R.A. Wynne, S. Xie, R.Y. Zhu

University of California, Riverside, Riverside, California, USA
R. Clare, J.W. Gary, G. Hanson

University of California, Santa Barbara - Department of Physics, Santa Barbara, California, USA
A. Barzdukas, L. Brennan, C. Campagnari, S. Carron Montero[82], K. Downham, C. Grieco, J.S. Guo, M.M. Hussain, D. Imani, J. Incandela, A. Krishna, M.W.K. Lai,

P. Masterson, J.J.H. Ockenfuss, J. Richman, S.N. Santpur, D. Stuart, T.Á. Vámi, X. Yan, D. Zhang

University of Colorado Boulder, Boulder, Colorado, USA
J.P. Cumalat, W.T. Ford, J. Fraticelli, A. Hart, M. Herrmann, S. Kwan, J. Pearkes, N. Schonbeck, K. Stenson, K. Ulmer, S.R. Wagner, N. Zipper, D. Zuolo

The Catholic University of America, Washington, DC, USA
R. Bartek, A. Dominguez, S. Raj, B. Sahu, A.E. Simsek, B. Singhal, S.S. Yu

University of Florida, Gainesville, Florida, USA
C. Aruta, P. Avery, C. Basile, D. Bourilkov, P. Chang, V. Cherepanov, M. Dittrich, R.D. Field, C. Huh, E. Koenig, M. Kolosova, J. Konigsberg, A. Korytov, G. Mitselmakher, K. Mohrman, A. Muthirakalayil Madhu, N. Rawal, S. Rosenzweig, Y. Takahashi, J. Wang

Florida Institute of Technology, Melbourne, Florida, USA
B. Alsufyani, S. Das, S. Demarest, L. Hasa, M. Hohlmann, M. Lavinsky, E. Yanes

Florida State University, Tallahassee, Florida, USA
T. Adams, A. Al Kadhim, D. Alam, A. Askew, S. Bower, R. Goff, R. Hashmi, A. Hassani, T. Kolberg, G. Martinez, M. Mazza, H. Prosper, P.R. Prova, R. Yohay

Fermi National Accelerator Laboratory, Batavia, Illinois, USA
M. Albrow, M. Alyari, O. Amram, G. Apollinari, A. Apresyan, L.A. Bauerdick, D. Berry, J. Berryhill, P.C. Bhat, K. Burkett, J.N. Butler, A. Canepa, G.B. Cerati, H. Cheung, F. Chlebana, C. Cosby, G. Cummings, I. Dutta, V.D. Elvira, J. Freeman, A. Gandrakota, Z. Gecse, L. Gray, D. Green, A. Grummer, S. Grünendahl, D. Guerrero, O. Gutsche, R.M. Harris, J. Hirschauer, V. Innocente, B. Jayatilaka, S. Jindariani, M. Johnson, R.S. Kim, S. Lammel, D. Lincoln, R. Lipton, T. Liu, K. Maeshima, D. Mason, P. McBride, P. Merkel, S. Mrenna, S. Nahn, J. Ngadiuba, D. Noonan, S. Norberg, V. Papadimitriou, N. Pastika, K. Pedro, C. Pena[83], C.E. Perez Lara, V. Perovic, F. Ravera, A. Reinsvold Hall[84], L. Ristori, M. Safdari, E. Sexton-Kennedy, E. Smith, N. Smith, A. Soha, L. Spiegel, S. Stoynev, J. Strait, L. Taylor, S. Tkaczyk, N.V. Tran, L. Uplegger, E.W. Vaandering, C. Wang, I. Zoi

University of Illinois Chicago, Chicago, Illinois, USA
M.R. Adams, N. Barnett, A. Baty, C. Bennett, N. Brandman-hughes, R. Cavanaugh, S.J. Das, R. Escobar Franco, O. Evdokimov, C.E. Gerber, H. Gupta, M. Hawksworth, A. Hingrajiya, D.J. Hofman, Z. Huang, J.h. Lee, C. Mills, S. Nanda, G. Nigmatkulov, B. Ozek, V. Pant, T. Phan, D. Pilipovic, R. Pradhan, E. Prifti, T. Roy, D. Shekar, N. Singh, F. Strug, A. Thielen, M. Tonjes, N. Varelas, M.A. Wadud, A. Wang, J. Yoo

Northwestern University, Evanston, Illinois, USA
S. Dittmer, K.A. Hahn, S. King, D. Li, M. Mcginnis, Y. Miao, D.G. Monk, M.H. Schmitt, A. Taliercio, M. Velasco, J. Wang, D. Wilbern

Purdue University Northwest, Hammond, Indiana, USA
N. Parashar, A. Pathak, E. Shumka

University of Notre Dame, Notre Dame, Indiana, USA
G. Agarwal, R. Band, S. Castells, A. Das, A. Datta, A. Ehnis, R. Goldouzian,

M. Hildreth, T. Ivanov, C. Jessop, K. Lannon, J. Lawrence, D. Lutton, J. Mariano, N. Marinelli, P. Mastrapasqua, A. Masud, T. McCauley, C. Mcgrady, C. Moore, Y. Musienko[23], H. Nelson, M. Osherson, A. Piccinelli, R. Ruchti, A. Townsend, Y. Wan, M. Wayne, H. Yockey

Purdue University, West Lafayette, Indiana, USA
S. Chandra, A. Gu, L. Gutay, L. He, M. Huwiler, M. Jones, A.W. Jung, I.G. Karslioglu, D. Kondratyev, J. Li, M. Liu, M. Macedo, G. Negro, N. Neumeister, G. Paspalaki, S. Piperov, N.R. Saha, J.F. Schulte, R. Sharma, F. Wang, A.L. Wesolek, A. Wildridge, W. Xie, Y. Yao, Y. Zhong

The University of Iowa, Iowa City, Iowa, USA
M. Alhusseini, D. Blend, K. Dilsiz[85], O.K. Köseyan, A. Mestvirishvili[58], O. Neogi, H. Ogul[86], Y. Onel, A. Penzo, C. Snyder

The University of Kansas, Lawrence, Kansas, USA
A. Abreu, L.F. Alcerro Alcerro, J. Anguiano, S. Arteaga Escatel, P. Baringer, A. Bean, R. Bhattacharya, M. Chukwuka, Z. Flowers, D. Grove, J. King, G. Krintiras, M. Lazarovits, C. Le Mahieu, J. Marquez, M. Murray, M. Nickel, E. Reynolds, C. Rogan, C. Royon, S. Rudrabhatla, S. Sanders, J.A. Velazquez Corral, G. Wilson

Kansas State University, Manhattan, Kansas, USA
A. Ahmad, B. Allmond, N. Islam, A. Ivanov, K. Kaadze, Y. Maravin, J. Natoli, G.G. Reddy, D. Roy, G. Sorrentino

Johns Hopkins University, Baltimore, Maryland, USA
B. Blumenfeld, J. Davis, A. Gritsan, Z. Huang, L. Kang, P. Maksimovic, N. Pinto, M. Roguljic, S. Sekhar, M.V. Srivastav, M. Swartz

University of Maryland, College Park, Maryland, USA
Z. Alton, D. Baden, A. Belloni, J. Bistany-riebman, S.C. Eno, N.J. Hadley, S. Jabeen, R.G. Kellogg, T. Koeth, B. Kronheim, J. Lee, P. Major, A. Mignerey, C. Palmer, C. Papageorgakis, M.M. Paranjpe, E. Popova[87], A. Shevelev, M. Wrotny, L. Zhang

Boston University, Boston, Massachusetts, USA
S. Cholak, Z. Demiragli, C. Erice, C. Fangmeier, C. Fernandez Madrazo, J. Fulcher, J. Garcia De Castro, F. Golf, S. Jeon, G. Linney, J. O'Cain, I. Reed, J. Rohlf, D. Sperka, I. Suarez, A. Tsatsos, E. Wurtz, A.G. Zecchinelli

Northeastern University, Boston, Massachusetts, USA
A. Aarif, G. Alverson, E. Barberis, S. Bein, J. Bonilla, B. Bylsma, M. Campana, R. Clark, Y. Han, I. Israr, M. Lu, N. Manganelli, R. Mccarthy, D.M. Morse, T. Orimoto, L. Skinnari, C.S. Thoreson, E. Tsai, D. Wood

Massachusetts Institute of Technology, Cambridge, Massachusetts, USA
C. Baldenegro Barrera, H. Bossi, S. Bright-Thonney, I.A. Cali, Y.c. Chen, P.c. Chou, M. D'Alfonso, K. Devereaux, J. Eysermans, C. Freer, G. Gomez Ceballos, M. Goncharov, G. Grosso, P. Harris, D. Hoang, A. Holtermann, G.M. Innocenti, K. Ivanov, G. Kopp, D. Kovalskyi, J. Lang, L. Lavezzo, Y.J. Lee, P. Lugato, C. Mcginn, E. Moreno, A. Novak, M.I. Park, C. Paus, C. Reissel, C. Roland, G. Roland, S. Rothman, T.a. Sheng, G. Stephans, D. Walter, J. Wang, Z. Wang, B. Wyslouch, T. Yang, K. Yoon

Wayne State University, Detroit, Michigan, USA
P.E. Karchin

University of Minnesota, Minneapolis, Minnesota, USA
A. Alpana, B. Crossman, W.J. Jackson, C. Kapsiak, D. Mahon, J. Mans, B. Marzocchi, R. Rusack, O. Sancar, R. Saradhy, N. Strobbe

Bethel University, St. Paul, Minnesota, USA
J.M. Hogan

University of Nebraska-Lincoln, Lincoln, Nebraska, USA
K. Bloom, D.R. Claes, S.V. Dixit, G. Haza, J. Hossain, C. Joo, I. Kravchenko, K.H.M. Kwok, Y. Mehra, J. Morris, A. Rohilla, J.E. Siado, A. Vagnerini, A. Wightman

Rutgers, The State University of New Jersey, Piscataway, New Jersey, USA
B. Chiarito, J.P. Chou, S. Donnelly, D. Gadkari, Y. Gershtein, E. Halkiadakis, C. Houghton, D. Jaroslawski, A. Kaur, A. Kobert, A. Lath, J. Martins, P. Meltzer, M. Perez Prada, K. Ramdin, B. Rand, J. Reichert, P. Saha, S. Salur, S. Somalwar, R. Stone, S.A. Thayil, S. Thomas, J. Vora

Princeton University, Princeton, New Jersey, USA
H. Bouchamaoui, G. Dezoort, P. Elmer, A. Frankenthal, M. Galli, B. Greenberg, K. Kennedy, Y. Lai, D. Lange, A. Loeliger, D. Marlow, I. Ojalvo, J. Olsen, F. Simpson, D. Stickland, C. Tully, S. Yoon

State University of New York at Buffalo, Buffalo, New York, USA
H. Bandyopadhyay, I. Iashvili, A. Kalogeropoulos, A. Kharchilava, A. Mandal, C. McLean, D. Nguyen, O. Poncet, S. Rappoccio, H. Rejeb Sfar, W. Terrill, D. Yu

Cornell University, Ithaca, New York, USA
J. Alexander, X. Chen, G. De Castro, J. Dickinson, A. Duquette, J. Fan, X. Fan, J. Grassi, P. Kotamnives, K. Krzyzanska, J. Monroy, G. Niendorf, M. Oshiro, J.R. Patterson, A. Ryd, J. Thom, H.A. Weber, B. Weiss, P. Wittich, Y. Wu, R. Zou, L. Zygala

University of Rochester, Rochester, New York, USA
A. Bodek, R. Demina, A. Garcia-Bellido, H.S. Hare, O. Hindrichs, Y.w. Kao, N. Parmar, P. Parygin[87], H. Seo, R. Taus, Y.h. Yu

The Ohio State University, Columbus, Ohio, USA
M. Carrigan, R. De Los Santos, L.S. Durkin, C. Hill, M. Joyce, L. Nestor, D.A. Wenzl, B.L. Winer, B. Yates

Carnegie Mellon University, Pittsburgh, Pennsylvania, USA
J. Alison, S. An, M. Cremonesi, V. Dutta, E.Y. Ertorer, T. Ferguson, T.A. Gómez Espinosa, A. Harilal, A. Kallil Tharayil, M. Kanemura, A. Khanal, C. Liu, M. Marchegiani, P. Meiring, S. Murthy, P. Palit, K. Park, M. Paulini, A. Roberts, Y. Zhou

University of Puerto Rico, Mayaguez, Puerto Rico, USA
S. Malik, R. Sharma

Brown University, Providence, Rhode Island, USA
G. Barone, G. Benelli, D. Cutts, S. Ellis, S. Gottlieb, L. Gouskos, M. Hadley,

L. Hay, U. Heintz, K.W. Ho, R. Jain, T. Kwon, L. Lambrecht, G. Landsberg, K.T. Lau, M. LeBlanc, J. Luo, S. Mondal, J. Roloff, T. Russell, S. Sagir[88], X. Shen, M. Stamenkovic, S. Sunnarborg, J. Tang, N. Venkatasubramanian

University of Tennessee, Knoxville, Tennessee, USA
A. Abdelhamid, D. Ally, A.G. Delannoy, J. Dervan, S. Fiorendi, J. Harris, T. Holmes, A.R. Kanuganti, N. Karunarathna, J. Lawless, L. Lee, E. Nibigira, B. Skipworth, S. Spanier, C. Thompson, A. Vendrasco

Vanderbilt University, Nashville, Tennessee, USA
U. Acharya, E. Appelt, Y. Chen, S. Greene, A. Gurrola, W. Johns, R. Kunnawalkam Elayavalli, A. Melo, D. Rathjens, F. Romeo, I. Shvetsov, S. Tuo, J. Velkovska, J. Zhang

Texas A&M University, College Station, Texas, USA
D. Aebi, M. Ahmad, T. Akhter, K. Androsov, A. Basnet, A. Bolshov, O. Bouhali[89], A. Cagnotta, S. Cooperstein, V. D'Amante, R. Eusebi, P. Flanagan, J. Gilmore, Y. Guo, T. Kamon, R. Mueller, G. Pizzati, A. Safonov

Rice University, Houston, Texas, USA
D. Acosta, A. Agrawal, C. Arbour, T. Carnahan, K.M. Ecklund, F.J. Geurts, I. Krommydas, N. Lewis, W. Li, J. Lin, X. Liu, C. Loizides, O. Miguel Colin, B.P. Padley, R. Redjimi, J. Rotter, C. Vico Villalba, M. Wulansatiti, E. Yigitbasi, Y. Zhang

Texas Tech University, Lubbock, Texas, USA
N. Akchurin, J. Damgov, Y. Feng, N. Gogate, W. Jin, S.W. Lee, C. Madrid, S. Magedov, A. Mankel, T. Peltola, I. Volobouev

Baylor University, Waco, Texas, USA
S. Abdullin, A. Brinkerhoff, E. Collins, M.R. Darwish, J. Dittmann, K. Hatakeyama, V. Hegde, J. Hiltbrand, B. McMaster, J. Samudio, S. Sawant, C. Sutantawibul, J. Wilson

University of Virginia, Charlottesville, Virginia, USA
B. Cardwell, H. Chung, B. Cox, J. Hakala, G. Hamilton Ilha Machado, R. Hirosky, M. Jose, A. Ledovskoy, C. Mantilla, R. Menon Raghunandanan, C. Neu, C. Ramón Álvarez, Z. Wu

University of Wisconsin - Madison, Madison, Wisconsin, USA
A. Aravind, S. Banerjee, K. Black, T. Bose, E. Chavez, R. Cruz, S. Dasu, P. Everaerts, C. Galloni, H. He, M. Herndon, A. Herve, C.K. Koraka, S. Lomte, R. Loveless, J. Marquez, A. Mohammadi, S. Mondal, T. Nelson, G. Parida, D. Pinna, A. Savin, V. Sharma, R. Simeon, W.H. Smith, D. Teague, M. Thakore, A. Thete, A. Warden

Authors affiliated with an international laboratory covered by a cooperation agreement with CERN
S. Afanasiev, V. Alexakhin, Y. Andreev, D. Budkouski, R. Chistov, M. Danilov, T. Dimova, I. Gorbunov, A. Kamenev, V. Karjavine, O. Kodolova[90], V. Korenkov, I. Korsakov, A. Kozyrev, A. Lanev, A. Malakhov, V. Matveev, A. Nikitenko[91,90], V. Palichik, V. Perelygin, S. Polikarpov, O. Radchenko, M. Savina, V. Shalaev, S. Shmatov, S. Shulha, Y. Skovpen, K. Slizhevskiy, V. Smirnov, O. Teryaev, A. Toropin, N. Voytishin, A. Zarubin, I. Zhizhin

Authors affiliated with an institute formerly covered by a cooperation agreement with CERN
L. Dudko, V. Kim[23], V. Murzin, V. Oreshkin, D. Sosnov

[1]Also at Yerevan State University, Yerevan, Armenia
[2]Also at Technische Universität Wien, Vienna, Austria
[3]Also at Ghent University, Ghent, Belgium
[4]Also at Istanbul NişantaşıUniversity, Istanbul, Türkiye
[5]Also at FACAMP - Faculdades de Campinas, Sao Paulo, Brazil
[6]Also at Universidade Estadual de Campinas, Campinas, Brazil
[7]Also at Federal University of Rio Grande do Sul, Porto Alegre, Brazil
[8]Also at The University of the State of Amazonas, Manaus, Brazil
[9]Also at University of Chinese Academy of Sciences, Beijing, China
[10]Also at University of Chinese Academy of Sciences, Beijing, China
[11]Also at School of Physics, Zhengzhou University, Zhengzhou, China
[12]Now at Henan Normal University, Xinxiang, China
[13]Also at University of Shanghai for Science and Technology, Shanghai, China
[14]Also at The University of Iowa, Iowa City, Iowa, USA
[15]Also at Nanjing Normal University, Nanjing, China
[16]Also at Center for High Energy Physics, Peking University, Beijing, China, Beijing, China
[17]Also at Helwan University, Cairo, Egypt
[18]Also at Zewail City of Science and Technology, Zewail, Egypt
[19]Also at British University in Egypt, Cairo, Egypt
[20]Now at Ain Shams University, Cairo, Egypt
[21]Also at Université de Haute Alsace, Mulhouse, France
[22]Also at Purdue University, West Lafayette, Indiana, USA
[23]Also at an institute formerly covered by a cooperation agreement with CERN
[24]Also at University of Hamburg, Hamburg, Germany
[25]Also at RWTH Aachen University, III. Physikalisches Institut A, Aachen, Germany
[26]Also at Bergische University Wuppertal (BUW), Wuppertal, Germany
[27]Also at Brandenburg University of Technology, Cottbus, Germany
[28]Also at Institute for Advanced Simulation - Jülich Supercomputing Centre, Juelich, Germany
[29]Also at CERN, European Organization for Nuclear Research, Geneva, Switzerland
[30]Also at HUN-REN ATOMKI - Institute of Nuclear Research, Debrecen, Hungary
[31]Now at Universitatea Babes-Bolyai - Facultatea de Fizica, Cluj-Napoca, Romania
[32]Also at MTA-ELTE Lendület CMS Particle and Nuclear Physics Group, Eötvös Loránd University, Budapest, Hungary
[33]Also at HUN-REN Wigner Research Centre for Physics, Budapest, Hungary
[34]Also at Physics Department, Faculty of Science, Assiut University, Assiut, Egypt
[35]Also at The University of Kansas, Lawrence, Kansas, USA
[36]Also at Punjab Agricultural University, Ludhiana, India
[37]Also at University of Hyderabad, Hyderabad, India
[38]Also at University of Visva-Bharati, Santiniketan, India
[39]Also at Indian Institute of Science (IISC), Bangalore, India
[40]Also at Institute of Physics, Bhubaneswar, India
[41]Also at Deutsches Elektronen-Synchrotron, Hamburg, Germany
[42]Also at Isfahan University of Technology, Isfahan, Iran
[43]Also at Sharif University of Technology, Tehran, Iran
[44]Also at Department of Physics, University of Science and Technology of Mazandaran, Behshahr, Iran
[45]Also at Department of Physics, Faculty of Science, Arak University, ARAK, Iran

[46]Also at Kocaeli University, Kocaeli, Türkiye
[47]Also at Centro Siciliano di Fisica Nucleare e di Struttura della Materia, Catania, Italy
[48]Also at James Madison University, Harrisonburg, Virginia, USA
[49]Also at Università degli Studi Guglielmo Marconi, Roma, Italy
[50]Also at Scuola Superiore Meridionale, Università di Napoli 'Federico II', Napoli, Italy
[51]Also at Fermi National Accelerator Laboratory, Batavia, Illinois, USA
[52]Also at Lulea University of Technology, Lulea, Sweden
[53]Also at Consiglio Nazionale delle Ricerche - Istituto Officina dei Materiali, Perugia, Italy
[54]Also at Boston University, Boston, Massachusetts, USA
[55]Also at UPES - University of Petroleum and Energy Studies, Dehradun, India
[56]Also at Institut de Physique des 2 Infinis de Lyon (IP2I), Villeurbanne, France
[57]Also at Department of Applied Physics, Faculty of Science and Technology, Universiti Kebangsaan Malaysia, Bangi, Malaysia
[58]Also at Georgian Technical University, Tbilisi, Georgia
[59]Also at Departamento de Física Instituto Superior Técnico Universidade de Lisboa, Lisbon, Portugal
[60]Also at Trincomalee Campus, Eastern University, Sri Lanka, Nilaveli, Sri Lanka
[61]Also at Saegis Campus, Nugegoda, Sri Lanka
[62]Also at National and Kapodistrian University of Athens, Athens, Greece
[63]Also at Ecole Polytechnique Fédérale Lausanne, Lausanne, Switzerland
[64]Also at Universität Zürich, Zurich, Switzerland
[65]Also at Stefan Meyer Institute for Subatomic Physics (SMI), Vienna, Austria
[66]Also at Near East University, Research Center of Experimental Health Science, Mersin, Türkiye
[67]Also at Konya Technical University, Konya, Türkiye
[68]Also at Izmir Bakircay University Faculty of Engineering and Architecture, Izmir, Türkiye
[69]Also at Adiyaman University, Adiyaman, Türkiye
[70]Also at Istanbul Sabahattin Zaim University, Istanbul, Türkiye
[71]Also at Marmara University, Istanbul, Türkiye
[72]Also at Milli Savunma University, Naval Academy, Istanbul, Türkiye
[73]Also at The Science and Technological research Council of Türkiye, Informatics and Information Security Research Center, Gebze/Kocaeli, Türkiye
[74]Also at Kafkas University, Kars, Türkiye
[75]Now at Istanbul Okan University, Istanbul, Türkiye
[76]Also at Istanbul University - Cerrahpasa, Faculty of Engineering, Istanbul, Türkiye
[77]Also at Istinye University, Istanbul, Türkiye
[78]Also at Mimar Sinan University, Istanbul, Istanbul, Türkiye
[79]Also at School of Physics and Astronomy, University of Southampton, Southampton, United Kingdom
[80]Also at Monash University, Faculty of Science, Clayton, Australia
[81]Also at Università di Torino, Torino, Italy
[82]Also at California Lutheran University, Thousand Oaks, California, USA
[83]Also at California Institute of Technology, Pasadena, California, USA
[84]Also at United States Naval Academy - Physics Department, Annapolis, Maryland, USA
[85]Also at Bingol University, Bingol, Türkiye
[86]Also at Sinop University, Sinop, Türkiye
[87]Now at another institute formerly covered by a cooperation agreement with CERN
[88]Also at Karamanoğlu Mehmetbey University, Karaman, Türkiye
[89]Also at Hamad Bin Khalifa University (HBKU), Doha, Qatar

[90]Now at Yerevan Physics Institute, Yerevan, Armenia
[91]Also at Imperial College, London, United Kingdom